This is to certify that the
dissertation entitled

POLYMER BRUSH MEMBRANES FOR
PERVAPORATION AND HIGH CAPACITY PROTEIN
BINDING

presented by

LEI SUN

has been accepted towards fulfillment
of the requirements for the

Ph.D.   degree in   Chemistry

_____
Major Professor's Signature

August 24, 2006
Date

MSU is an Affirmative Action/Equal Opportunity Institution

PLACE IN RETURN BOX to remove this checkout from your record.
TO AVOID FINES return on or before date due.
MAY BE RECALLED with earlier due date if requested.

DATE DUE	DATE DUE	DATE DUE
		AUG 5 1 8 0 3

POLYMER BRUSH MEMBRANES FOR PERVAPORATION

AND HIGH CAPACITY PROTEIN BINDING

By

Lei Sun

A DISSERTATION

Submitted to
Michigan State University
In partial fulfillment of the requirements
For the degree of

DOCTOR OF PHILOSOPHY

Department of Chemistry

2006

ABSTRACT

POLYMER BRUSH MEMBRANES FOR PERVAPORATION AND HIGH CAPACITY PROTEIN BINDING

By

Lei Sun

Atom transfer radical polymerization (ATRP) of 2-hydroxyethyl methacrylate from the surface of porous alumina supports yields polymer-brush membranes that can be readily modified to control their properties. Derivatization of poly(2-hydroxyethyl methacrylate) (PHEMA) coatings with octyl, hexadecyl, or pentadecafluorooctyl side chains provides films that are sufficiently hydrophobic to allow highly selective pervaporation of volatile organic compounds from water. Moreover, the polymerization and derivatization reactions readily yield defect-free films with thicknesses of 200 nm or less, and this minimal thickness results in fluxes of ~1.4 kg/m^{2}h (0.05 wt% VOCs at 22 °C) through fluorinated films. These fluxes are generally an order of magnitude greater than those through high-performance poly(dimethyl siloxane) pervaporation membranes. The use of different monomers may further enhance the flux and selectivity of pervaporation membranes prepared by ATRP.

In related work, ATRP of PHEMA brushes inside the pores of alumina supports followed by functionalization of PHEMA with nitrilotriacetate-Cu^{2+} complexes yields membranes that adsorb proteins via coordination of Cu^{2+} to histidine residues. Adsorption isotherms show that these membranes have binding capacities as high as 0.9 mg of bovine serum albumin (BSA) per cm^2 of external membrane surface area (150

mg/cm^3 of membrane), and breakthrough curves indicate that saturation of the membranes with BSA or myoglobin occurs in less than 15 min. Nine cycles of protein loading, elution, and membrane regeneration result in no detectable loss of binding capacity. The unusually high capacity of these membranes for rapid protein binding makes them attractive for applications such as purification of his tagged proteins.

Expansion on the protein adsorption work demonstrates that polymer brushes derivatized with Ni^{2+} complexes are very attractive for purification of his tagged proteins. Protein binding experiments with films on gold substrates show that PHEMA-NTA-Ni^{2+} brushes are capable of selectively binding large amounts (3.1 μg/cm^2) of his tagged ubiquitin (HisU). Porous alumina membranes modified with derivatized brushes also show remarkable capacities (0.72 mg/cm^2) for the binding of HisU. Most importantly, gel electrophoresis studies show that these high-capacity membranes are highly selective for purification of his tagged proteins. Even in a 20-fold excess of BSA, membranes gave 99% HisU.

To My Husband

ACKNOWLEDGMENTS

The first person I would like to thank is my advisor Merlin Bruening. I joined his group in 2002 and have been working with him for 4 years. During these four years, I have known him as a pleasant person, a great advisor as well as an excellent scientist. His understanding, encouraging and personal guidance have provided a good basis for the present thesis. He is the most considerate advisor a student could ever ask for.

I also acknowledge Professor Baker who as my second supervisor provided tremendous help to me.

Dr. Jinhua Dai has been a great mentor to me. He, as a true scientist, has taught me how to do great research. I dedicate my greatest acknowledgement to him.

Thank my committee members Dr Blanchard, Dr Borhan and Dr Swain for their kind help and great suggestions.

I would like to give my thanks to all Bruening group members. The last four years has been a wonderful experience for me to be with talented people like Malai, Dan, Matt, Sri, Jamie, Christin, Lu, Maneesha, Parul, Fei and David.

Last but not least, I would like to express my deepest gratitude to my husband. I am very grateful to him for his long-distance support.

TABLE OF CONTENTS

LIST OF TABLES

LIST OF SCHEMES

LIST OF FIGURES

xi

LIST OF ABBREVIATIONS

AFM	Atomic Force Microscopy
AIBN	Azobisisobutyronitrile
ATRP	Atom transfer radical polymerization
BSA	Bovine serum albumin
DMAP	4-dimethylaminopyridine
DMF	Dimethylformamide
DPE	1,1-Diphenylethylene
EDC	1-[3-(dimethylamino)propyl]-3-ethylcarbodiimide hydrochloride
EDTA	Ethylenediamine tetraacetic acid
ENB	5-Ethylidene-2-norbornene
FTIR	Fourier transform infrared spectroscopy
GPS	3-glycidoxypropyltrimethoxysilane
IMAC	Immobilized metal-affinity chromatography
LCST	Liquid Critical Solution Temperature
NHS	N-hydroxysuccinimide
NMP	Nitroxide-mediated polymerization
ODMS	Octadecylmethyldiethoxysilane
ODT	Octadecanethiol
OEG	Oligo(ethylene glycol)
PAAm	Poly(acrylamide)
PDMS	Polydimethylsiloxane
PE	Polyelectrolyte
PEG	Poly(ethylene glycol)
PHEMA	Poly(2-hydroxyethyl) methacrylate
PMMA	Poly(methyl methacrylate)
PNIPAM	Poly(N-isopropylacrylamide)
PPEI	Poly(N-propionylethylenimine)
PS	Polystyrene
PSA	Pressure-sensitive adhesive
PSGMA	Poly(sodium sulphonated glycidyl methacrylate)
PVDF	Poly(vinylidene fluoride)
RAFT	Reversible addition fragmentation chain transfer
RGD	Arginine-glycine-aspartic acids
ROMP	Ring-opening metathesis polymerization
SA	Succinic anhydride
SAM	Self assembled monolayer
SIP	Surface initiated polymerization
TEMPO	2, 2, 6, 6-Tetramethyl-1-piperidinyloxy
VOCs	Volatile organic compounds

Chapter 1　　　Introduction and Background

This dissertation describes the growth of polymer brushes on and in porous supports to form high-flux pervaporation membranes as well as membrane absorbers capable of purifying proteins modified with histidine$_x$ tags. The research builds on previous studies of the synthesis and application of polymer brushes, so to put this work in perspective, this introduction first describes polymer brushes and several of their extensively investigated applications. Subsequently, I discuss a number of recent techniques for synthesizing polymer brushes in a controlled fashion. Sections 1.3 and 1.4 of the introduction then present brief background on the importance of pervaporation membranes and membrane absorbers, respectively, and show why polymer brushes might be attractive for these applications. Finally, I present an outline of the dissertation.

1.1. Polymer Brushes

1.1.1. Definition and Assets of Brushes

Polymer brushes are assemblies of macromolecules bound to a substrate with a chain density high enough to force the polymers to extend from the surface.[1] The brushes
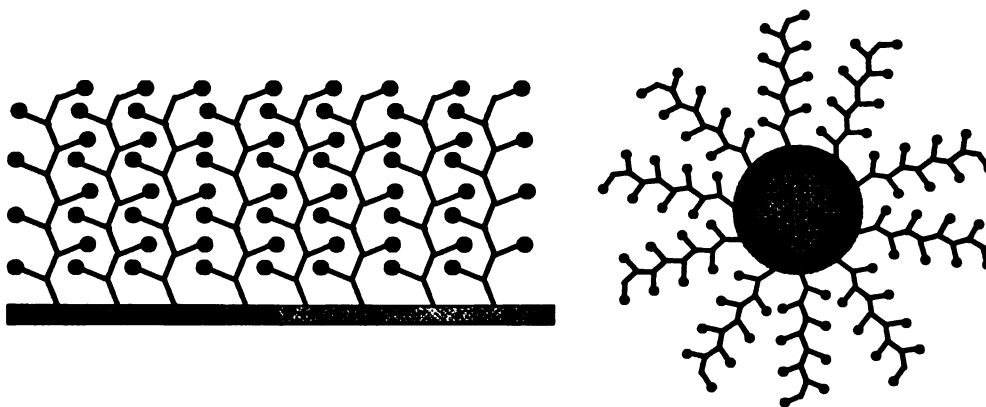
Figure 1.1.　　Polymer brushes on a flat or spherical surface.

can be held on the surface by either physisorption or covalent bonding, usually near one end of the polymer chain.[2] Because of their surface confinement, in appropriate solvents polymer brushes are extended away from the rigid substrate boundary and can be highly swollen, which makes them attractive platforms for capture and purification of proteins, as demonstrated herein.[3-5] The high swelling of polymer brushes should also allow molecules to rapidly diffuse through them, which is important for both rapidly capturing biomolecules and allowing fast transport of small molecules in pervaporation separations. An additional asset of polymer brushes is that they contain a high density of functional groups that can be readily derivatized to tailor brush properties for specific applications.

1.1.2. Applications of Brushes

Polymer brushes first found application in the early 1950s, when Clayfield and coworkers grafted poly(ethylene oxide) onto colloidal particles to effectively prevent flocculation.[6] More recently, brushes have been employed as materials for lithographic masks, adhesion promoters, lubrication, nonfouling coatings, and responsive surfaces, as described below.[2]

1.1.2-a. Polymer Brushes as Lithographic Resists

Lithography is a process used in semiconductor device fabrication to transfer a pattern from a photo mask to the surface of a wafer. Patterned polymer brushes have drawn significant attention for lithography because of the diversity of chemical structures suitable for brush formation and the physical/mechanical robustness of the grafted films. Micropatterning of functional polymer brushes on substrates is of crucial importance to the development of biochips, microarrays, and microdevices for cell-growth, regulation of protein adsorption, and drug delivery.[7] Ober and coworkers prepared oligo(ethylene

2

glycol) (OEGn)-containing styrene polymer brushes and compared the biocompatibility of these brushes with that of assemblies of surface-bound OEGn-terminated silanes with selected chain lengths.[8] The monomer (4-(Oligoethyleneoxy)oxymethylstyrene) was prepared by reaction of 4-chloromethylstyrene and monomethoxy OEG derivatives of varying lengths in the presence of sodium hydride. Surface initiated nitroxide-mediated polymerization was used to polymerize this monomer to form polymer brushes. Polymer brushes possessed a superior ability to inhibit protein adsorption and cell adhesion when compared to surface assemblies with the same OEGn length. They attributed this result to the greater thickness and surface coverage of polymer brushes with respect to monolayers of OEGn-terminated silanes.

Various techniques have been reported for fabricating patterned polymer brushes, including microcontact printing, UV/electron-beam lithography, scanning-probe lithography, and imprint lithography.[9] Microcontact patterning (also called soft lithography) was principally introduced by Whitesides and coworkers and is a remarkably simple technique that allows generation of patterned surfaces in any laboratory.[10] In this procedure (Figure 1.2),
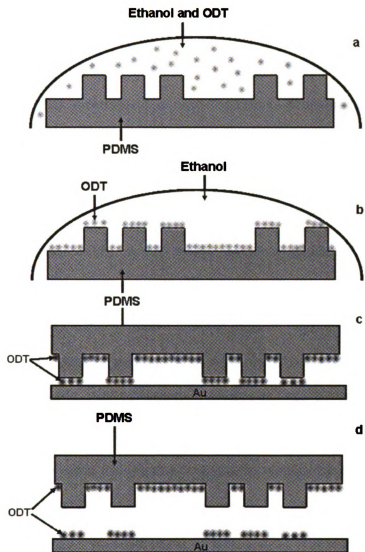
Figure 1.2. The Microcontact printing process. (a) a patterned PDMS stamp is placed in ethanol containing octadecanethiol (ODT); (b) ODT from the solution lightly adsorbs to the PDMS stamp; (c) The PDMS stamp with the ODT is placed on the gold substrate; (d) The stamp is removed and the ODT remains adsorbed to the gold. (Redrawn from *Angew. Chem. Int. Ed.* **1998**, *37*, 550-575.)

an elastomeric polydimethylsiloxane (PDMS) stamp is used to transfer a monolayer of molecules of an ink to a surface at contacted regions. After printing, a different self assembled monolayer (SAM) can be formed on the unmodified regions of the surface by exposing the patterned substrate to a dilute solution containing a second adsorbing molecule. If one of the two adsorbed molecules is an initiator of polymerization, polymer brushes can be grown from these initiators to amplify the surface pattern.[11-13] Hawker and coworkers prepared patterned brushes using atom transfer radical polymerization (ATRP) and speculated that the brushes would provide a significantly more robust resist than a simple monolayer.[11] Huck and coworkers successfully grew thick poly(N-isopropylacrylamide) (PNIPAM) brushes using surface initiated polymerization (SIP) from patterned monolayers to prepare smart micro-patterned domains.[14] PNIPAM is a very interesting material that is widely investigated due to its inverse solubility-temperature relationship in water, i.e., PNIPAM dissolves in water at low temperature, but becomes insoluble when the solution temperature reaches the liquid critical solution temperature (LCST), 32 $^{\circ}$C. Atomic force microscopy (AFM) experiments showed that patterned PNIPAM chains grown from a surface display a reversible phase transition accompanied by measurable changes in adhesion between the surface and the AFM tip. A hydrophilic to hydrophobic change occurs when raising the temperature from 25 $^{\circ}$C to 35 $^{\circ}$C.

Zauscher and coworkers reported a "top-down/bottom-up" technique to fabricate patterned polymer brush arrays on the micrometer and nanometer length scales.[15] Their approach combined the traditional electron beam lithography technique (top down) with SIP (bottom up). The primary advantage of electron beam lithography is that it provides a

way to overcome the diffraction limit of light to prepare features in the sub-µm regime. Electron beam widths were projected to be on the order of nanometers as of the year 2005. The electron beam can also be replaced with UV irradiation.[16] The combination of SIP and electron beam lithography gives control over polymer functionality, shape, feature dimension and inter-feature spacing on the nanometer length scale. This technique yielded patterned polymer brushes with a height of about 300 nm and width of 1.8 µm.

Scanning probe lithography is an emerging area of research in which the scanning tunneling microscope or AFM is used to pattern nanometer-scale features. Zauscher presented a strategy to fabricate stimulus-responsive, surface-confined PNIPAM brush nanopatterns prepared in an approach that combines "nanoshaving", a scanning probe lithography method, with SIP.[17]

Another mechanism for formation of polymer-brush nanopatterns is a new nonconventional lithographic method called nanoimprint lithography.[18] This method is regarded as one of the "10 emerging technologies that will change the world" by MIT Technology Review.[19] The key advantage of this lithographic technique is the ability to pattern sub-25 nm structures over a large area with a high-throughput and low-cost.[20] In the first step of nanoimprint lithography, a mold with nanostructures on its surface is pressed into a thin resist cast on a substrate, followed by removal of the mold. This step duplicates the nanostructures on the mold in the resist film. The second step is the pattern transfer where an anisotropic etching process, such as reactive ion etching is used to remove the residual resist in the compressed area. Carter and his coworkers patterned polystyrene (PS), poly(methyl methacrylate) (PMMA), and poly(2-hydroxyethyl) methacrylate (PHEMA) into submicrometer sized features on a silicon wafer using a

combination of nanoimprint lithography and living free radical polymerization.[21] (Initiators were attached to exposed areas of the pattern and polymerization from these initiators followed.) They also grew polydihexylfluorene brushes from a nanoimprint-patterned surface using metal-catalyzed step-growth condensation polymerization.[19] Polymer brushes of well-defined nanoscopic structure, molecular weight, and controllable molecular architecture were obtained and have potential application in a variety of different areas such as molecular-scale electronics, magnetic storage, optoelectronics, and biotechnology.[21]

In one final approach to the use of polymer brushes to amplify surface patterns, Luzinov and coworkers developed the use of capillary force lithography and SIP to generate patterned binary brushes containing poly(ethylene glycol) methyl ether methacrylate and PNIPAM.[9] They found that when an ultrathin PS pattern was deposited, over a layer of polymerization initiator already anchored to a surface (Figure 1.3), the pattern could withstand subsequent polymerization conditions and stay intact during brush synthesis, provided that no solvent for PS was involved. Thus, no monomer and catalyst were delivered to the initiator located under the PS-protected areas. They utilized this interesting phenomenon and achieved a variety of combinations of binary patterned polymer brushes.
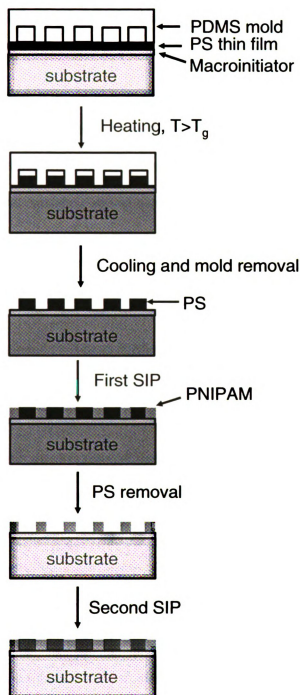
Figure 1.3. Schematic diagram showing the formation of patterned surfaces by capillary force lithography and SIP. (Redrawn from *J. Am. Chem. Soc.* **2006,** *128*, 8106-8107.)

1.1.2-b. Polymer Brushes as Adhesion Promoters

Adhesion at polymer/polymer and polymer/solid interfaces is of great importance for numerous applications from microelectronics to the aircraft industry.[22] For both permanent and reversible adhesion, it is essential that the chemical composition and morphology of the interfaces to be joined are well controlled. Polymer brushes provide a controlled and tailorable surface, and because they are often covalently bonded to surfaces, they can promote adhesion to the substrates on which they reside.

Creton and coworkers investigated the adhesive properties of binary heterogeneous polymer brushes made from a mixture of end-functionalized PS and poly(2-vinylpyridine) chains.[22] The adhesive properties were tested using a soft hydrophobic pressure-sensitive adhesive (PSA), which contains a symmetric (PS-polyisoprene-PS) triblock copolymer and a low molecular weight, high-Tg resin that is completely miscible with the isoprene phase. To test the adhesive properties of the binary polymer brushes, a silicon wafer coated with the binary brush film is glued on the end of a cylindrical stainless steel probe. The probe then approaches and comes in contact with the PSA layer deposited on a glass microscope slide. By observing the events occurring at the adhesive/brush interface with a CCD camera and recording the stress/strain curve, the adhesive properties of the binary brushes were investigated. The adhesive properties of the binary brush structure can be reversibly switched by exposing the brush to solvents that bring PS or poly(2-vinylpryridine) to the surface. When PS is at the surface, adhesion to the hydrophobic PSA is strong, while little adhesion occurs when poly(2-vinylpyridine) is at the surface. This class of adhesives is gaining increasing interest in industry and medicine for its low toxicity and ease of use. However, more

work is needed on model systems to better understand the subtle interactions taking place at the interface between a brush with mixed composition and an adhesive.

Polymer brushes can also be modified to control cellular adhesion. The ability to spatially control such adhesion on a biocompatible substrate is an important factor in designing new biomaterials for use in wound healing and tissue engineering applications. Since arginine-glycine-aspartic acids (RGD) were found to promote cell adhesion in 1984, numerous materials have been functionalized with RGD for academic studies or medical applications.[23, 24] Current efforts to precisely engineer cell-adhesive or non-adhesive surfaces often focus on including the RGD peptide sequence in a SAM.[25, 26] Metter's group recently developed a novel method for creating RGD-ligand density gradients in anionic polymer brushes (poly(methacrylic acid) salts) to control the spatial attachment of fibroblasts across patterned surfaces.[27] By utilizing a controlled photopolymerization technique, polymer brushes exhibiting spatially defined gradients in chain density are created. Subsequently these brushes are functionalized with RGD to create ligand density gradients capable of inducing cell adhesion on an otherwise weakly adhesive substrate. Their studies of cell adhesion indicated that these ligand-functionalized surfaces are noncytotoxic, with cellular adhesion increasing with RGD-ligand density across the gradient of polymer brush density.

Polymer brushes are much more flexible than SAMs because of their long chain lengths. The flexibility and high density of functional groups in polymer brushes, as well as the ability to modify the surfaces of both inorganic and polymeric materials, give these materials significant advantages over SAMs for the preparation of ligand-functionalized materials.[26]

1.1.2-c. Polymer Brushes as Lubricants

The use of lubricants to reduce friction between rubbing surfaces has been documented since antiquity.[28] More recently, research has focused on boundary lubrication by surfactant-like species coating the surfaces. Klein and coworkers first discovered that polymer brushes can facilitate the sliding of one surface over another in 1994.[29] They determined the normal (F_{normal}) and shear (F_{shear}) forces between curved, molecularly smooth mica surfaces using a surface forces apparatus, and then attached PS brushes to the mica surfaces and measured the shear forces again.[30] The shear forces with polymer brushes were orders of magnitude lower than the forces needed for sliding the bare surfaces. The attachment of polymer brushes resulted in an entropy-driven long-range equilibrium separation of the surfaces, which gave decreased friction. Theoretical studies suggested only a limited interpenetration of the brushes, so as the surfaces slide past each other, there is rapid relaxation of the interpenetrating chains and low friction.

After proving that the presence of neutral polymer brushes may lead to a massive reduction in sliding friction between the surfaces to which they are attached, Klein further showed that hydrated ionic brushes can also act as extremely efficient lubricants between sliding charged surfaces.[30] They created a diblock copolymer brush of poly(methyl methacrylate) and poly(sodium sulphonated glycidyl methacrylate) (PMMA-b-PSGMA) on mica. The copolymer contains hydrophobic (PMMA) and hydrophilic polyelectrolyte (PSGMA) blocks (Figure 1.4). Effective friction coefficients with these polyelectrolyte (PE) brushes are lower than about 0.0006 – 0.001 even at low sliding velocities and at pressures of up to several atmospheres. These low values of the effective friction coefficient reveal a remarkable capacity for lubrication by the PE, di-block brushes. The
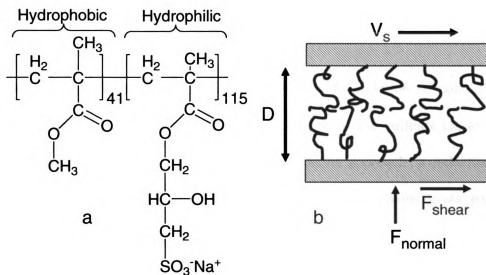
Figure 1.4. (a) Chemical structure of PMMA-b-PSGMA copolymer. (b) Schematic representation of F_{shear} and F_{normal} between the brush-bearing surfaces. (Redrawn from *J. Polym. Sci., Part B: Polym. Phys.* **2005**, *43*, 193-204.)

authors attributed this to the exceptional resistance to mutual interpenetration displayed by the compressed, counterion-swollen brushes, together with the fluidity of the hydration layers surrounding the charged, rubbing polymer segments. They also mentioned that these charged polymer brushes may have applications as biolubricants in artificial implants.

1.1.2-d. Polymer Brushes as Stabilizers of Colloidal Particles

Interactions between polymer-coated colloidal particles have been an important issue for both industrial applications and scientific investigations.[31] These interactions form one of the bases of steric stabilization of colloidal dispersions that are widely used in industry.[32] Since Clayfield and coworkers found that polymer brushes can effectively

prevent flocculation and maintain the stability of colloids,[6] much research has been performed in this area.[33-37]

In the absence of a macromolecular covering, flocculation of colloids occurs rapidly because attractive van der Waals forces between the colloids cause them to aggregate. However, when two polymer-coated particles approach, a reduction in the number of configurations available to the flexible polymer chains gives rise to an "entropic" repulsive force between the particles, which may keep colliding particles separated such that the van der Waals interaction energy is insufficient for coherence.[38]

The Birshtein group found that colloidal stability is significantly influenced by a mechanism called capillary condensation in a binary solvent system. Capillary condensation occurs in porous particles when multilayer adsorption from a vapor proceeds to the point at which pore spaces are filled with liquid separated from the gas phase. In particular, when the particles are somewhat hydrophilic, there will be a molecularly thin film of water adsorbed onto their surfaces. When two particles come near to each other, there will be a thick water film between the two particles. Consequently, the particles cannot separate without breaking the water film, and such films can hold particles together. Birshtein's group referred to this process as capillary condensation mediated flocculation and showed theoretically that one way to protect particles from capillary condensation flocculation is to graft hydrophobic polymer brushes onto their surfaces.[37]
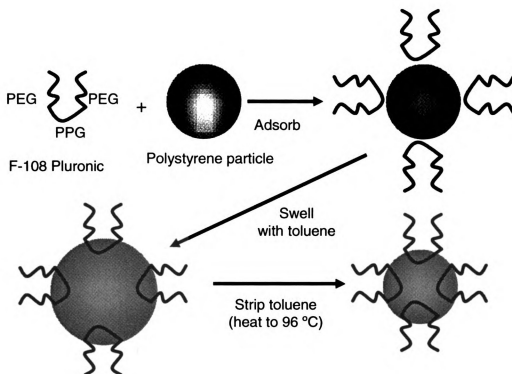
Figure 1.5. Swelling-based method for preparing stable, functionalized polymer colloids. (Redrawn from *J. Am. Chem. Soc.* **2005**, *127*, 1592-1593.)

Very recently, Crocker and coworkers used a swelling-based method to prepare stable, brush-functionalized polymer colloids (Figure 1.5). They first adsorbed block copolymer surfactants, poly(ethylene glycol)-b-poly(propylene glycol)-b-poly(ethylene glycol), from deionized water onto the surfaces of the PS particles and then swelled the particles with a small amount of toluene, allowing the hydrophobic block of the surfactant to penetrate the surface. Finally, they deswelled the particles by stripping the solvent. Optical microscope images show the high stability of these particles. Unlike physical adsorption, the swelling method permanently anchors the molecules to the polymer surfaces, and the poly(ethylene glycol) chains of the anchored polymer provide a steric barrier to aggregation, even at high ionic strength.[33]

1.1.2-e. Polymer Brushes as Nonfouling Coatings

Biofouling is a ubiquitous phenomenon that can occur on surfaces ranging from living marine organisms (known as epibiosis) to synthetic surfaces such as separation membranes. Most frequently biofouling is an undesirable process that needs to be prevented. For example the buildup of biofoulant films in groundwater wells can limit the rate of water recovery. Elimination of biofouling will require biocompatible materials that eradicate, or largely reduce, the nonspecific adsorption of proteins and other biomolecules. In recent years special attention has been given to the modification of protein–surface interactions using grafted polymer brushes.[39] It is believed that the role of the polymers tethered to the surface is to present a steric barrier to approaching
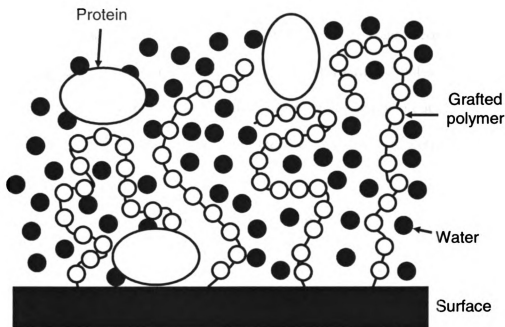
Figure 1.6. Schematic representation of protein molecules in contact with a polymer brush. (Redrawn from *Curr. Opin. Solid State Mater. Sci.* **1997,** *2,* 337-344.)

proteins (Figure 1.6).[40] To be specific, the protein approaches the polymer surface by diffusion and is affected by the van der Waals attraction between the polymer brush and protein through water. Further approach of the protein initiates the compression of polymer chains, which induces a steric repulsion effect; an additional van der Waals attraction becomes important between the substrate and protein through the water solvated polymer brush layer. The van der Waals component with the substrate decreases with increasing surface density and chain length of terminally attached polymer chains. Thus, high density of polymer brushes tends to prevent more protein adsorption.

Surfaces coated by terminally grafted, water soluble chains are highly resistant to protein adsorption in aqueous media.[41] In 1997, Szleifer wrote a review article discussing the understanding of the ability of tethered polymer chains to prevent protein adsorption along with the up-to-date experimental status of these systems. Some theoretical studies that enable calculation of the interactions of proteins with tethered polymer layers are also included in the review. In the last 10 years, experimental and theoretical studies that utilize polymer brushes to prevent nonspecific protein adsorption appeared continuously.[39, 41-46]

Among all the polymer brushes used for antifouling, poly(ethylene glycol) (PEG) is the most widely used. The ability of PEG films to reduce the adsorption of proteins onto surfaces has opened a broad field of applications in biotechnology.[40] Both the ability of PEG to prevent protein adsorption and its low toxicity have resulted in various attempts to create surfaces presenting PEG to the environment.[45]

Chilkoti et al synthesized PEG brushes from gold using SIP and examined the adsorption of different proteins onto these modified gold slides.[42] They observed no

protein adsorption from pure solutions of fibronectin or 10% or 100% fetal bovine serum. Wang and coworkers extended the formation of brushes using SIP to poly(vinylidene fluoride) (PVDF) substrates.[43] The fluorine atoms on the polymer surface served as direct initiation sites. Then they used ATRP to prepare poly(2-(N, N-dimethylamino) ethyl methacrylate) and poly(ethylene glycol) methacrylate brushes from PVDF. Protein adsorption experiments revealed substantial resistance to fouling for both grafted films in comparison with the native PVDF surface.

1.1.2-f. Polymer Brushes as Responsive Materials

Some polymer brushes can act as materials that respond to environmental conditions such as pH, temperature or photo-irradiation, and PE brushes are particularly notable in this regrard.[47] The conformation and swelling of PE brushes strongly depends on the ionic strength, valence of counter ions, and the pH of the solutions to which they are exposed. Stamm et al. synthesized a mixed PE brush of carboxy terminated poly(acrylic acid) and poly(2-vinylpyridine)) on silicon wafers. They first absorbed 3-glycidoxypropyltrimethoxysilane (GPS) on the silicone wafer. Then a grafted layer of carboxy terminated poly(tert-butyl acrylate) was prepared via spin coating of this polymer on the GPS modified Si wafer and subsequent annealing in a vacuum oven at 150 °C for 20 min. Carboxy terminated poly(2-vinylpyridine) was then grafted on the same surface using a similar procedure. Finally, hydrolysis of poly(tert-butyl acrylate) yielded poly(acrylic acid). The charge of the mixed PE brush can switch rapidly with a change in pH, and the swelling of the brushes also changes dramatically. The responsive/switching behavior of the PE brush can be explored to tune surface properties

in aqueous environments by applying a pH signal, which is of potential interest for microfluidic technologies, smart nanodevices, and drug delivery systems.[48]

PNIPAM exhibits large swelling changes in aqueous media in response to small changes in temperature (Scheme 1.1). As mentioned before, the LCST of PNIPAM is
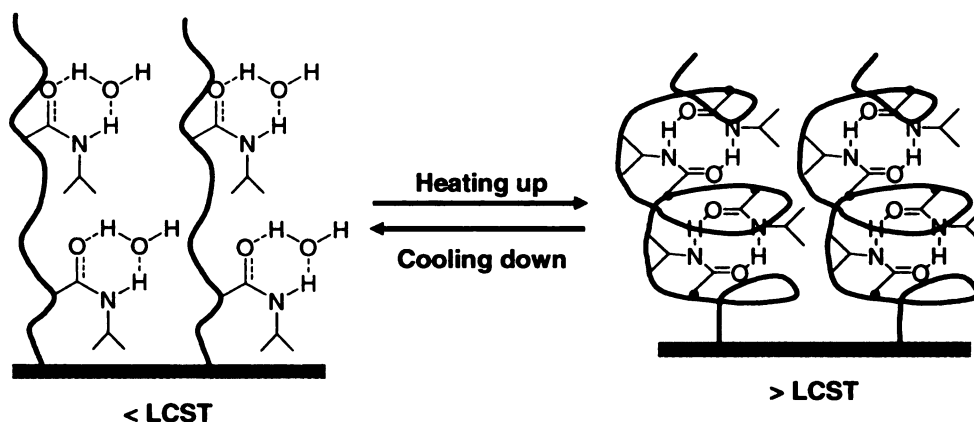
Scheme 1.1. Diagram of the reversible formation of intermolecular hydrogen bonds between PNIPAM chains and water molecules (left) and intramolecular hydrogen bonding between C=O and N-H groups in PNIPAM chains (right) below and above the LCST. (Redrawn from *Angew. Chem. Int. Ed.* **2004**, *43*, 357-360.)

near 32 °C. PNIPAM chains hydrate to form expanded structures in water when the solution temperature is below its LCST but become compact structures by dehydration when heated up above the LCST.[49] Temperature-responsive properties of PNIPAM brushes have been utilized in a variety of applications including controlled drug delivery[50] and solute separation.[51]
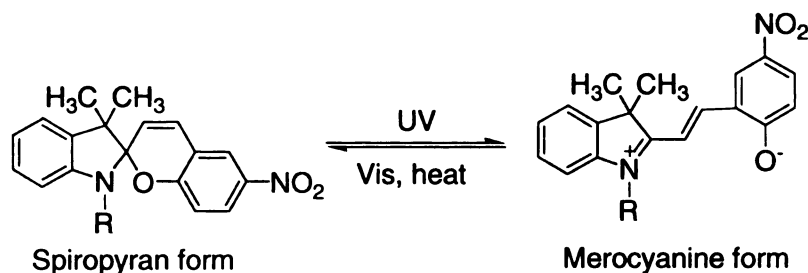
Scheme 1.2. Photochromic transformation of spiropyran. (Redrawn from *Macromolecules* **1998**, *31*, 2606-2610.)

To realize a photo response in polymer brushes, Imanishi et al. grafted a spiropyran-containing methacrylate-MMA block copolymer onto a glass filter. The photoisomerization of the spiropyran groups (Scheme 1.2) might induce structural variations in the macromolecular chain, and it also yields changes in film color.[52] The appearance of a blue color upon ultraviolet light irradiation indicated isomerization of the pendant spiropyran groups to merocyanine groups, and this color change occurred reversibly upon ultraviolet and visible light irradiations. Toluene permeation through the glass filter modified with the grafted copolymer increased upon ultraviolet-light irradiation, and decreased after visible-light irradiation.

1.2. Growth of Polymer Brushes from Surfaces

1.2.1. Surface Initiated Polymerization

Because polymer brushes have many potential applications, the preparation of these materials on solid substrates has been investigated extensively. Successful synthetic techniques for forming brushes can be divided into two large categories: "grafting to" methods[53] and "grafting from" methods.[54, 55] In "grafting to" approaches,

preformed end functionalized polymer molecules react with functional groups on a substrate to form polymer brushes. The "grafting to" technique results in relatively low densities of polymer chains on the surface because steric hindrance prevents incoming polymer chains from diffusing through the film to reactive sites on the substrate.

When higher grafting densities are needed, the "grafting from" approach is the method of choice for brush formation. "Grafting from" is accomplished by covalently anchoring initiators on the substrate and then activating these initiators to start polymerization. The polymer brushes grown from the surface by this technique possess high chain densities (~1 chain per 2 nm^2) because monomers, rather than polymer chains must diffuse to the surface for film growth to occur. [3]

"Grafting to" can be accomplished with a number of polymerization techniques including free-radical, cationic, and anionic polymerization, as well as ring-opening metathesis polymerization (ROMP), ATRP, nitroxide-mediated polymerization (NMP), and reversible addition fragmentation chain transfer (RAFT) polymerization. The following sections will focus on the synthesis of polymer brushes using these various SIP techniques.

1.2.2. Surface Initiated Free Radical Polymerization

Free radical polymerization is a relatively versatile tool to grow polymer brushes on a surface because it allows the use of a variety of monomers, including those with polar and unprotected functional groups.[56] Immobilized azo compounds are usually used as initiators in surface initiated free radical polymerization because they can be readily activated at low temperatures or with UV light. To immobilize the initiator, a difunctional anchor molecule is frequently linked to the surface of the substrate and the

initiating azo species is linked to this anchor molecule in one or several additional steps.[57] However, if the surface reactions are not quantitative, the stepwise generation of the initiator monolayers can lead to low initiator densities that consequently reduce the density of brushes.

To avoid these problems, Rühe and coworkers developed a system in which the complete initiator is attached to the substrate in one step as shown in Scheme 1.3.[55, 58, 59] The initiator system contains an anchoring group (A) that connects the molecule to the surface, the initiator itself (I-I*), and a cleavable group (ⓘ) that allows for the detachment of the polymer brushes after polymerization. (Detachment of the brushes is useful for analysis of the polymer composition using methods such as gel-permeation chromatography.) The complete initiator is first self assembled on the substrate, and in a subsequent reaction the initiator is activated and polymer is grown in situ from the surface of the substrate. Rühe and coworkers reported the free radical polymerization of styrene using SAMs of azo initiators covalently bound to high surface area silica gels[54] and studied the kinetics and mechanism of this free radical polymerization.[55] Very recently, they grew mixed polymer brushes consisting of PS and PMMA on a silicon surface using this polymerization technique. These mixed polymer brushes show nanophase separation into defined patterns, depending on the molecular parameters of the brushes.[60, 61] This nanopattern has a domain memory effect, which is defined as the ability of single patterns of the brush topography to recover after erasure and regeneration of the nanopattern by exposure to selective and nonselective solvents, respectively. To be specific, the size, shape, and position of the PS-PMMA domains are found to vary with the nature of the solvent to which the brushes are exposed. The brushes are treated first

with toluene (good solvent for both blocks), which leads to strong swelling and structure erasure. Subsequent exposure to acetone (a selective solvent for PMMA) leads to a film that contains PMMA chains at the surface and PS chains in its interior.

Bruening and Huang extended this method of polymerization to include siloxane-based initiators attached to thin oxide surfaces formed on SAMs on Au.[56] That study was performed because Au surfaces are homogeneous and compatible with a broad variety of surface analytical techniques including ellipsometry, contact angle measurements, AFM, Fourier transform infrared spectroscopy (FTIR), surface plasmon resonance, and quartz crystal microbalance gravimetry. In addition, contact-printing schemes allow patterning of layers on Au surfaces.[13] Bruening and Huang also applied free-radical polymerization to grow PS from azo-initiator thiol monolayers attached directly to a planar Au substrate. However, the stability of alkanethiol monolayers appears to decrease in the presence of free radicals in solution. Desorbed alkanethiols may serve as efficient chain-transfer reagents that hinder polymerization. To overcome this problem, they utilized a simple cross-linking procedure (Scheme 1.4) to enhance the stability of SAMs and make thermal radical polymerization from Au surfaces more effective.
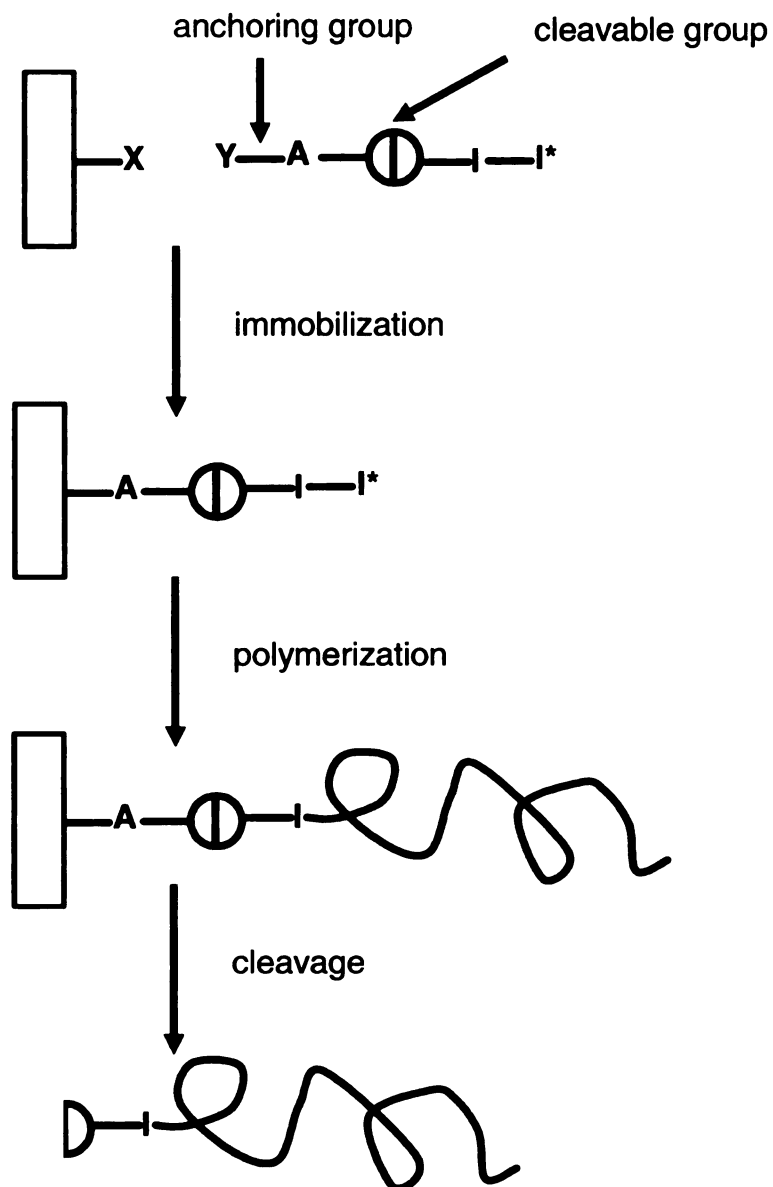
Scheme 1.3. Schematic description of the preparation of polymer brushes by radical polymerization from covalently immobilized initiators. (Redrawn from *Macromolecules* **1998**, *31*, 592-601.)
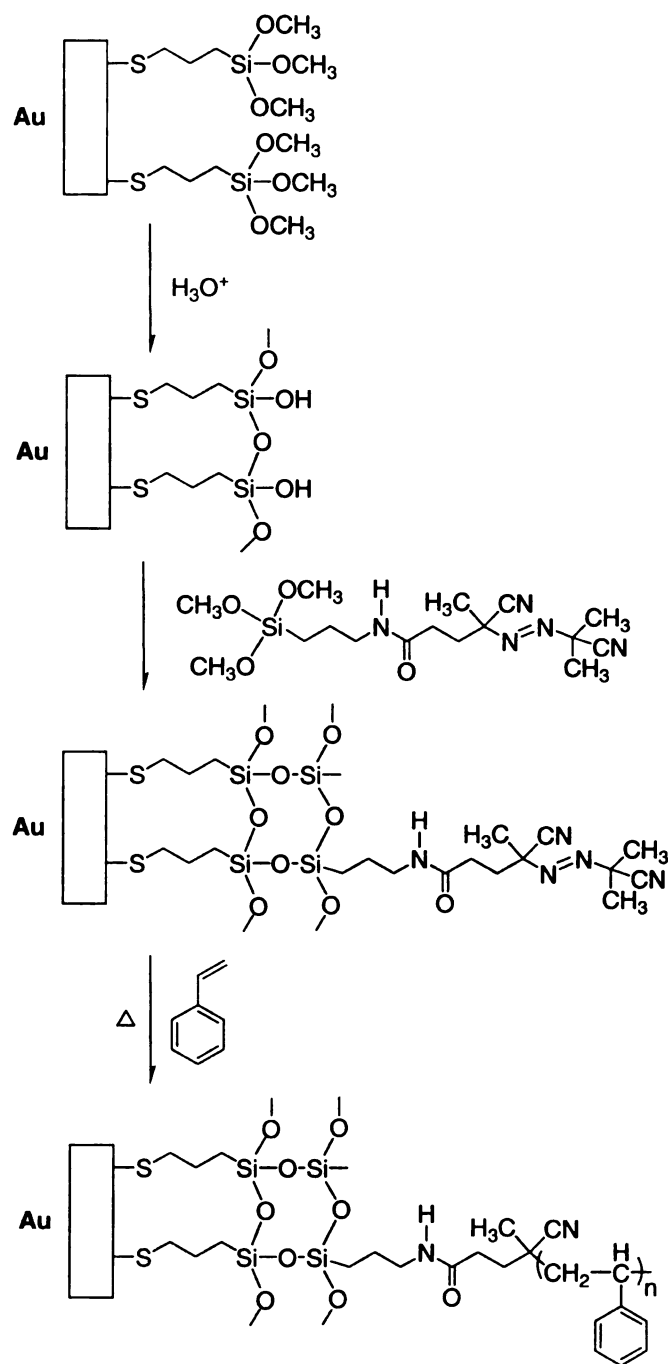
Scheme 1.4. Free radical polymerization from initiator layers attached to cross-linked thiol monolayers on Au. (Figure redrawn from *Langmuir* **2001,** *17,* 1731-1736.)

1.2.3. Surface Initiated Anionic Polymerization

Among the surface initiated polymerization techniques, living anionic polymerizations are very attractive for possible control of polymer architecture.[62] Anionic polymerization has been used to grow polymer brushes from a variety of substrates such as silica,[63] clay nanoparticles[64] and flat surfaces.[62, 65, 66]

Jordan et al. presented the first report of surface initiated anionic polymerization, with the growth of styrene from a SAM on gold.[65] A SAM of 4'-bromo-4-mercaptobiphenyl was self assembled on gold and reacted with s-BuLi to obtain 4'-lithio-4-mercaptobiphenyl, which served as the initiator for the anionic polymerization of styrene. This synthetic approach results in homogeneous "brush type" PS layers with a very high grafting density as well as surprisingly high stability.
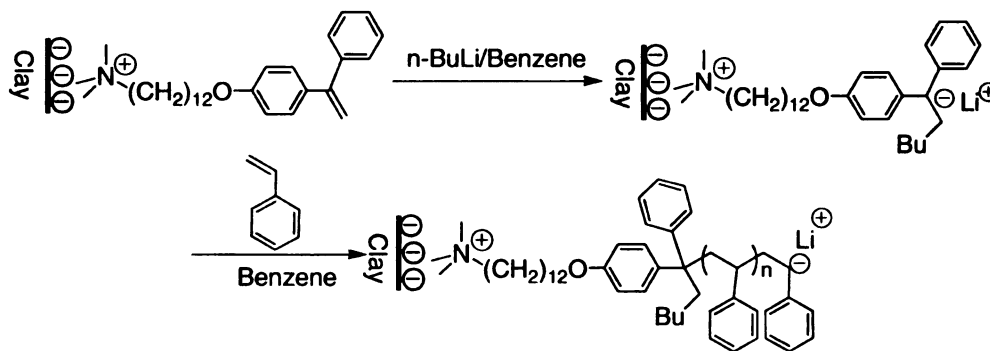
Scheme 1.5. Schematic illustration of anionic SIP from clay surfaces. (Redrawn from *Langmuir* **2002,** *18,* 4511-4518.)

However, controlled anionic polymerization requires the proper choice of initiator, monomer, and solvent as well as high purity reagents and an inert atmosphere.[67] Recently, Advincula et al. reported the synthesis of polymer brushes on clay nanoparticles using 1,1-diphenylethylene (DPE) initiators (Scheme 1.5).[64, 68] Anionic SIP

directly from clay particles is difficult, because the hydrophilic lamellar hosts inevitably contain moisture, which can terminate a propagating living anion. To overcome this problem, they demonstrated that by using a DPE derivative as the initiator and carefully controlling the polymerization conditions (high temperature and high vacuum to remove excess water), SIP from silicate clay surfaces is feasible. They inferred a "living" nature for anionic polymerization of PS from the DPE initiators on nanoparticles by demonstrating a linear relationship between monomer concentration and molecular mass and observing the appearance/disappearance of a red-colored Li-DPE anion complex. They then investigated the feasibility of anionic SIP of homopolymers and block copolymers using SAMs of DPE derivatives on Si, SiOx and Au surfaces. The initiator precursor DPE was functionalized with alkylsilane or alkylthiol groups and grafted onto planar Si wafers and Au-coated surfaces, respectively. n-BuLi was used to activate the DPE initiator, which allowed the anionic polymerization of PS or PS-b-polyisoprene to proceed in benzene solution with both types of substrates.

1.2.4. Surface Initiated Cationic Polymerization

Compared to anionic polymerizations, cationic polymerizations are not as well studied and have not been made suitable for complex macromolecular synthesis.[69] Factors that influence surface initiated cationic polymerization include solvent polarity and additives.[70]

OH

+Au
————————
EtOH, rt, 16h

OH OH OH OH

O(SO₂CF₃)₂
————————
1 day,
vapor phase

SO_2CF_3
O

R

R=

S

C_2H_5

N O

0°C, reflux

C_2H_5
OTf

O
N

R

C_2H_5
n N O

————————
7 days,
CHCl₃,reflux

C_2H_5
OTf
O
N

C_2H_5
O
N
n-1

R

HN
ALKYL
ALKYL

————————
1 day,
CHCl₃, rt

ALKYL ALKYL

OTf NH

C_2H_5
O
N
n-1

R

terminal
functionality

polymer

SAM

Au
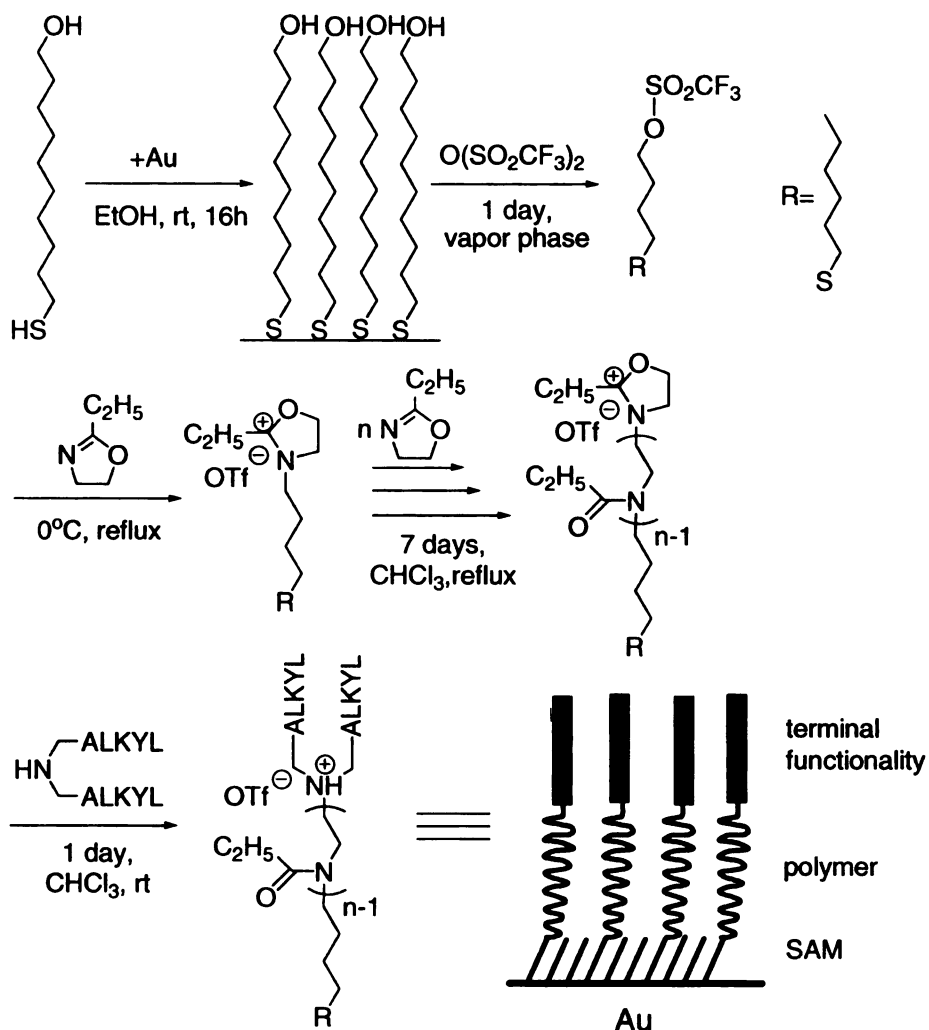
Scheme 1.6. Surface initiated cationic polymerization of 2-oxazolines.

(Redrawn from *J. Am. Chem. Soc.* **1998,** *120,* 243-247.)

Jordan and Ulman presented the surface initiated cationic ring opening polymerization of a 2-substituted 2-oxazoline to give poly(N-acylethylenimine).[71] They first formed a SAM of triflate groups attached to n-alkyl chains as the initiator (Scheme 1.6). After 7 days of polymerization, the resulting polymer brush layer (10 nm thick) of linear poly(N-propionylethylenimine) (PPEI) was of uniform thickness and was found to

be very stable. PPEI modified surfaces are of interest for their low toxicity and denaturing potential toward numerous proteins as well as their resistance to protein adsorption. Later, the Ulman group extended the polymerization of PPEI to the surface of gold nanoparticles.[72] 3D ω-functionalized SAMs of thiolates on gold nanoparticles were used to initiate the polymerization, and the resulting gold/polymer nanocomposite was found to be thermally stable.

Because the surface area per polymer chain is generally greater than the surface area per initiator bound to a surface, only a fraction of the immobilized initiators can initiate polymerization. Zhao et al. described the cationic polymerization of tethered PS brushes on silicate substrates and presented a discussion of initiator efficiency. They used nondeuterated (2-(4-(11-triethoxysilylundecyl) phenyl-2-methoxypropane) and deuterated (2-(4-trichlorosilylphenyl)-2-methoxy-d_3-propane) initiators to form the SAM on the silicate substrate. FTIR-ATR was used to estimate the initiator efficiency, which was about 7%.

1.2.5. Surface Initiated Ring-opening Metathesis Polymerization

Surface initiated ring opening polymerization is an attractive tool for coating surfaces with thin layers of polycaprolactone, polylactide and other polymers. ROMP of strained cyclic monomers, in particular functionalized norbornenes, has attracted recent attention for the synthesis of polymers with useful electrical properties.[73] Whitesides and coworkers formed a variety of patterned polymer films using the ROMP catalyst developed by Schwab et al. [74,75] [$(Cy_3P)_2Cl_2Ru$=CHPh, Cy=cyclohexyl]. The surface bound catalytic sites were produced by forming a trichlorosilane-derived SAM containing norbornene groups, and then exposing the SAM to a solution of the above catalyst.

Subsequent exposure of the substrate to norbornene-based monomers produced a polymeric film on the surface. Typical polymerization times were 30 min and film thicknesses were about 90 nm.[76]

Zauscher et al. combined AFM anodization lithography with ROMP to produce nanopatterned polymer brushes.[77] They showed for the first time that AFM anodization lithography, a form of field-induced scanning probe lithography, offers a powerful means to nanopattern semiconductor surfaces. First, anodic oxide patterns were generated on octadecylmethyldiethoxysilane (ODMS)-SAM coated silicon substrates (Scheme 1.7). Next, a 5-(bicycloheptenyl)triethoxysilane linker was covalently tethered to the patterned area, allowing for the subsequent attachment of a Ru-based metathesis catalyst. Finally, a nanopattern was amplified by immersing the patterned substrate in a monomer solution containing 5-ethylidene-2-norbornene (ENB).
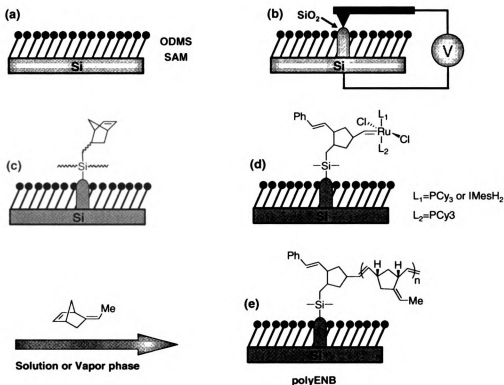
Scheme 1.7. Stepwise fabrication of polymeric nanostructures by surface initiated ROMP on SiO_2 nanopatterns generated by anodization lithography. a) ODMS resist SAMs were pre-coated on silicon substrates; b) anodization lithography was performed by applying a positive bias voltage to the p-type Si/SiO_2 substrate; c) Nbn-Si(OEt)$_3$ linkers were then covalently attached to the patterned SiO_2 features; d) A Ru-based metathesis catalyst (first- or second-generation Grubbs catalyst) was then covalently tethered to the linkers; e) ROMP of ENB was performed in solution or vapor phase. (Scheme and caption taken from *Small* **2006,** *2,* 848 – 853.)

1.2.6. Surface Initiated Controlled Radical Polymerization

Controlled radical polymerization has attracted much attention over the past decade because it provides simple and robust synthetic routes to well-defined, low-polydispersity polymers. Among the controlled radical polymerization techniques, NMP, ATRP, and RAFT polymerizations have already been applied to SIP by immobilizing either a dormant species or a conventional radical initiator on the surface.[78]

The living character of NMP depends on the reversible capping of the active chain-end radical with a nitroxide leaving group. The first application of NMP to surface initiated graft polymerization was reported by Hussemann et al. in 1999.[79] They succeeded in densely grafting PS using a surface-bound dormant species with a 2, 2, 6, 6-tetramethyl-1-piperidinyloxy (TEMPO) moiety (Scheme 1.8). A free dormant compound with TEMPO was also added to the solution to help control the polymerization. The stable TEMPO will cleave during the initiating process and subsequently reversibly cap the chain-end radicals to control the concentration of radicals at a given time. PS brushes over 100 nm thick were produced in 16 hours using this method. The living nature of the grafting was suggested by the formation of a block copolymer brush.
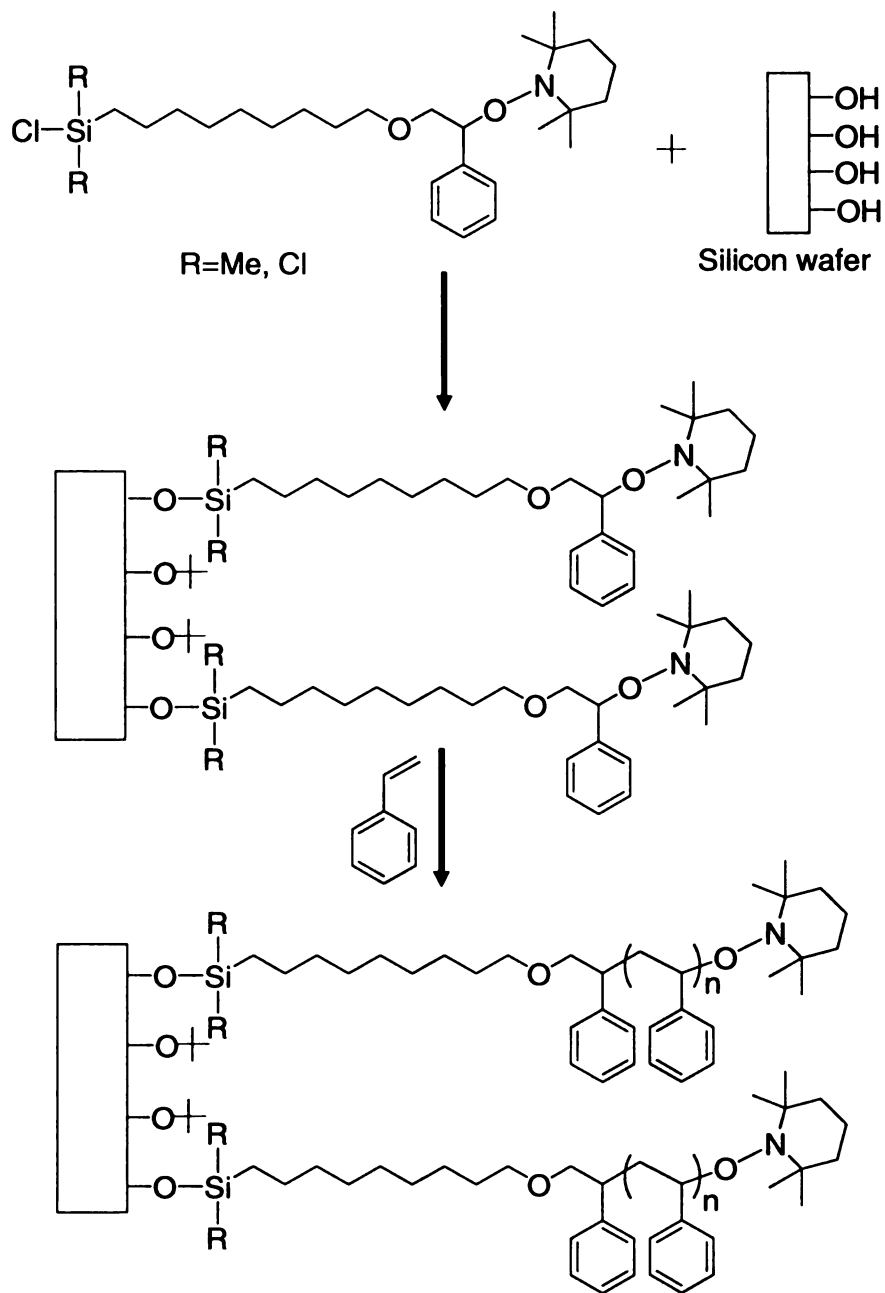
Scheme 1.8. Synthesis of polystyrene brushes by TEMPO-mediated radical polymerization. (Redrawn from *Macromolecules* **1999**, *32*, 1424-1431.)

RAFT polymerization is another important technique for controlled radical polymerization. In RAFT, chain growth is initiated using a conventional free radical initiator such as azobisisobutyronitrile (AIBN) and mediated by a dithioester chain transfer agent. Baum and Brittain prepared styrene, methyl methacrylate, and N,N-dimethylacrylamide brushes under RAFT conditions using silicate surfaces that were modified with surface-immobilized azo initiators (Scheme 1.9).[80] 2-Phenylprop-2-yl dithiobenzoate was added as a free (unbound) RAFT agent to control the graft
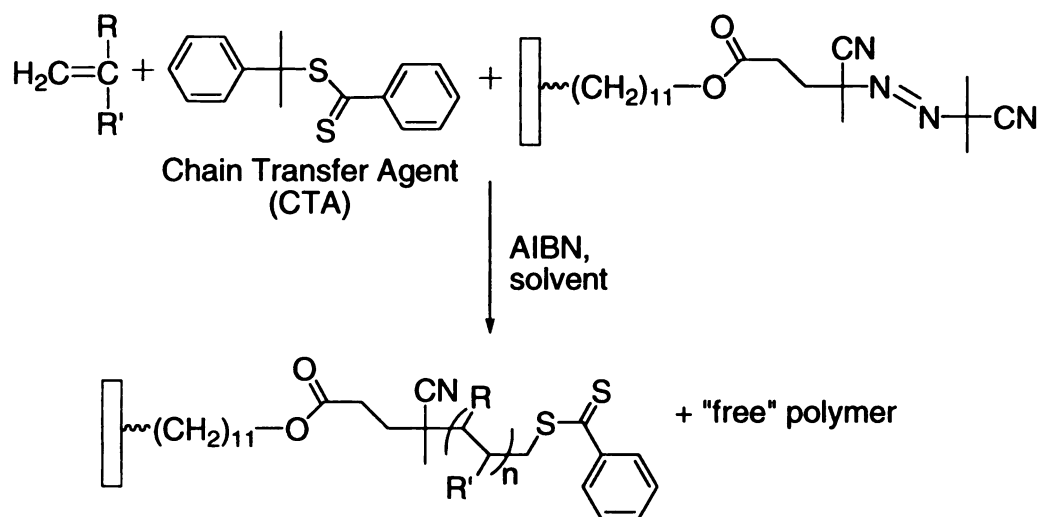
Scheme 1.9. General process of surface-initiated RAFT polymerizations using 2-phenylprop-2-yl dithiobenzoate as the chain transfer agent and a substrate-immobilized azo initiator. (Redrawn from *Macromolecules* **2002**, *35*, 610-615.)

polymerization. At temperatures up to 90 °C and times of up to 48 hours, PMMA brushes with a thickness of 28 nm and poly(N,N-dimethylacrylamide) and PS brushes up to 11 nm thick were grown. Although RAFT is relatively slow compared to ATRP and NMP,

the fact that this technique supported the easy re-initiation of the polymer chains suggests it is a highly controlled process.

1.2.7. Surface Initiated Atom Transfer Radical Polymerization

Since Matyjaszewski and Sawamoto first reported the use of ATRP in 1995,[81, 82] this technique has become one of the most widely employed techniques for the formation of polymer brushes. Among all the controlled radical polymerization techniques, it is particularly successful and has attracted commercial interest because it utilizes a simple experimental setup and employs readily accessible and inexpensive catalysts (usually copper complexes formed with aliphatic amines, imines, or pyridines, many of which are commercially available), as well as simple initiators (often alkyl halides).[83] ATRP is probably the most robust and efficient controlled radical polymerization technique for preparing well-defined polymers with controlled topology, composition and functionality. This technique is compatible with a variety of functionalized monomers and the living/controlled character of the ATRP process yields polymers with a low polydispersity (Mw/Mn).[84]

The controlled nature of ATRP is due to the reversible activation–deactivation reaction between the growing polymer chains and a copper–ligand species. Scheme 1.10 shows the mechanism of ATRP.

$$RX + Cu\ (I)\ X\ /\ bpy \underset{k_{deact}}{\overset{k_{act}}{\rightleftharpoons}} \quad R\bullet \quad + \quad Cu\ (II)\ X_2\ /\ bpy$$

+M k_p k_t Termination
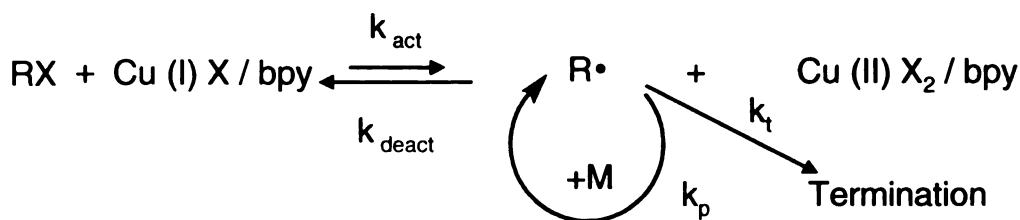
Scheme 1.10. Mechanism of ATRP. (Adapted from *J. Am. Chem. Soc.* **1998,** *120,* 243-247.)

Typically, ATRP utilizes a transition metal complex as a catalyst (e.g., Cu(I)X/bpy) and an initiator with a transferable halogen. The transition metal complex acts as a halogen atom transfer agent between active and dormant chain ends. Fast deactivation by the $Cu(II)X_2$/ligand complex, where X is the transferred halogen atom, leads to a low concentration of propagating radicals, thus ensuring that chain termination and radical transfer reactions are minimized so that polymer chains are able to grow at slow, but nearly constant rates to yield a narrow molecular weight distribution.

Monomers which have been successfully polymerized by ATRP include styrenes,[85] acrylates,[86] and acrylonitrile.[87] All of these compounds contain substituents capable of stabilizing propagating radicals (e.g., phenyl or carbonyl groups).[88] In contrast, ATRP is not compatible with monomers containing carboxylic acid groups (because the carboxylic acid side groups react with the metal complexes to form carboxylate salts which are inefficient catalysts for ATRP) and halogenated or alkylsubstituted alkenes (due to their low intrinsic reactivity toward radical polymerization).

A variety of transition metal catalysts have been successfully used in ATRP, including Cu,[89, 90] Fe,[91] Ru,[92] Ni,[93] Mo, [94]and Rh[95] complexes. Among these transition

metal catalyst systems, the Cu halide system is the most popular due to its compatibility

with various monomers. To increase the solubility of Cu salts in organic media and to

i) bidentate ligands
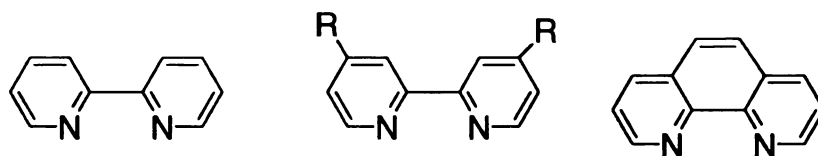
ii) tridentate ligands
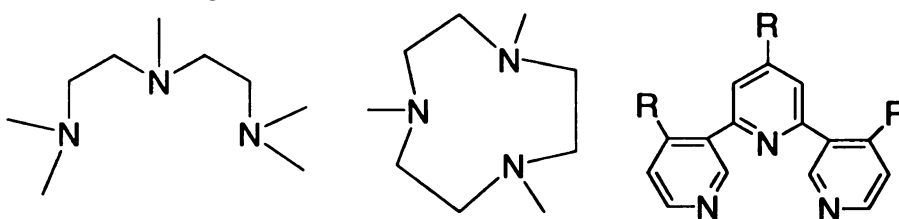
iii) tetradentate ligands
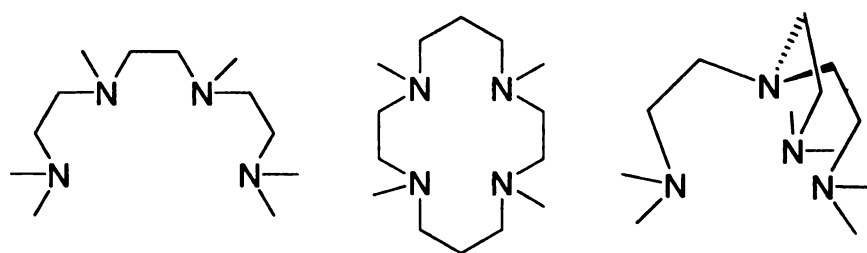
Scheme 1.11. Ligands used for copper-mediated ATRP. (Redrawn from

Curr. Org. Chem, **2002,** *6,* 67-82.)

adjust the redox potential of the metal center for appropriate reactivity, various

polydentate nitrogen based ligands, such as phenanthroline and its derivatives, and

pyridineimines, have been used for copper-mediated ATRP (Scheme 1.11).[96]

Ejaz et al. first succeeded in using ATRP to synthesize dense polymer brushes

(low-polydispersity PMMA) on silicon wafers.[97] They deposited the initiator by the

Cl
|
SO₂

Initiating group for ATRP

= H₃CO—Si—OCH₃   Spread   Hydrolysis
      H₃CO   on the water surface

CH₂
CH₂
H₃CO—Si—OCH₃
H₃CO

HO—Si—OH
HO

Monolayer formation

Compression

Condensation   Water

LB Trough

Deposition

Fixation   Si wafer   Graft Polymn

Water   of MMA
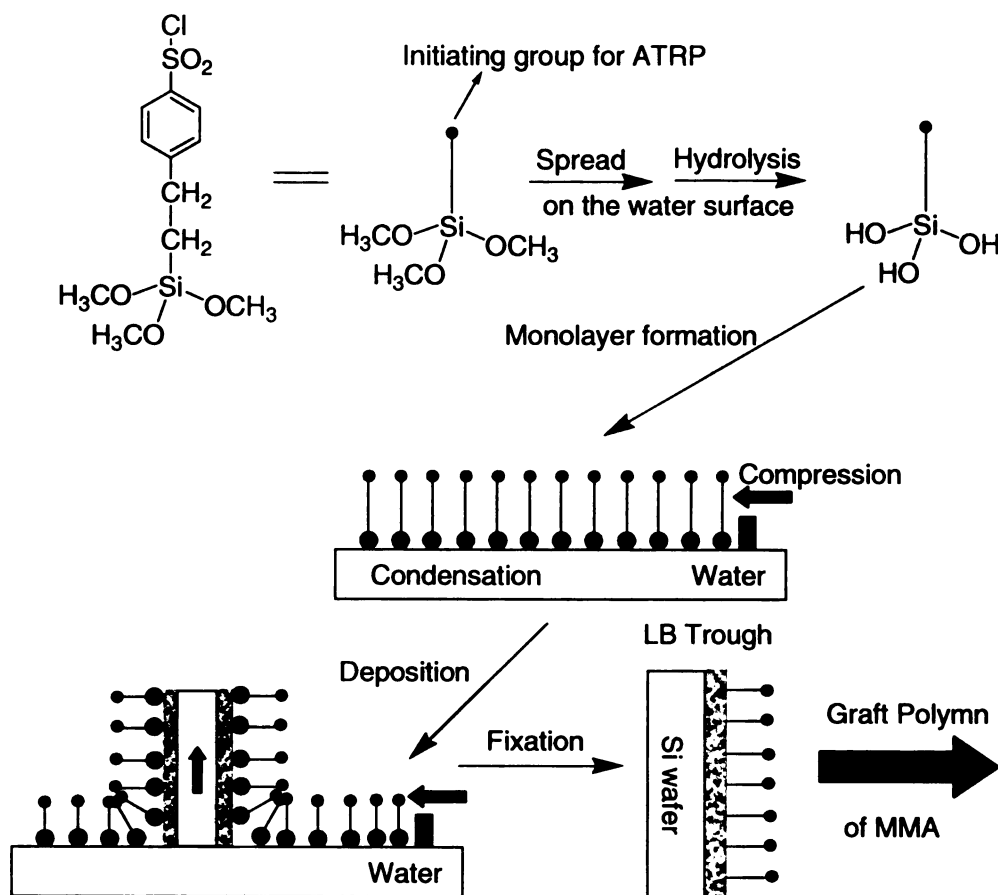
Scheme 1.12. Schematic illustration of the immobilization of ATRP

initiators using the LB technique. (Redrawn from *Macromolecules* **1998**, *31*,

5934-5936.)

Langmuir–Blodgett technique and subsequently exposed this substrate to monomer and

the ATRP catalyst (Scheme 1.12). PMMA film thicknesses of up to 80 nm were

achieved in less than 12 hours at 90 °C, as measured by ellipsometry.

Au-coated substrates provide a model surface that is readily characterized and

complimentary to Si, but due to the limited thermal stability of the S – Au bond in

initiator monolayers, ATRP can only be carried out at a relatively low temperature. Kim

and coworkers reported surface-confined ATRP of MMA on gold surfaces using room-

temperature ATRP.[98] The use of very active Cu-Me₆TREN complexes as catalysts allowed for successful room-temperature polymerization of dense PMMA brushes on gold. Based on solution studies by Armes and coworkers,[99] Huang and coworkers found that room-temperature, water-accelerated ATRP allows for growth of thick polymer films in short reaction times. They obtained 700 nm thick PHEMA films in just 12 hours using water as the solvent.[3] Huck and coworkers observed a similar effect in the aqueous-based polymerization of poly(glycidyl methacrylate).[100, 101] They were able to grow 125 nm-thick poly(glycidyl methacrylate) brushes in 100 min.

Surface initiated ATRP was applied not only on planar substrates but also on various types of fine particles. Patten extended the technique to silica nanoparticles.[102, 103] In his procedure, (2-(4-chloromethylphenyl)ethyl) dimethylethoxysilane initiator was deposited on the surface of the nanoparticles, and well-defined PS chains were grown from the modified nanoparticle surfaces. Besides silica nanoparticles, ATRP of polymers on gold,[104, 105] iron oxide[106] and magnetic particles has been demonstrated.[107]

Porous materials with polymer brushes grafted on them are also fascinating targets for chromatographic and other applications such as the membrane absorbers described herein. Wirth et al. reported the grafting of poly(acrylamide) (PAAm) on a porous silica gel and showed the protein separation ability of these materials.[108] A living PAAm thin film is grown from a self assembled benzyl chloride monolayer on silica gel using Cu(bpy)₂Cl to control the radical polymerization. To test for intact pore structure of the PAAm-modified silica gel, a size-exclusion separation was performed for sodium azide and four proteins: thyroglobulin (MW, 669,000), ovalbumin (MW, 44,000), ribonuclease A (MW, 13,700), and aprotinin (MW, 6,500). The five species eluted in

order of decreasing molecular weight, as expected for a size exclusion separation. This proved that the polymerization is sufficiently well controlled that films grown on nanoporous silica leave the pores intact. Later on, they applied ATRP of acrylamide to coat the channels of PDMS microchips and studied the electrophoretic behavior of proteins in these channels.[109] Bare PDMS is adsorptive toward proteins due to its hydrophobicity, and it would be valuable to be able to modify the surface of PDMS to make it permanently hydrophilic and resistant to protein adsorption. By growing PAAm in the PDMS channels, adsorption of bovine serum albumin was largely reduced.

1.3. Introduction to Pervaporation Membranes

Membrane separation techniques such as microfiltration, ultrafiltration, reverse osmosis, dialysis, electrodialysis, gas separation, and pervaporation have been applied to industrial, medical, and biological fields.[110, 111] Pervaporation is an especially promising membrane-based technique in which a liquid mixture contacts the surface of a membrane, and selective transport of one component through the membrane to a vapor phase (often a modest vacuum) affords separation (Figure 1.7).[112] It is attractive because it allows for the separation of azeotropic mixtures and often requires less energy than conventional distillation.[113] Many of the successes with pervaporation involve the removal of water from organic solvents, but the reverse separation has also been demonstrated. Hydrophilic membranes allow selective pervaporation of water for dehydration of organic solvents, while hydrophobic films often permit selective passage of volatile organic compounds (VOCs) from aqueous solutions for water remediation or VOC analysis by membrane- introduction mass spectrometry.
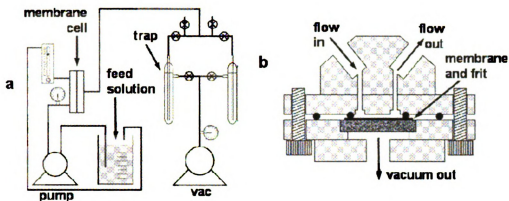
Figure 1.7. Schematic diagrams of (a) a pervaporation system and (b) a cross-sectional view of the membrane cell of the apparatus. (Figure taken from *J. Membr. Sci.* **2005,** *248,* 161-170.)

In the pervaporation process, the separation effectiveness of a membrane is quantified by two parameters, flux and selectivity.[112] The membrane selectivity comes from the different solubilities and diffusivities of the components in the membrane. A solution-diffusion model is generally used to describe the transport of molecules in
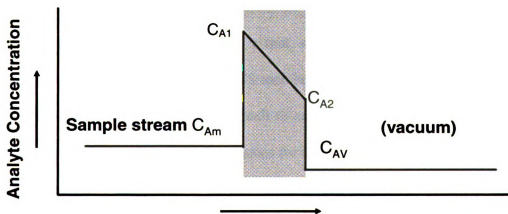
Figure 1.8. Schematic diagram of a solution-diffusion model.

membranes. In this model (Figure 1.8), the permeation process can be divided into three steps: (1) sorption into the membrane at the feed side (often assumed to be at equilibrium), (2) diffusion through the membrane, and (3) desorption at the permeate side. Solubility is a thermodynamic property, and diffusivity is a kinetic property, but they both affect the selectivity.[114]

Selective removal of organics from water is very important in chemical analysis and purification of waste streams.[115] The solution-diffusion mechanism suggests that pervaporation of organic compounds from water will require a material with high sorption selectivity for the organic molecule and a minimal diffusion selectivity for water.[116-118] Hydrophobic polymers with high free volumes, especially PDMS, provide these characteristics, and there are a number of reports of selective pervaporation of volatile organic compounds through such materials.[119-121]

In addition to selectivity, both analytical and preparative pervaporation applications require high fluxes that necessitate the use of membranes that are as thin as possible.[122, 123] However, due to the mechanical weakness of ultrathin polymer films, high-flux membranes generally consist of a thin, selective skin layer on a nonselective, highly porous support.[124] Although PDMS membranes provide high selectivity towards removal of organics from water, it's difficult to achieve defect-free skin layers that are less than 500 nm thick using simple techniques for forming PDMS membranes.[125]

To overcome this problem, polymer brushes can be used as selective layers on porous supports. As mentioned previously in this chapter, there are a lot of controlled polymerization techniques available to grow polymer brushes on a porous support. ATRP is especially useful for preparing well-defined polymers with controlled topology,

41

composition and functionality, and polymer brushes prepared by this technique will be well suited to cover the pores of porous membrane but not block their interior pores.

1.4. Importance of Membrane Absorbers

Potential therapeutic applications of proteins along with rapid developments in biotechnology and genetic engineering have greatly increased the rate of production of various proteins and enzymes.[126, 127] Sales of therapeutic proteins are projected to reach a remarkable value of $90 Billion in 2009.[128] Accompanying this increase in the scale of protein production is a need for fast and convenient purification techniques. Affinity chromatography is probably the most convenient way to purify proteins due to its ability to separate biomolecules based on their biological interactions,[127, 129] but the rate of separations with packed-bead affinity columns is limited by slow diffusion of biomacromolecules within bead pores.[129-131]

Compared to column chromatography, membrane chromatography has a lower pressure drop, higher flow rate, and higher productivity as a result of the microporous/macroporous structure of the thin membrane.[132] Flow through membrane pores greatly enhances mass transport to binding sites. Easy packing and scale-up of membranes is an additional asset of membrane chromatography. Consequently, this technique is a promising large-scale separation process for the isolation, purification, and recovery of proteins and enzymes. Many publications have reported the performance of adsorptive membranes (ion-exchange membranes, affinity membranes, and hydrophobic interaction membranes), as well as their theoretical description and optimal design.[127, 129, 133]

42

Despite their potential, the major disadvantage of membrane absorbers is their low binding capacity relative to beads. The specific surface area of membranes is simply not as great as that of beads. This can be overcome to some extent through the use of polymer chains grafted in membrane pores and binding of multilayers of proteins to these polymers. For example, Ulbricht and Yang achieved a lysozyme-binding capacity of 20 mg/cm^3 by grafting poly(acrylic acid) to polypropylene membranes modified with adsorbed photoinitiators.[4]

Our research aims at utilizing the controlled growth of polymer brushes in porous membranes to develop affinity membranes with remarkably high protein-binding capacities. The use of ATRP to grow PHEMA from initiators bound to a porous alumina surface affords relatively fine control over polymer molecular weight, which allows large increases in capacity without clogging of membrane pores. PHEMA brushes are particularly attractive because they can be functionalized to exploit a number of affinity interactions.[112, 134, 135] Specifically, functionalization of PHEMA with nitrilotriacetate-Cu^{2+} complexes results in protein binding via metal-ion affinity interactions, and the microporous alumina support provides a ~500-fold increase in surface area relative to two-dimensional supports.

1.5. Outline of the Dissertation

In Chapter 2 of this dissertation, I report preparation of composite pervaporation membranes via ATRP of 2-hydroxyethyl methacrylate from the surface of porous alumina membranes and subsequent derivatization of PHEMA using a series of acid chlorides. The pervaporation performance of a series of derivatized PHEMA membranes

is compared to provide correlations between membrane chemistry and transport properties. Sorption studies, which helped us elucidate the factors behind the selectivities of different films, will also be presented in this chapter. Last but not the least, I compare the performance of our membranes with related membrane systems that have been described in the literature.

Chapter 3 of this dissertation first describes the growth, characterization, and derivatization of polymer brushes to yield protein-binding materials. To quantify the binding capacity of these polymer brushes on gold substrates, we developed a simple technique which utilizes both FTIR and ellipsometry for calibration of IR absorbances. Subsequently, chapter 3 presents synthesis and derivatization of polymer brushes inside the pores of porous alumina membranes. Simple surface area calculations clarify why we need to grow polymer brushes inside of highly porous membranes. Finally, protein binding studies in membranes and a comparison with related research illustrate the extremely high protein-binding capacity of our polymer brushes.

In chapter 4, I show that derivatized polymer brushes are very attractive for purification of histindine$_x$-tagged proteins. Brushes formed on a gold substrate were capable of selectively binding the equivalent of many monolayers of his tagged ubiquitin. Porous alumina membranes modified with derivatized brushes also show remarkable capacities for the binding of his tagged ubiquitin. Gel electrophoresis studies show that these high-capacity membranes are highly selective for purification of his tagged proteins.

In the last chapter, I will present the conclusions drawn from my research and some proposed future work.

1.6. References

1. Milner, S. T., *Science* **1991,** *251*, 905-914.

2. Bhat, R. R.; Tomlinson, M. R.; Wu, T.; Genzer, J., *Adv. Polym. Sci.* **2006,** *198*, 51-124.

3. Huang, W.; Kim, J.-B.; Bruening, M. L.; Baker, G. L., *Macromolecules* **2002,** *35*, 1175-1179.

4. Ulbricht, M.; Yang, H., *Chem. Mater.* **2005,** *17*, 2622-2631.

5. Brown, H. R.; Char, K.; Deline, V. R., *Macromolecules* **1990,** *23*, 3383-3385.

6. Ash, S. G.; Clayfield, E. J., *J. Colloid Interface Sci.* **1976,** *55*, 645-657.

7. Xu, F. J.; Kang, E. T.; Neoh, K. G., *J. Mater. Chem.* **2006,** *16*, 2948-2952.

8. Andruzzi, L.; Senaratne, W.; Hexemer, A.; Sheets, E. D.; Ilic, B.; Kramer, E. J.; Baird, B.; Ober, C. K., *Langmuir* **2005,** *21*, 2495-2504.

9. Liu, Y.; Klep, V.; Luzinov, I., *J. Am. Chem. Soc.* **2006,** *128*, 8106-8107.

10. Xia, Y.; Whitesides, G. M., *Angew. Chem. Int. Ed.* **1998,** *37*, 550-575.

11. Shah, R. R.; Merreceyes, D.; Husemann, M.; Rees, I.; Abbott, N. L.; Hawker, C. J.; Hedrick, J. L., *Macromolecules* **2000,** *33*, 597-605.

12. Schmelmer, U.; Jordan, R.; Geyer, W.; Eck, W.; Golzhauser, A.; Grunze, M.; Ulman, A., *Angew. Chem. Int. Ed.* **2003,** *42*, 559-563.

13. Husemann, M.; Mecerreyes, D.; Hawker, C. J.; Hedrick, J. L.; Shah, R.; Abbott, N. L., *Angew. Chem. Int. Ed.* **1999,** *38*, 647-649.

14. Jones, D. M.; Smith, J. R.; Huck, W. T. S.; Alexander, C., *Adv. Mater.* **2002,** *14*, 1130-1134.

15. Ahn, S. J.; Kaholek, M.; Lee, W.-K.; LaMattina, B.; LaBean, T. H.; Zauscher, S., *Adv. Mater.* **2004,** *16*, 2141-2145.

16. Padeste, C.; Solak, H. H.; Brack, H.-P.; Slaski, M.; Gursel, S. A.; Scherer, G. G., *J. Vac. Sci. Technol., B* **2004,** *22*, 3191-3195.

17. Kaholek, M.; Lee, W.-K.; LaMattina, B.; Caster, K. C.; Zauscher, S., *Nano Lett.* **2004,** *4*, 373-376.

18. Krauss, P. R.; Chou, S. Y., *J. Vac. Sci. Technol., B* **1995,** *13,* 2850-2852.

19. Beinhoff, M.; Appapillai, A. T.; Underwood, L. D.; Frommer, J. E.; Carter, K. R., *Langmuir* **2006,** *22,* 2411-2414.

20. Chou, S. Y.; Krauss, P. R.; Renstrom, P. J., *J. Vac. Sci. Technol., B* **1996,** *14,* 4129-4133.

21. von Werne, T. A.; Germack, D. S.; Hagberg, E. C.; Sheares, V. V.; Hawker, C. J.; Carter, K. R., *J. Am. Chem. Soc.* **2003,** *125,* 3831-3838.

22. Retsos, H.; Gorodyska, G.; Kiriy, A.; Stamm, M.; Creton, C., *Langmuir* **2005,** *21,* 7722-7725.

23. Pierschbacher, M. D.; Ruoslahti, E., *Nature* **1984,** *309,* 30-33.

24. Hersel, U.; Dahmen, C.; Kessler, H., *Biomaterials* **2003,** *24,* 4385-4415.

25. Houseman, B. T.; Mrksich, M., *Biomaterials* **2001,** *22,* 943-955.

26. Maheshwari, G.; Brown, G.; Lauffenburger, D. A.; Wells, A.; Griffith, L. G., *J. Cell Sci.* **2000,** *113,* 1677-1686.

27. Harris, B. P.; Kutty, J. K.; Fritz, E. W.; Webb, C. K.; Burg, K. J. L.; Metters, A. T., *Langmuir* **2006,** *22,* 4467-4471.

28. Israelachvili, J. N.; Tabor, D., *Nature* **1973,** *241,* 148-149.

29. Klein, J.; Kumacheva, E.; Mahalu, D.; Perahla, D.; Fetters, L. J., *Nature* **1994,** *370,* 634-636.

30. Raviv, U.; Giasson, S.; Kampf, N.; Gohy, J.-F.; Jerome, R.; Klein, J., *Nature* **2003,** *425,* 163-165.

31. Singh, C.; Pickett, G. T.; Zhulina, E.; Balazs, A. C., *J. Phys. Chem. B* **1997,** *101,* 10614-10624.

32. Roan, J.-R.; Kawakatsu, T., *J. Chem. Phys.* **2002,** *116,* 7295-7310.

33. Kim, A. J.; Manoharan, V. N.; Crocker, J. C., *J. Am. Chem. Soc.* **2005,** *127,* 1592-1593.

34. Zaman, A. A.; Bjelopavlic, M.; Moudgil, B. M., *J. Colloid Interface Sci.* **2000,** *226,* 290-298.

35. Walker, H. W.; Grant, S. B., *Langmuir* **1996,** *12,* 3151-3156.

36.   Yan, Y. D.; Glover, S. M.; Jameson, G. J.; Biggs, S., *Int. J. Miner. Process.* **2004,** *73*, 161-175.

37.   Leermakers, F. A. M.; Zhulina, E. B.; van Male, J.; Mercurieva, A. A.; Fleer, G. J.; Birshtein, T. M., *Langmuir* **2001,** *17*, 4459-4466.

38.   Gerber, P. R.; Moore, M. A., *Macromolecules* **1977,** *10*, 476-481.

39.   Satulovsky, J.; Carignano, M. A.; Szleifer, I., *Proc. Natl. Acad. Sci. U. S. A.* **2000,** *97*, 9037-9041.

40.   Szleifer, I., *Curr. Opin. Solid State Mater. Sci.* **1997,** *2*, 337-344.

41.   Halperin, A., *Langmuir* **1999,** *15*, 2525-2533.

42.   Ma, H.; Hyun, J.; Stiller, P.; Chilkoti, A., *Adv. Mater.* **2004,** *16*, 338-341.

43.   Chen, Y.; Liu, D.; Deng, Q.; He, X.; Wang, X., *J. Polym. Sci., Part A: Polym. Chem.* **2006,** *44*, 3434-3443.

44.   Drobek, T.; Spencer, N. D.; Heuberger, M., *Macromolecules* **2005,** *38*, 5254-5259.

45.   Brown, A. A.; Khan, N. S.; Steinbock, L.; Huck, W. T. S., *Eur. Polym. J.* **2005,** *41*, 1757-1765.

46.   Chilkoti, A.; Ma, H. USA 2005-US4947, 20050217, 2005.

47.   Ito, Y.; Park, Y. S., *Polym. Adv. Technol.* **2000,** *11*, 136-144.

48.   Houbenov, N.; Minko, S.; Stamm, M., *Macromolecules* **2003,** *36*, 5897-5901.

49.   Takei, Y. G.; Aoki, T.; Sanui, K.; Ogata, N.; Sakurai, Y.; Okano, T., *Macromolecules* **1994,** *27*, 6163-6166.

50.   Kost, J.; Langer, R., *Adv. Drug Delivery Rev.* **2001,** *46*, 125-148.

51.   Feil, H.; Bae, Y. H.; Feijen, J.; Kim, S. W., *J. Membr. Sci.* **1991,** *64*, 283-294.

52.   Park, Y. S.; Ito, Y.; Imanishi, Y., *Macromolecules* **1998,** *31*, 2606-2610.

53.   Luzinov, I.; Julthongpiput, D.; Malz, H.; Pionteck, J.; Tsukruk, V. V., *Macromolecules* **2000,** *33*, 1043-1048.

54.   Matyjaszewski, K.; Miller, P. J.; Shukla, N.; Immaraporn, B.; Gelman, A.; Luokala, B. B.; Siclovan, T. M.; Kickelbick, G.; Vallant, T.; Hoffmann, H.; Pakula, T., *Macromolecules* **1999,** *32*, 8716-8724.

55. Prucker, O.; Rühe, J., *Langmuir* **1998**, *14*, 6893-6898.

56. Huang, W.; Skanth, G.; Baker, G. L.; Bruening, M. L., *Langmuir* **2001**, *17*, 1731-1736.

57. Sugawara, T.; Matsuda, T., *Macromolecules* **1994**, *27*, 7809-7814.

58. Prucker, O.; Rühe, J., *Macromolecules* **1998**, *31*, 592-601.

59. Prucker, O.; Rühe, J., *Macromolecules* **1998**, *31*, 602-613.

60. Santer, S.; Kopyshev, A.; Donges, J.; Yang, H.-K.; Rühe, J., *Langmuir* **2006**, *22*, 4660-4667.

61. Santer, S.; Kopyshev, A.; Yang, H.-K.; Rühe, J., *Macromolecules* **2006**, *39*, 3056-3064.

62. Advincula, R.; Zhou, Q.; Park, M.; Wang, S.; Mays, J.; Sakellariou, G.; Pispas, S.; Hadjichristidis, N., *Langmuir* **2002**, *18*, 8672-8684.

63. Zhou, Q.; Nakamura, Y.; Inaoka, S.; Park, M.-K.; Wang, Y.; Mays, J.; Advincula, R., *Polym. Mater. Sci. Eng.* **2000**, *82*, 290-291.

64. Fan, X.; Zhou, Q.; Xia, C.; Cristofoli, W.; Mays, J.; Advincula, R., *Langmuir* **2002**, *18*, 4511-4518.

65. Jordan, R.; Ulman, A.; Kang, J. F.; Rafailovich, M. H.; Sokolov, J., *J. Am. Chem. Soc.* **1999**, *121*, 1016-1022.

66. Ingall, M. D. K.; Honeyman, C. H.; Mercure, J. V.; Bianconi, P. A.; Kunz, R. R., *J. Am. Chem. Soc.* **1999**, *121*, 3607-3613.

67. Quirk, R. P.; Mathers, R. T.; Cregger, T.; Foster, M. D., *Macromolecules* **2002**, *35*, 9964-9974.

68. Zhou, Q.; Fan, X.; Xia, C.; Mays, J.; Advincula, R., *Chem. Mater.* **2001**, *13*, 2465-2467.

69. Advincula, R., *Adv. Polym. Sci.* **2006**, *197*, 107-136.

70. Zhao, B.; Brittain, W. J., *Macromolecules* **2000**, *33*, 342-348.

71. Jordan, R.; Ulman, A., *J. Am. Chem. Soc.* **1998**, *120*, 243-247.

72. Jordan, R.; West, N.; Ulman, A.; Chou, Y.-M.; Nuyken, O., *Macromolecules* **2001**, *34*, 1606-1611.

73.   Edmondson, S.; Osborne, V. L.; Huck, W. T. S., *Chem. Soc. Rev.* **2004**, *33*, 14-22.

74.   Jeon, N. L.; Choi, I. S.; Whitesides, G. M.; Kim, N. Y.; Laibinis, P. E.; Harada, Y.; Finnie, K. R.; Girolami, G. S.; Nuzzo, R. G., *Appl. Phys. Lett.* **1999**, *75*, 4201-4203.

75.   Schwab, P.; Grubbs, R. H.; Ziller, J. W., *J. Am. Chem. Soc.* **1996**, *118*, 100-110.

76.   Kim, N. Y.; Jeon, N. L.; Choi, I. S.; Takami, S.; Harada, Y.; Finnie, K. R.; Girolami, G. S.; Nuzzo, R. G.; Whitesides, G. M.; Laibinis, P. E., *Macromolecules* **2000**, *33*, 2793-2795.

77.   Lee, W.-K.; Caster, K. C.; Kim, J.; Zauscher, S., *Small* **2006**, *2*, 848-853.

78.   Tsujii, Y.; Ohno, K.; Yamamoto, S.; Goto, A.; Fukuda, T., *Adv. Polym. Sci.* **2006**, *197*, 1-45.

79.   Husseman, M.; Malmstroem, E. E.; McNamara, M.; Mate, M.; Mecerreyes, D.; Benoit, D. G.; Hedrick, J. L.; Mansky, P.; Huang, E.; Russell, T. P.; Hawker, C. J., *Macromolecules* **1999**, *32*, 1424-1431.

80.   Baum, M.; Brittain, W. J., *Macromolecules* **2002**, *35*, 610-615.

81.   Wang, J.-S.; Matyjaszewski, K., *J. Am. Chem. Soc.* **1995**, *117*, 5614-5615.

82.   Kato, M.; Kamigaito, M.; Sawamoto, M.; Higashimura, T., *Macromolecules* **1995**, *28*, 1721-1723.

83.   Matyjaszewski, K.; Spanswick, J., *Mater. Today* **2005**, *8*, 26-33.

84.   Matyjaszewski, K.; Xia, J., *Chem. Rev.* **2001**, *101*, 2921-2990.

85.   Teare, D. O. H.; Barwick, D. C.; Schofield, W. C. E.; Garrod, R. P.; Ward, L. J.; Badyal, J. P. S., *Langmuir* **2005**, *21*, 11425-11430.

86.   Brar, A. S.; Saini, T., *J. Polym. Sci., Part A: Polym. Chem.* **2006**, *44*, 1975-1984.

87.   Hou, C.; Ying, L.; Wang, C., *J. Appl. Polym. Sci.* **2006**, *99*, 1050-1054.

88.   Matyjaszewski, K., *Curr. Org. Chem.* **2002**, *6*, 67-82.

89.   Wang, J.-S.; Matyjaszewski, K., *Macromolecules* **1995**, *28*, 7901-7910.

90.   Wang, J.-S.; Matyjaszewski, K., *Macromolecules* **1995**, *28*, 7572-7573.

91. Gibson, V. C.; O'Reilly, R. K.; Wass, D. F.; White, A. J. P.; Williams, D. J., *Macromolecules* **2003**, *36*, 2591-2593.

92. Saenz-Galindo, A.; Textle, H. M.; Jasso, A. R.; Torres-Lubian, J. R., *J. Polym. Sci., Part A: Polym. Chem.* **2005**, *44*, 676-680.

93. Duquesne, E.; Habimana, J.; Degee, P.; Dubois, P., *Macromolecules* **2005**, *38*, 9999-10006.

94. Maria, S.; Stoffelbach, F.; Mata, J.; Daran, J.-C.; Richard, P.; Poli, R., *J. Am. Chem. Soc.* **2005**, *127*, 5946-5956.

95. Mecerreyes, D.; Moineau, G.; Dubois, P.; Jerome, R.; Hedrick, J. L.; Hawker, C. J.; Malmstrom, E. E.; Trollsas, M., *Angew. Chem. Int. Ed.* **1998**, *37*, 1274-1276.

96. Tang, W.; Matyjaszewski, K., *Macromolecules* **2006**, *39*, 4953-4959.

97. Ejaz, M.; Yamamoto, S.; Ohno, K.; Tsujii, Y.; Fukuda, T., *Macromolecules* **1998**, *31*, 5934-5936.

98. Kim, J.-B.; Bruening, M. L.; Baker, G. L., *J. Am. Chem. Soc.* **2000**, *122*, 7616-7617.

99. Wang, X. S.; Jackson, R. A.; Armes, S. P., *Macromolecules* **2000**, *33*, 255-257.

100. Jones, D. M.; Brown, A. A.; Huck, W. T. S., *Langmuir* **2002**, *18*, 1265-1269.

101. Jones, D. M.; Huck, W. T. S., *Adv. Mater.* **2001**, *13*, 1256-1259.

102. von Werne, T.; Patten, T. E., *J. Am. Chem. Soc.* **1999**, *121*, 7409-7410.

103. von Werne, T.; Patten, T. E., *J. Am. Chem. Soc.* **2001**, *123*, 7497-7505.

104. Nuss, S.; Bottcher, H.; Wurm, H.; Hallensleben, M. L., *Angew. Chem. Int. Ed.* **2001**, *40*, 4016-4018.

105. Ohno, K.; Koh, K.-m.; Tsujii, Y.; Fukuda, T., *Macromolecules* **2002**, *35*, 8989-8993.

106. Li, G.; Fan, J.; Jiang, R.; Gao, Y., *Chem. Mater.* **2004**, *16*, 1835-1837.

107. Marutani, E.; Yamamoto, S.; Ninjbadgar, T.; Tsujii, Y.; Fukuda, T.; Takano, M., *Polymer* **2004**, *45*, 2231-2235.

108. Huang, X.; Wirth, M. J., *Anal. Chem.* **1997**, *69*, 4577-4580.

109. Xiao, D.; Van Le, T.; Wirth, M. J., *Anal. Chem.* **2004**, *76*, 2055-2061.

110. Ohshima, T.; Miyata, T.; Uragami, T.; Berghmens, H., *J. Mol. Struct.* **2005**, *739*, 47-55.

111. Vane, L. M., *J. Chem. Technol. Biotechnol.* **2006**, *81*, 1328.

112. Sun, L.; Baker, G. L.; Bruening, M. L., *Macromolecules* **2005**, *38*, 2307-2314.

113. Sullivan, D. M.; Bruening, M. L., *J. Membr. Sci.* **2005**, *248*, 161-170.

114. Doong, S. J.; Ho, W. S.; Mastondrea, R. P., *J. Membr. Sci.* **1995**, *107*, 129-146.

115. Kujawski, W., *Sep. Sci. Technol.* **2000**, *35*, 89-108.

116. Mishima, S.; Kaneoka, H.; Nakagawa, T., *J. Appl. Polym. Sci.* **1999**, *71*, 273-287.

117. Chandak, M. V.; Lin, Y. S.; Ji, W.; Higgins, R. J., *J. Appl. Polym. Sci.* **1998**, *67*, 165-175.

118. Samdani, A. R.; Mandal, S.; Pangarkar, V. G., *Sep. Sci. Technol.* **2003**, *38*, 1069-1092.

119. Kujawski, W.; Ostrowska-Gumkowska, B., *Sep. Sci. Technol.* **2003**, *38*, 3669-3687.

120. Uragami, T.; Ohshima, T.; Miyata, T., *Macromolecules* **2003**, *36*, 9430-9436.

121. Trong Nguyen, Q.; Bendjama, Z.; Clement, R.; Ping, Z., *Phys. Chem. Chem. Phys.* **2000**, *2*, 395-400.

122. Olsson, J.; Tragardh, G.; Lipnizki, F., *Sep. Sci. Technol.* **2002**, *37*, 1199-1223.

123. Nijhuis, H. H.; Mulder, M. H. V.; Smolders, C. A., *J. Membr. Sci.* **1991**, *61*, 99-111.

124. Yoshida, W.; Cohen, Y., *J. Membr. Sci.* **2004**, *229*, 27-32.

125. Blume, I.; Wijmans, J. G.; Baker, R. W., *J. Membr. Sci.* **1990**, *49*, 253-286.

126. Arica, M. Y.; Testereci, H. N.; Denizli, A., *J. Chromatogr. A* **1998**, *799*, 83-91.

127. Kawai, T.; Saito, K.; Lee, W., *J. Chromatogr. B* **2003**, *790*, 131-142.

128. Therapeutic Proteins, h. w. m. c. p. d. a. p. x. r., accessed March 2006.

129. Zou, H.; Luo, Q.; Zhou, D., *J. Biochem. Bioph. Methods* **2001**, *49*, 199-240.

130. Che, S.; Liu, Z.; Ohsuna, T.; Sakamoto, K.; Terasaki, O.; Tatsumi, T., *Nature* **2004**, *429*, 281-284.

131. Clairbois, A. S.; Letourneur, D.; Muller, D.; Jozefonvicz, J., *J. Chromatogr. B* **1998**, *706*, 55-62.

132. Zeng, X.; Ruckenstein, E., *Biotechnol. Prog.* **1999**, *15*, 1003-1019.

133. Reichert, U.; Linden, T.; Belfort, G.; Kula, M.-R.; Thommes, J., *J. Membr. Sci.* **2002**, *199*, 161-166.

134. Miller, M. D.; Baker, G. L.; Bruening, M. L., *J. Chromatogr. A* **2004**, *1044*, 323-330.

135. Bayramoglu, G.; Yilmaz, M.; Arica, M. Y., *Colloids Surf., A* **2004**, *243*, 11-21.

Chapter 2

Polymer Brush Membranes for Pervaporation

2.1. Introduction

This chapter describes our efforts to utilize polymer brushes as the skin layer of pervaporation membranes, where polymer brushes are grown only from the surface of the substrate so that they cover underlying pores without filling them.

Our hypothesis in this area is that polymer brushes grown on top of porous supports may provide a platform for preparing ultrathin skin layers and enhancing flux. In support of this hypothesis, this chapter reports preparation of composite pervaporation membranes via ATRP[1-4] of HEMA[5-7] from the surface of a porous substrate (Scheme 2.1). Although this work employs porous alumina as a support, formation of brush membrane skins should be possible from a wide range of porous materials such as cellulose,[8] PDMS,[9] PS[10] and PEs adsorbed on various surfaces.[11] To make PHEMA membranes sufficiently hydrophobic for pervaporation of organic analytes from water, we derivatize them with hydrophobic acid chlorides, i.e., octanoyl chloride, palmitoyl chloride, and pentadecafluorooctanoyl chloride. Jennings previously showed that derivatization of PHEMA can yield hydrophobic films,[12, 13] and we reported that fluorinated PHEMA membranes show modest selectivities in gas separations.[11] However, derivatized PHEMA films are much more attractive for pervaporation than gas separations, as they allow unusually high pervaporation fluxes (>1 kg/m^{2}h). The ability to derivatize PHEMA with a variety of hydrophobic molecules permits comparison of different

53
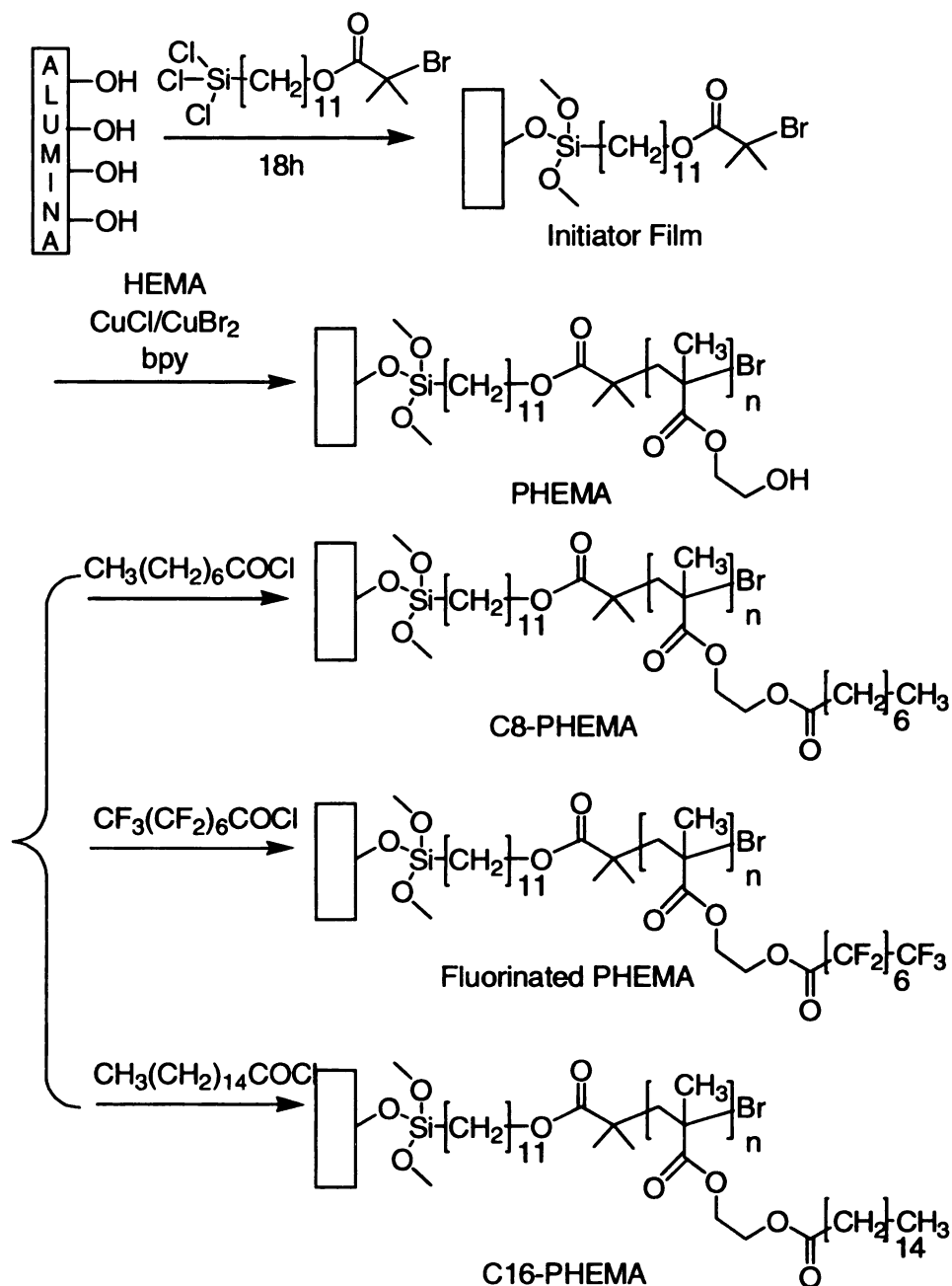
Scheme 2.1. Attachment of a trichlorosilane initiator to a porous alumina support, ATRP from the immobilized initiator, and derivatization of PHEMA with acid chlorides.

membrane materials without the need to develop new polymerization processes, and this chapter compares the pervaporation properties of three different elaborations of PHEMA. Sorption studies help elucidate the factors behind the selectivities of different films.

2.2. Experimental Section

2.2.1. Materials

Octanoyl chloride (99%), palmitoyl chloride (98%), pentadecafluorooctanoyl chloride (97%), dimethylformamide (DMF, anhydrous, 99.8%), tetrahydrofuran (THF, anhydrous, inhibitor free, 99.8%), 11-mercaptoundecanol (97%), 2-bromopropionyl bromide (97%), ethyl 2-bromoisobutyrate (98%), CuCl (99.999%), CuBr$_2$ (99%), and 2,2'-bipyridine (bpy, 99%) were used as received from Aldrich. 2-hydroxyethyl methacrylate (HEMA, Aldrich, 97%, inhibited with 300 ppm hydroquinone monomethyl ether) was purified by passing it through a column of activated basic alumina (Spectrum), and the trichlorosilane initiator (11-(2-bromo-2-methyl)propionyloxy)undecyltrichlorosilane) was synthesized according to a literature procedure.[3] Sorption and pervaporation tests employed deionized water (Milli-Q, 18.2 MΩcm) and one of the following solvents: ethyl alcohol (EtOH, 100%, Pharmco), ethyl acetate (EtOAc), dichloromethane (CH$_2$Cl$_2$), trichloroethylene (TCE), or benzene. Other than ethanol, solvents were analytical grade and purchased from Aldrich. Anodisc™ porous alumina membranes (Fisher) with 0.02 μm-diameter surface pores were used as supports for membrane formation, while gold-coated wafers (200 nm of sputtered Au on 20 nm Cr on a Si (100) wafer) were used as substrates for ellipsometry, contact angle measurements, and reflectance Fourier Transform Infrared (FTIR) spectroscopy.

2.2.2. Polymerization of HEMA and Subsequent Derivatization

The alumina substrates were first cleaned in a UV/ozone cleaner (Boekel model 135500) for 15 minutes, inserted into a glove box, and immersed in a 2 μM solution of trichlorosilane initiator in anhydrous THF for ~12 h. After removal from the glove box, samples were rinsed with acetone, sonicated in DMF for 5 minutes, rinsed with water and acetone, and finally dried with a flow of nitrogen. Deposition of initiators on Au-coated wafers occurred through formation of a mercaptoundecanol monolayer and subsequent derivatization of this layer with 2-bromopropionyl bromide as described in the literature.[7]

Polymerization of HEMA occurred by immersion of the initiator-coated substrate in an aqueous HEMA solution containing a Cu catalyst system (Scheme 2.1).[5] To prepare this polymerization solution, 15 mL of purified monomer was added to 15 mL of deionized water, and this solution was degassed via three freeze-pump-thaw cycles. Next, 82.5 mg (0.825 mmol) of CuCl, 54 mg (0.24 mmol) of $CuBr_2$, and 320 mg (2.04 mmol) of bpy were quickly added to the mixture, which was then subjected to another freeze-pump-thaw cycle and stirred until a homogeneous, dark brown solution formed. Initiator-coated substrates and the sealed flask containing the polymerization solution were then transferred to a glove bag that was purged with nitrogen for about 1 h. The polymerization solution was finally transferred to the container holding the substrates, and polymerization was carried out for 2 h. After polymerization, substrates were removed from the container, sonicated in DMF for 10 minutes, rinsed with water followed by acetone, and dried with a flow of nitrogen. Subsequent derivatizations of PHEMA were carried out by immersing the PHEMA-coated substrates in DMF solutions containing 0.2 M octanoyl chloride, pentadecafluorooctanoyl chloride, or palmitoyl

chloride and 0.1 M pyridine. After a 2 h immersion in the solution of acid chloride, substrates were rinsed with DMF followed by ethanol, and dried with a flow of nitrogen.

2.2.3. Characterization of Membranes

Film growth on alumina supports was verified by field-emission scanning electron microscopy (FESEM, Hitachi S-4700II, acceleration voltage of 10 kV). Membranes were freeze-fractured under liquid N_2 and sputter-coated (Pelco model SC-7) on both sides with 5 nm of gold prior to FESEM. Ellipsometric thickness determinations were performed using a rotating analyzer ellipsometer (model M-44, J.A. Woollam). We assumed a film refractive index of 1.5, except in the case of the fluorinated film, where both refractive index and thickness were fit to ellipsometric data. These ellipsometric studies were carried out with films grown from gold-coated wafers. For each polymer film, thicknesses were measured at three different spots and averaged. Reflectance FTIR spectroscopy of films on gold-coated wafers was performed with a Nicolet Magna-IR 560 instrument using a Pike grazing angle (80°) accessory. Static water contact-angle measurements (Firsttenangstroms contact angle analyzer) on alumina membranes were also performed before and after derivatization.

2.2.4. Pervaporation Experiments

Our home-built pervaporation apparatus was described previously.[14] Briefly, the solution was pumped across the surface of a membrane (effective area of 3.1 cm^2) that was supported by a stainless steel frit. The membrane cell was connected to a coiled stainless steel feed tube, and both the membrane cell and coiled tube were immersed into a thermostated water bath to control the temperature of the feed solution. On the permeate side of the membrane, a vacuum pressure of 0.06 mbar was applied, and the

permeate was collected in one of two liquid nitrogen-cooled traps. Feed solution was usually pumped across the membrane at a flow rate of 5 mL/min, but in a few experiments, we did vary flow rate to determine if there were large boundary layer effects on transport. In pervaporation of 0.05 wt% EtOAc, CH_2Cl_2, or TCE through C8-PHEMA at 65 °C, variation of feed flow rates from 1.4 mL/min to 11 mL/min yielded minimal changes in flux (<3% variation) and selectivity (<10% variation). Pervaporation of 0.05 wt% CH_2Cl_2 through fluorinated PHEMA membranes at 22 °C also showed little dependence on flow rate, suggesting that boundary layer effects are negligible. Tubing on the permeate side was warmed with heating tape to avoid condensation. Finally, prior to sample collection, pervaporation was performed for at least 1 h to achieve stable, steady-state fluxes, and then the samples were collected in a second trap. The masses of the collected samples were measured using an electronic balance, and the composition of the permeate was determined by gas chromatography (Shimadzu GC-17A equipped with a Restek RTx-BAC1 column), using methanol as an internal standard. In cases where the permeate separated into organic and aqueous phases, the sample was diluted sufficiently with water to achieve a homogeneous mixture.

The separation effectiveness of pervaporation is quantified by two parameters, flux and selectivity. Flux (J) can be calculated using equation 1,

$$J = \frac{Q}{At} \qquad (1)$$

where Q is the mass of the permeate collected in time t, and A is the area of the membrane exposed to the feed solution. In the case of a binary feed of components A and B, selectivity or separation factor, α_B^A, can be expressed by equation 2,

$$\alpha_B^A = \frac{y_A/y_B}{x_A/x_B} \qquad (2)$$

where x and y represent mass fractions in the feed and permeate, respectively. Reported selectivities and fluxes are averages of results from three different membranes.

2.2.5. Sorption Measurements

Sorption experiments were performed with bulk polymers because of the inherent difficulties in measuring sorption in ultrathin films. Derivatized HEMA monomers were first synthesized by allowing acid chlorides to react with HEMA, and then these monomers were polymerized in solution. Specifically, HEMA (10 mL, 0.08 mol) was placed in a 250 mL round-bottom flask and dissolved in 100 mL of anhydrous dichloromethane. The flask was sealed with a septum, and pyridine (8 mL, 0.1 mol) was added to this solution followed by 0.09 mol of the desired acid chloride. The solution was purged with nitrogen for 1 h and stirred overnight at room temperature. The mixture was extracted with 1 M aqueous HCl, dried over Na_2SO_4, and the solvent was removed by rotary evaporation. The product was purified by column chromatography (20% EtOAc in hexanes, basic alumina as stationary phase) and dried under vacuum to obtain monomers as colorless oils. C8-HEMA (18 g, 90% yield), ^{1}H NMR (300 MHz, $CDCl_3$) δ 6.17-6.04 (1H, d), 5.65-5.49 (1H, d), 4.47-4.19 (4H, m), 2.45-2.19 (2H, m), 2.06-1.84 (3H, s), 1.76-1.49 (2H, m), 1.42-1.23 (8H, m), 1.01-0.75 (3H, m). C16-HEMA (25 g, 85% yield), ^{1}H NMR (300 MHz, $CDCl_3$) δ 6.19-6.03 (1H, d), 5.65-5.48 (1H, d), 4.44-4.22 (4H, m), 2.47-2.19 (2H, m), 2.03-1.85 (3H, s), 1.72-1.47 (2H, m), 1.44-1.10 (24H, m), 0.98-0.76 (3H, m). Fluorinated-HEMA (30 g, 70% yield), ^{1}H NMR (300 MHz,

CDCl$_3$) δ 6.23-6.02 (1H, d), 5.70-5.49 (1H, d), 4.39-4.16 (2H, m), 3.94-3.67 (2H, m), 2.07-1.83 (3H, s).

For polymerization, 0.05 mol of monomer was added to a 100 mL Schlenk flask and degassed by three freeze-pump-thaw cycles. The flask was then inserted into a glove box, and 40 mL of anhydrous dichloromethane was added to the monomer. Next CuBr$_2$, CuCl, and bpy (0.82 mmol, 0.24 mmol, and 2.0 mmol, respectively) were added to the solution followed by the initiator, 0.50 mmol of ethyl 2-bromoisobutyrate. After 10 h, the flask was taken out of the glove box, and the brown solution was extracted with aqueous 1 M HCl to remove the copper complex. Evaporation of the solvent yielded colorless, viscous polymers. Those polymers were then dissolved in acetone (3 g/10 mL), and 2 mL of this polymer solution was cast on a 2 × 1 cm gold-coated Si wafer. After letting the acetone evaporate for 4 h at room temperature, the cast films were dried overnight in an oven at 60 °C, and finally removed from the substrate.

To measure sorption selectivities and polymer swelling by solvents, the derivatized bulk PHEMA films were immersed for 24 h in room-temperature aqueous solutions containing 0.05 wt % of a volatile organic compound (VOC). After that, the films were taken out of the vessel, wiped quickly with filter paper, and weighed. Degree of sorption of the VOC solution into the membranes was determined using equation 3, where m_0 and m_1 denote the weights of the dried membrane and the swollen membrane, respectively.

$$\text{Degree of sorption} = (m_1 - m_0) / m_0 \times 100 \qquad (3)$$

To measure sorption selectivity, we employed a literature procedure. Briefly, solvent-swollen membranes were dried with filter paper and placed in a trap that was

quickly cooled with liquid nitrogen and subsequently evacuated.[15] The sample was then

heated with a blow drier, and the vapor was collected in a second, cooled flask that was

connected to the first by a valve. The mass of the bulk polymer was then measured again

to make sure that we had removed essentially all of the water and solvent. The

concentration of the VOC in the collected solution was determined by gas

chromatography, and the separation factor was calculated using equation 2 with y

representing the composition of the adsorbed liquid that was eventually collected.

2.3. Results and Discussion

2.3.1. FTIR and SEM Characterization of Derivatized PHEMA Membranes

PHEMA is relatively hydrophilic and, hence, would not be expected to allow

selective pervaporation of VOCs from water. However, each repeat unit of PHEMA has

a hydroxyl group that can be easily esterified with a variety of acid chlorides. We let

PHEMA films react with octanoyl chloride, palmitoyl chloride and

pentadecafluorooctanoyl chloride in the presence of a base to obtain polymers with

hydrophobic side chains (Scheme 2.1). The static water contact angle on native PHEMA

films is 50°, but contact angles increase to 75°, 95°, and 98° for porous alumina-supported

films derivatized with octanoyl chloride (C8-PHEMA), palmitoyl chloride (C16-

PHEMA), and pentadecafluorooctanoyl chloride (fluorinated PHEMA), respectively.

These values fall between the advancing and receding contact angles reported by

Jennings and coworkers.[13, 16] To verify derivatization of PHEMA using reflectance FTIR

spectroscopy, we grew films on gold-coated wafers as described previously.[5, 13] Figure

2.1 shows the reflectance FTIR spectra of PHEMA films before and after esterification.

Nearly complete disappearance of the OH stretch at 3500 cm^{-1} and a doubling of the carbonyl (CO) stretch at 1700 cm^{-1} suggest >90% conversion of the hydroxyl groups to esters for C8- and C16-PHEMA films.[5] In the case of fluorinated PHEMA, the OH stretch also disappears, but the peak due to the newly formed ester carbonyl appears at 1790 cm^{-1}, rather than at the position of the initial ester of PHEMA. (The electronegativity of the F atoms results in the shifted position of the carbonyl stretch.)
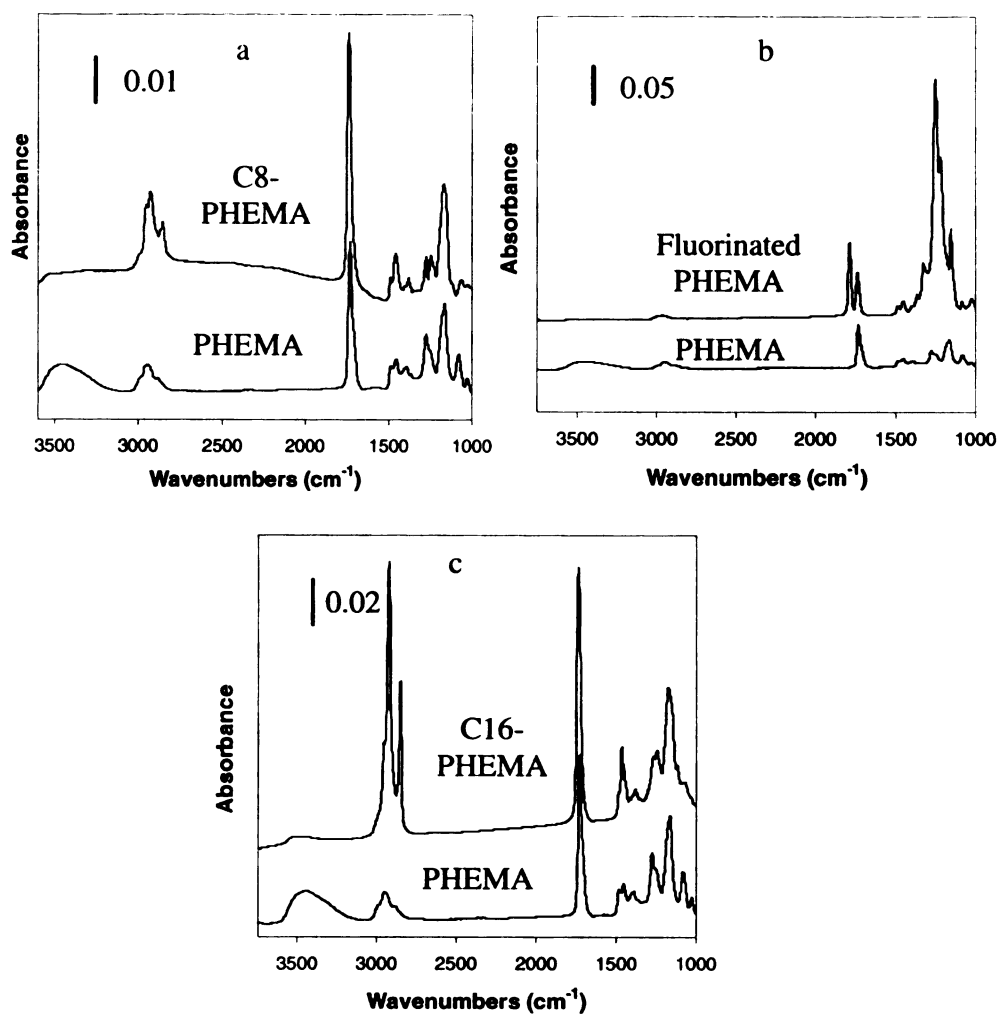
Figure 2.1. Reflectance FTIR spectra of PHEMA films on gold before and after derivatization with (a) octanoyl chloride, (b) pentadecafluorooctanoyl chloride, and (c) palmitoyl chloride.

Figure 2.2 shows cross-sectional FESEM images of PHEMA, C8-PHEMA, C16-PHEMA, and fluorinated PHEMA films grown from porous alumina supports. Before derivatization, the thickness of PHEMA films is about 50 nm, as shown in Figure 2.2(a), and the film fully covers substrate pores. Ellipsometric measurements of PHEMA films grown on gold-coated wafers under the same conditions also give a film thickness of 50 nm. After derivatization with octanoyl chloride, the molecular weight of the polymer

(a)	(b)
(c)	(d)
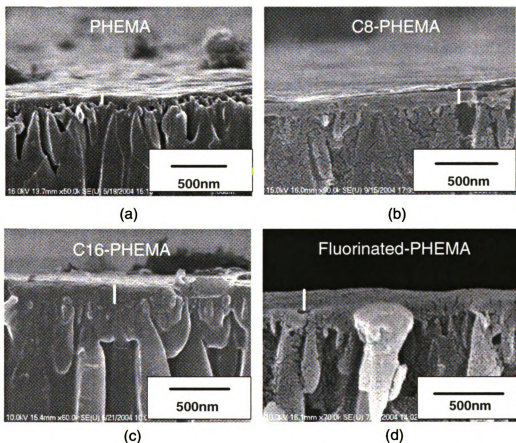
Figure 2.2. Cross-sectional FESEM images of alumina supports coated with (a) PHEMA, (b) C8-PHEMA, (c) C16-PHEMA, and (d) fluorinated PHEMA.

repeat unit should approximately double, so we would expect that the thickness of C8-PHEMA films would be about twice that for PHEMA, assuming a similar density for

64

both films.[5] Both ellipsometry results and SEM images such as that in Figure 2.2(b) indicate that film thickness does indeed double upon reaction with octanoyl chloride.

For C16-PHEMA, we would expect to see a 180% increase in film thickness based solely on the molecular weight of the new repeat unit. Ellipsometric measurements show a thickness increase of 125%. The SEM image in Figure 2.2(c) suggests a ~200% increase in thickness, but it is difficult to determine exactly where the film begins in this image. In the case of fluorinated films, the polymer density should be higher than that of hydrogenated aliphatic polymers,[17, 18] so it is not difficult to understand why we saw only a 170% increase in film thickness in ellipsometry in spite of a 300% increase in the molecular weight of the monomer unit. The FESEM image suggests a 240% increase in thickness. We should note that the high density of fluorinated PHEMA reflects the high atomic mass of fluorine relative to H and does not imply a low free volume for the fluorinated film. Most importantly, the PHEMA membranes and their derivatives are an order of magnitude or more thinner than typical PDMS membranes and other types of hydrophobic membranes currently used in pervaporation.[19-21] Moreover, the ATRP process (Scheme 2.1) allows effective control over the thickness of the membranes by changing the polymerization time.

2.3.2. Pervaporation of Ethyl acetate-water Mixtures Using Derivatized PHEMA

2.3.2-a. Effect of Feed Concentration

We initially employed EtOAc/water mixtures to probe the pervaporation properties of derivatized PHEMA membranes as a function of feed concentration and temperature. Figures 2.3, 2.4, and 2.5 show that trends in flux and selectivity related to feed composition vary dramatically among the different membranes. For C8-PHEMA
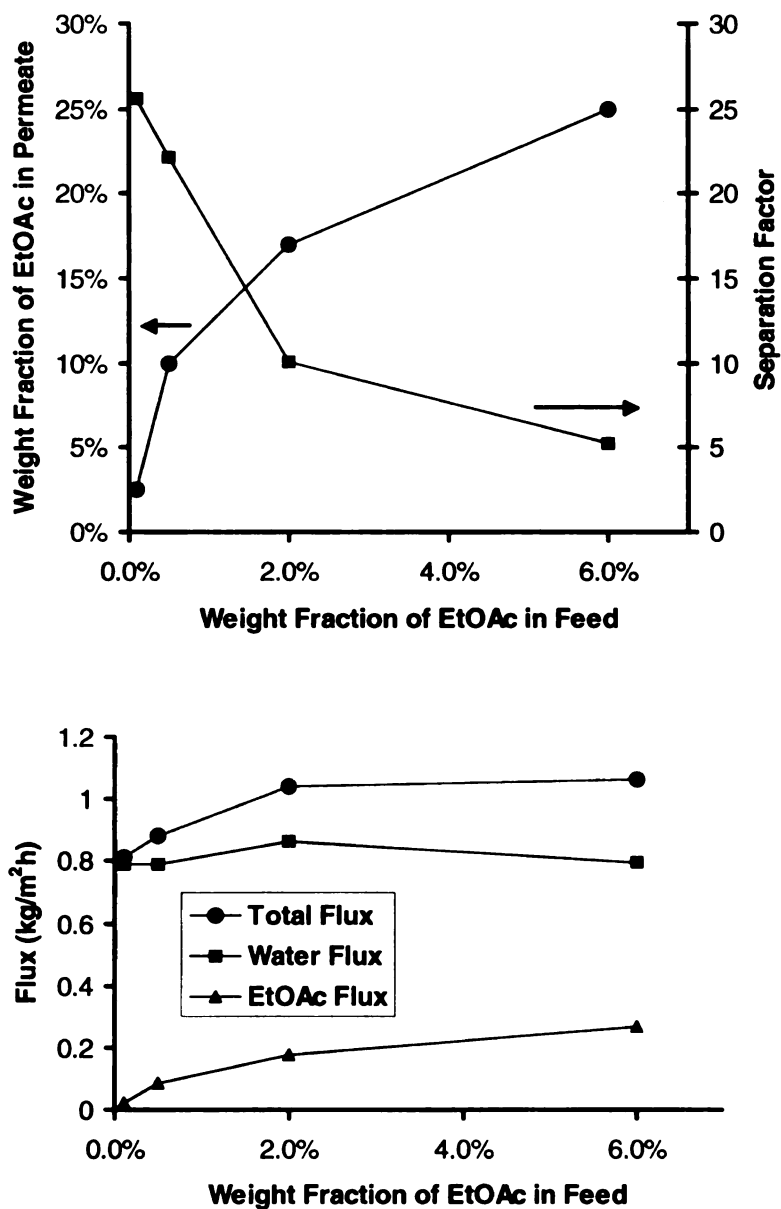
Figure 2.3. Permeate composition (top), separation factor (top), and flux (bottom) in pervaporation of several ethyl acetate/water mixtures through C8-PHEMA membranes at 50 °C. The standard deviations of flux values and ethyl acetate weight fractions in the permeate were less than 15%.
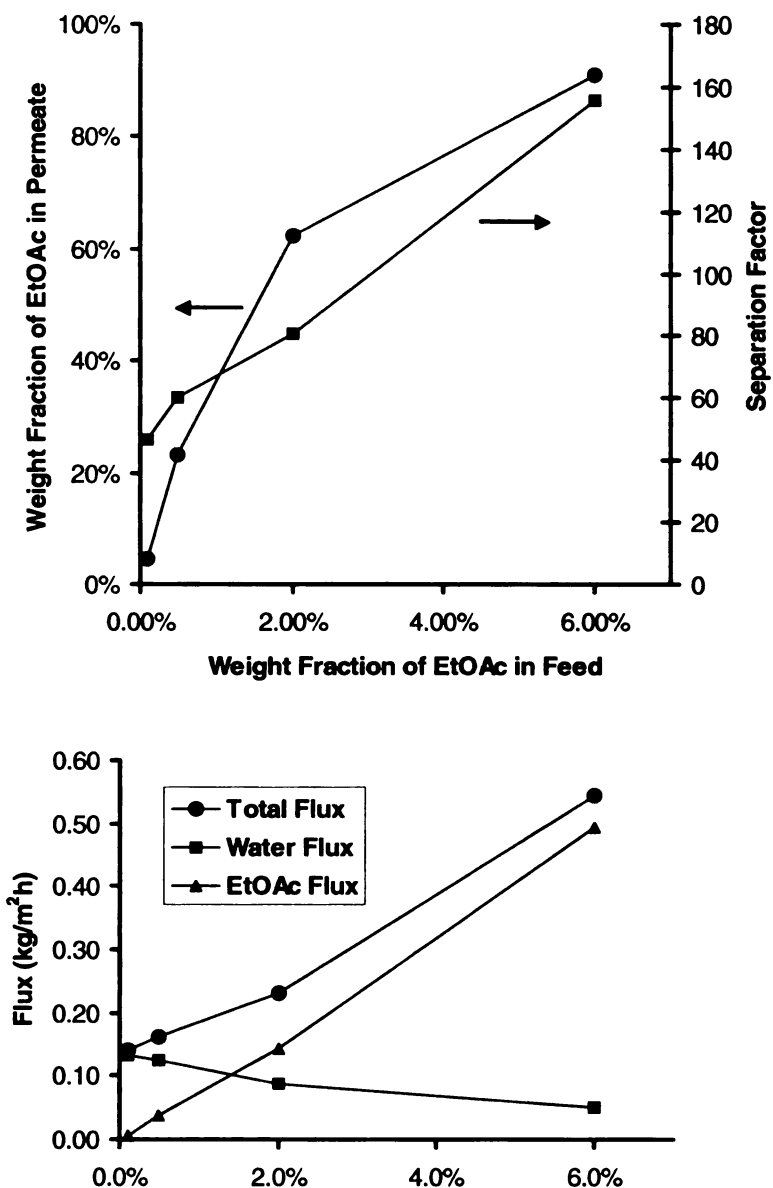
Figure 2.4. Permeate composition (top), separation factor (top), and flux (bottom) in pervaporation of several ethyl acetate/water mixtures through C16-PHEMA membranes at 50 °C. The standard deviations of flux values and ethyl acetate weight fractions in the permeate were less than 15%.
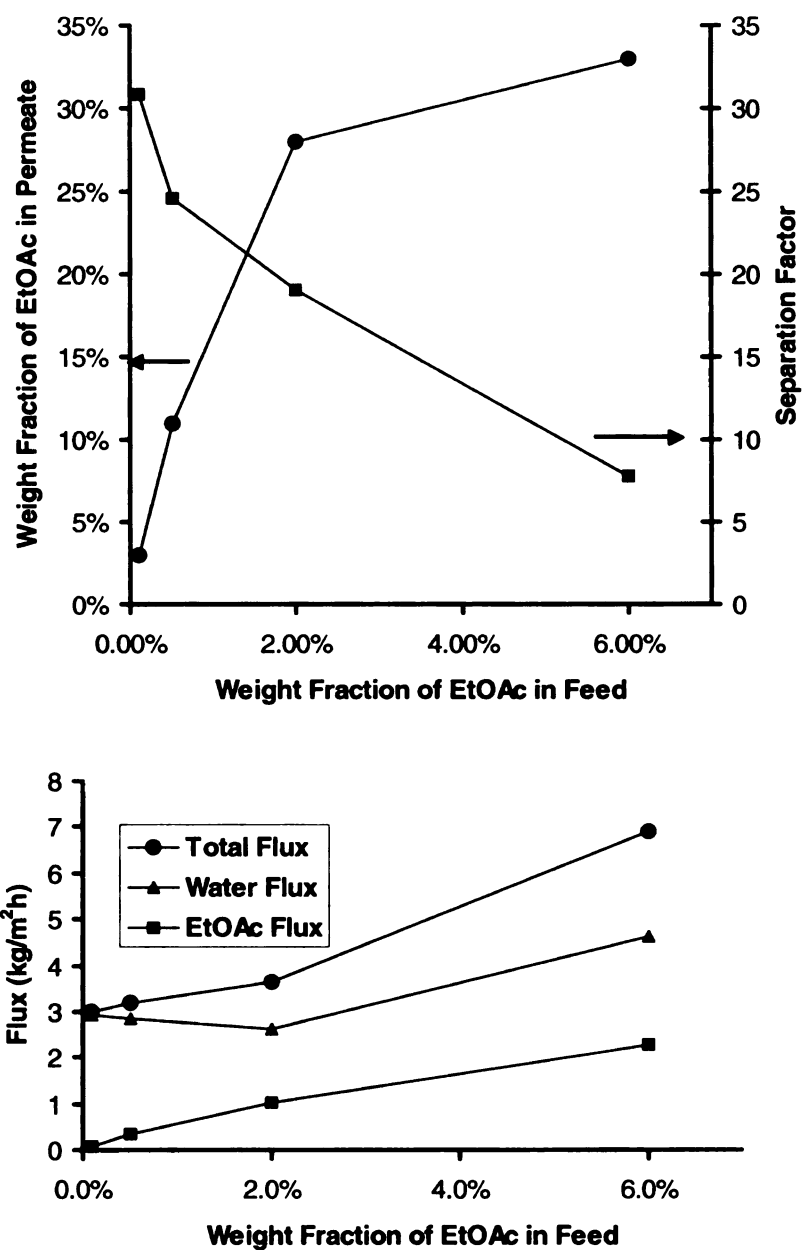
Figure 2.5. Permeate composition (top), separation factor (top), and flux (bottom) in pervaporation of several ethyl acetate/water mixtures through fluorinated-PHEMA membranes at 50°C. The standard deviations of flux values and ethyl acetate weight fractions in the permeate were less than 15%.

membranes (Figure 2.3), the total flux increases modestly from 0.8 to 1.1 kg/m^{2}h as the EtOAc concentration in the feed goes from 0.1% to 6%. In contrast, total flux increases 4-fold on going from 0.1 to 6% EtOAc with C16-PHEMA membranes (Figure 2.4), although even with 6% EtOAc, fluxes through C16-PHEMA are half of those through C8-PHEMA. Fluorinated PHEMA membranes allow the highest fluxes (3- to 6-fold higher than with C8-PHEMA), with a doubling in flux as EtOAc concentration goes from 0.1 to 6% (Figure 2.5).

The trends in flux values are likely a reflection of differences in side chain packing in the different membrane systems. Hexadecyl side chains should pack in a more crystalline arrangement than shorter octyl side chains, so one would expect lower fluxes through C16-PHEMA membranes. (C16-PHEMA films are also 50% thicker than C8-PHEMA membranes, but this should result in only a ~33% lower flux for these membranes.) The more hydrophobic C16-PHEMA should also be more susceptible to plasticization than C8-PHEMA, which is consistent with the large increase in flux through C16-PHEMA on going from 2% to 6% EtOAc. In the case of fluorinated PHEMA, the perfluorooctyl chain is bulkier than typical octyl chains, and this likely leads to higher free volume and, hence, higher permeability for the fluorinated PHEMA relative to C8-PHEMA.[22, 23] Although the fluorinated films have a slightly higher water contact angle than C16-PHEMA, the fluorinated systems appear to be less prone to plasticization, as suggested from a smaller relative increase in flux on going from 0.1 to 6% EtOAc. This may reflect the fact that typical hydrocarbons are less soluble in fluorinated than hydrogenated aliphatic chains.[24]

69

Separation factors also seem to depend on polymer packing. At low EtOAc concentrations (0.1%), separation factors are similar for all three membranes (25, 45, and 30, for C8-PHEMA, C16-PHEMA, and fluorinated PHEMA, respectively). However, separation factors for C8-PHEMA and fluorinated PHEMA decrease with increasing EtOAc concentration, while selectivities of C16-PHEMA membranes show a 4-fold increase on going from 0.1 to 6% EtOAc (Figures 2.3, 2.4, and 2.5). Perhaps due to the tight packing in C16-PHEMA films, absorbed EtOAc molecules block the transport of water. Such an effect was seen previously in the separation of TCE from water using a fluoroalkyl methacrylate-grafted PDMS membrane.[25]

2.3.2-b. Effect of Feed Temperature

Figure 2.6 shows the fluxes and selectivities for pervaporation of EtOAc solutions through C8-PHEMA membranes at several temperatures. In agreement with other studies,[26-28] flux increases with increasing feed temperature, while selectivity remains essentially constant. Generally, as temperature increases, the thermal motion of polymer chains and permeate molecules intensifies, leading to more rapid diffusion of analytes through the membrane and, hence, higher fluxes. In contrast, temperature changes do not greatly alter separation factors because solubility (sorption) selectivity among permeating molecules is not a strong function of temperature.[26]

High pervaporation temperatures could also affect membrane performance by inducing polymer degradation. To test the stability of C8-PHEMA membranes, we performed pervaporation of 0.05 wt% EtOAC at 65 °C before and after storage of the membrane in the hot pervaporation solution for one week. The week-long exposure to 65 °C 0.05 wt% EtOAc in water had no significant effect on pervaporation. Additionally,

we examined the stability of C16-PHEMA and fluorinated PHEMA films on gold wafers using FTIR spectroscopy. Storage of these films in 65 °C 0.05 wt% EtOAc in water for one week yielded no change in their IR spectra other than a uniform ~10% decrease in intensity, which is probably due to desorption of a small quantity of polymer from the gold surface. The desorption could result from a small amount of physisorbed polymer or the instability of the Au-thiol linkage at high temperatures.[29]
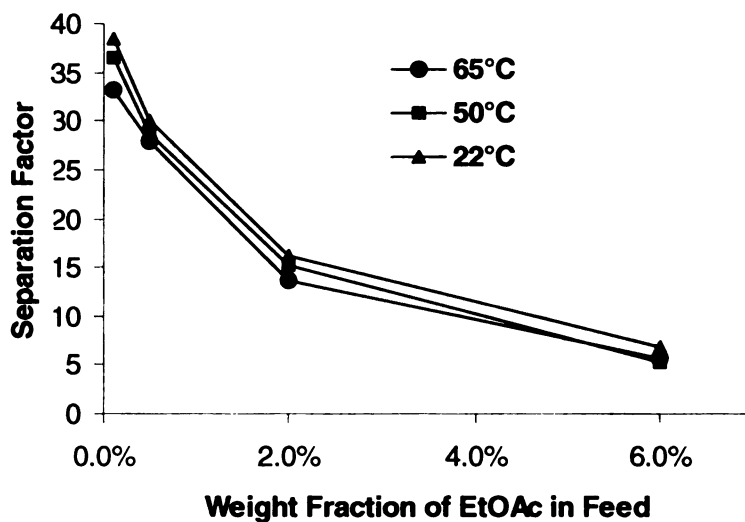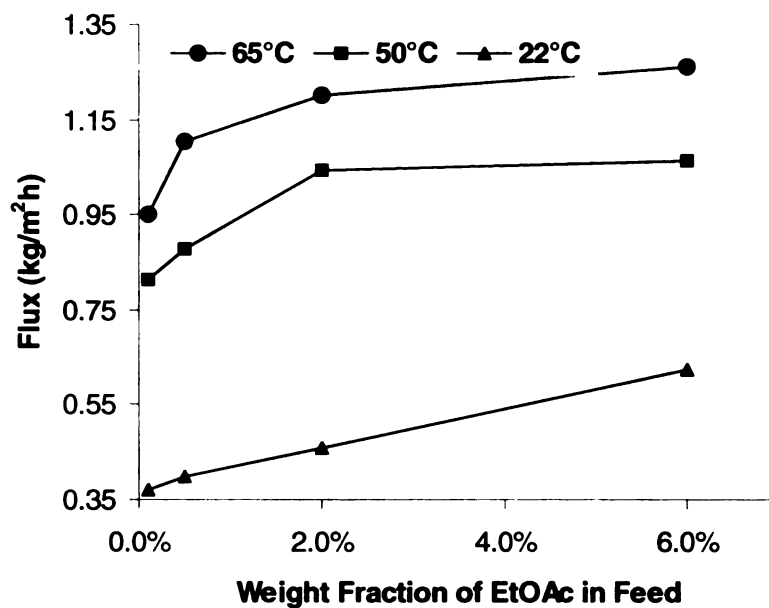
Figure 2.6. Flux (top) and separation factor (bottom) for pervaporation of water/ethyl acetate mixtures through C8-PHEMA membranes at several temperatures. The standard deviations of flux values and separation factors were less than 15%.

2.3.3. Pervaporation of Different Organic Compounds through Derivatized PHEMA Membranes

To further compare the properties of the derivatized PHEMA membranes, we examined pervaporation of a series of VOCs in water. We utilized a relatively low VOC concentration (0.05 %) in these experiments to avoid plasticization and ensure that the VOCs remained soluble. For all VOCs, flux decreased in the order fluorinated PHEMA (1.2-1.5 kg/m^{2}h) >C8-PHEMA (0.3-0.5 kg/m^{2}h) >C16-PHEMA (0.1 – 0.2 kg/m^{2}h). However, VOC/water separation factors did not vary greatly among the three types of membranes (Table 2.1). Selectivity did increase with the hydrophobicity of the VOC (decreasing water solubility) from EtOH to TCE, with the exception of CH$_2$Cl$_2$. The higher than expected CH$_2$Cl$_2$/water selectivity may occur in part because the small molar

Table 2.1. Molecular properties[22] of several VOCs and separation factors (VOC/Water) for pervaporation (22 °C) of 0.05% solutions through C8-PHEMA, C16-PHEMA, and fluorinated PHEMA membranes.

Compound	Molar Volume (mL/mol)	B.P. (°C)	Solubility in water (wt%)	Separation Factor		
				C8	C16	Fluorinated
Water	18.0	100	———	———	———	———
EtOH	58.5	78	Miscible	2.0±0.5	3.0±0.3	1.0 ±0.5
EtOAc	98.5	77	8.24	48±3	56±5	49±1
CH$_2$Cl$_2$	63.9	40	2.00	330±30	430±60	430±60
benzene	89.0	80	0.18	190±30	250±20	240±20
TCE	90.2	87	0.11	430±50	540±50	510±90

volume of CH_2Cl_2 relative to EtOAc, benzene, and TCE results in more rapid diffusion of CH_2Cl_2.[30] The low boiling point of CH_2Cl_2 may also increase its pervaporative transport.

2.3.4. Sorption Behavior and the Solution-diffusion Model

In the solution-diffusion model, transport through membranes includes both sorption and diffusion. To decouple the effects of diffusion and sorption on selectivity, we measured sorption directly for all three PHEMA derivatives. To attain sufficient sensitivity for these measurements, we employed bulk polymers rather than thin polymer brushes grown from a surface, but sorption properties of bulk polymers and thin films should be similar. Table 2.2 shows that both the degrees of sorption and VOC/water

Table 2.2. Degrees of sorption and sorption selectivities for five VOCs (0.05% aqueous solutions) in C8-PHEMA, C16-PHEMA, and fluorinated PHEMA films. Measurements were performed at 22 °C, and solubilities of the VOCs in water are given for reference.

Compound	Solubility in water (wt%)	Degree of Sorption			Selectivity		
		C8	C16	Fluorinated	C8	C16	Fluorinated
EtOH	Miscible	4.2±0.7	3.7±0.4	6.4±0.7	8.1±1.2	12.3±0.5	3.5±1.2
EtOAc	8.24	48±5	10±1	59±7	203±30	369±5	120±17
CH_2Cl_2	2.00	50±8	20±2	68±7	520±5	645±6	450±23
benzene	0.18	55±12	27±1	88±9	580±56	1600±20	310±30
TCE	0.11	68±9	32±2	99±15	1540±90	3700±50	570±80

sorption selectivities for the three derivatized PHEMA membranes generally increase with decreasing water solubility of the VOCs, as would be expected. The fluorinated

membrane provides the only exception to this trend with the sorption selectivity of benzene being 30% lower than that of CH_2Cl_2.

Among the three membranes, C16-PHEMA exhibits both the highest sorption selectivity and the lowest degree of sorption. This is consistent with the high hydrophobicity of this polymer and a low free volume. The fluorinated polymer has the highest degree of sorption of the three derivatives, suggesting again that this material has a high free volume. However, with the exception of CH_2Cl_2, sorption selectivities for C8-PHEMA are 70% to 170% greater than those for fluorinated PHEMA. Although the fluorinated membrane has a higher water contact angle than C8-PHEMA, the low solubility of organics in fluorous phases likely reduces VOC/water sorption selectivity.[25]

Table 2.3. Separation factors (22 °C) for pervaporation (α_{PV}), sorption (α_S), and diffusion (α_D) of VOCs (0.05% aqueous solutions) in C8-PHEMA, C16-PHEMA, and fluorinated PHEMA membranes.

Compound	Molar Volume (mL/mol)	C8-PHEMA			C16-PHEMA			Fluorinated PHEMA		
		α_{PV}	α_S	α_D	α_{PV}	α_S	α_D	α_{PV}	α_S	α_D
EtOH	58.5	2.0	8.1	0.25	3.0	12.3	0.24	1.0	3.5	0.26
EtOAc	98.5	48	203	0.24	56	369	0.15	49	120	0.41
CH_2Cl_2	63.9	330	520	0.63	430	645	0.67	430	460	0.93
benzene	89.0	190	580	0.33	250	1600	0.16	240	310	0.77
TCE	90.2	430	1540	0.28	540	3700	0.14	510	570	0.89

The pervaporation separation factor, α_{PV}, in the solution-diffusion model is simply the product of the sorption selectivity, α_S, and the diffusion selectivity, α_D. Table 2.3 contains values of α_{PV} and α_S along with calculated values of α_D for all three membranes. Because of the small molar volume of water (18 mL/mol), α_D is less than 1 for all of the membranes. The higher diffusion selectivity for the fluorinated membranes (lower water/VOC selectivity) is probably another reflection of a high free volume. Among the VOCs, CH_2Cl_2 shows the largest α_D, which would be expected for this relatively small molecule. However, ethanol has an even lower molar volume than CH_2Cl_2, but its α_D is around 0.25 for all of the membranes. Perhaps ethanol is diffusing through the membrane in a hydrated state.[31] Trends in α_D for EtOAc, benzene, CH_2Cl_2, and TCE correlate reasonably well with molar volume, with the exception of TCE in the fluorinated membrane.

2.3.5. Comparison with Related Membrane Systems

Table 2.4 compares the pervaporation performance of fluorinated PHEMA membranes with several PDMS membranes. Blume and coworkers coated microporous polymer supports with PDMS to achieve 3.5-μm thick PDMS skins (row 1, Table 2.4).[32] Those membranes show TCE/water pervaporation selectivities that are similar to those of fluorinated PHEMA, but the fluorinated PHEMA allows a 7-fold higher flux because it is 20-times thinner. When normalized to film thickness, the PDMS membranes are more permeable than fluorinated PHEMA, but Blume and coworkers reported that their coating method could not produce defect-free films with thicknesses less than 0.5 μm.

In the case of commercial PERVAP 1060 and 1070 membranes, EtOAc/water selectivity is 10- to 20-fold higher for the commercial membranes than for fluorinated

PHEMA. However, EtOAc flux is 2.5 to 10-fold higher for fluorinated PHEMA, again because of the minimal thickness of the polymer brushes (Table 2.4). (Both PERVAP

Table 2.4. Comparison of the pervaporation performance of fluorinated PHEMA and several PDMS membranes.

Membrane	VOC	Feed Concentration (wt%)	T (°C)	Membrane Thickness (μm)	Total Flux (kg/m²h)	Separation Factor
PDMS [32]	TCE	0.05	30	3.5	0.2	440
Fluorinated PHEMA	TCE	0.05	22	0.17	1.5	510
PDMS [20] (PERVAP 1060)	EtOAc	1	30	8	0.4 [a]	300
PDMS [20] (PERVAP 1070)	EtOAc	1	30	10	0.1 [a]	450
Fluorinated PHEMA	EtOAc	1	22	0.17	1 [a]	25
PDMSDMMA [33]	benzene	0.05	40	270	0.0514	1853
Fluorinated PHEMA	benzene	0.05	22	0.17	1.5	240

[a] EtOAc flux only.

1060 and PERVAP 1070 are composite membranes with a PDMS skin, but PERVAP 1070 is filled with zeolites.) In a recent paper, Uragami and coworkers polymerized PDMS dimethyl methacrylate macromonomers to prepare extremely selective membranes for pervaporation of benzene from water.[33] These membranes have 8-fold higher benzene/water selectivities than fluorinated PHEMA, but again the polymer brush membranes allow much higher fluxes. All of these comparisons neglect the fact that the transport through PHEMA membranes was measured at lower temperatures than those used with the comparison membranes. Higher pervaporation temperatures could result in

as much as a doubling of flux, so transport through fluorinated PHEMA is generally an order of magnitude or more greater than that reported for high-performance membranes. Additionally, decreasing the thickness of fluorinated PHEMA films may also allow further increases in flux. Although these comparisons demonstrate the high fluxes that can be achieved by using ultrathin polymer brushes as the skin layers in composite membranes, they also show that it may be possible to achieve even higher fluxes and selectivities if polymer brushes with different compositions can be prepared. Our future work will focus on this area.

2.4. Conclusions

Membranes for selective pervaporation of VOCs were prepared by ATRP of HEMA from the surface of porous alumina followed by derivatization of the resulting PHEMA films with hydrophobic acid chlorides. Reflectance FTIR spectroscopy and FESEM measurements confirm the derivatization process and show that the derivatized PHEMA skin layers fully cover the porous alumina substrates. The VOC/water pervaporation selectivities of these membranes reach values as high as 500, and the minimal thickness of the PHEMA films allows fluxes that are an order of magnitude higher than those of currently used pervaporation membranes. Flux through fluorinated PHEMA is higher than through C8- or C16-PHEMA, presumably because the bulky fluorinated side chains pack less tightly than alkyl chains. C16-PHEMA exhibits the highest sorption selectivities, but the tight packing of the C16 chains likely results in significant water/organic diffusion selectivity. Overall, tradeoffs between diffusion and sorption selectivities result in similar pervaporation selectivities for fluorinated PHEMA, C8-PHEMA and C16-PHEMA. Given the similar selectivities, the fluorinated system

appears to be most promising because of its high flux. ATRP of other monomers from

porous surfaces may yield membranes with even higher fluxes and selectivities.

2.5. References

1. Huang, W.; Baker, G. L.; Bruening, M. L., *Angew. Chem., Int. Ed.* **2001**, *40*, 1510-1512.

2. Kim, J.-B.; Bruening, M. L.; Baker, G. L., *J. Am. Chem. Soc.* **2000**, *122*, 7616-7617.

3. Matyjaszewski, K.; Xia, J., *Chem. Rev.* **2001**, *101*, 2921-2990.

4. Wang, J.-S.; Matyjaszewski, K., *J. Am. Chem. Soc.* **1995**, *117*, 5614-5615.

5. Huang, W.; Kim, J.-B.; Bruening, M. L.; Baker, G. L., *Macromolecules* **2002**, *35*, 1175-1179.

6. Jones, D. M.; Huck, W. T. S., *Adv. Mater.* **2001**, *13*, 1256-1259.

7. Kim, J.-B.; Huang, W.; Bruening, M. L.; Baker, G. L., *Macromolecules* **2002**, *35*, 5410-5416.

8. Carlmark, A.; Malmstroem, E. E., *Biomacromolecules* **2003**, *4*, 1740-1745.

9. Xiao, D.; Zhang, H.; Wirth, M., *Langmuir* **2002**, *18*, 9971-9976.

10. Luo, N.; Husson, S. M.; Hirt, D. E.; Schwark, D. W., *J. Appl. Polym. Sci.* **2004**, *92*, 1589-1595.

11. Balachandra, A. M.; Baker, G. L.; Bruening, M. L., *J. Membr. Sci.* **2003**, *227*, 1-14.

12. Bantz, M. R.; Brantley, E. L.; Weinstein, R. D.; Moriarty, J.; Jennings, G. K., *J. Phys. Chem. B* **2004**, *108*, 9787-9794.

13. Brantley, E. L.; Holmes, T. C.; Jennings, G. K., *J. Phys. Chem. B* **2004**, *108*, 16077-16084.

14. Sullivan, D. M.; Bruening, M. L., *J. Membr. Sci.* **2005**, *248*, 161-170.

15. Chang, Y.-H.; Kim, J.-H.; Lee, S.-B.; Rhee, H.-W., *J. Appl. Polym. Sci.* **2000**, *77*, 2691-2702.

16. Brantley, E. L.; Jennings, G. K., *Macromolecules* **2004**, *37*, 1476-1483.

17. Alentiev, A. Y.; Shantarovich, V. P.; Merkel, T. C.; Bondar, V. I.; Freeman, B. D.; Yampolskii, Y. P., *Macromolecules* **2002**, *35*, 9513-9522.

18.   De Angelis, M. G.; Merkel, T. C.; Bondar, V. I.; Freeman, B. D.; Doghieri, F.; Sarti, G. C., *Macromolecules* **2002,** *35*, 1276-1288.

19.   Jonquieres, A.; Clement, R.; Lochon, P.; Neel, J.; Dresch, M.; Chretien, B., *J. Membr. Sci.* **2002,** *206*, 87-117.

20.   Kujawski, W., *Sep. Sci. Technol.* **2000,** *35*, 89-108.

21.   Okumus, E.; Gurkan, T.; Yilmaz, L., *J. Membr. Sci.* **2003,** *223*, 23-38.

22.   Kim, J. H.; Chang, B. J.; Lee, S. B.; Kim, S. Y., *J. Membr. Sci.* **2000,** *169*, 185-196.

23.   Nagel, C.; Guenther-Schade, K.; Fritsch, D.; Strunskus, T.; Faupel, F., *Macromolecules* **2002,** *35*, 2071-2077.

24.   Nakamura, M.; Samejima, S.; Kawasaki, T., *J. Membr. Sci.* **1988,** *36*, 343-351.

25.   Mishima, S.; Kaneoka, H.; Nakagawa, T., *J. Appl. Polym. Sci.* **1999,** *71*, 273-287.

26.   Ki Hong, Y.; Hi Hong, W., *J. Membr. Sci.* **1999,** *159*, 29-39.

27.   Matsuda, H.; Yanagishita, H.; Negishi, H.; Kitamoto, D.; Ikegami, T.; Haraya, K.; Nakane, T.; Idemoto, Y.; Koura, N.; Sano, T., *J. Membr. Sci.* **2002,** *210*, 433-437.

28.   Sano, T.; Yanagishita, H.; Kiyozumi, Y.; Mizukami, F.; Haraya, K., *J. Membr. Sci.* **1994,** *95*, 221-228.

29.   Huang, W.; Skanth, G.; Baker, G. L.; Bruening, M. L., *Langmuir* **2001,** *17*, 1731-1736.

30.   Johnson, T.; Thomas, S., *J. Appl. Polym. Sci.* **1999,** *71*, 2365-2379.

31.   Radovanovic, P.; Thiel, S. W.; Hwang, S. T., *J. Membr. Sci.* **1990,** *48*, 55-65.

32.   Blume, I.; Wijmans, J. G.; Baker, R. W., *J. Membr. Sci.* **1990,** *49*, 253-286.

33.   Uragami, T.; Ohshima, T.; Miyata, T., *Macromolecules* **2003,** *36*, 9430-9436.

Chapter 3

High-Capacity, Protein-Binding Membranes Based on Polymer Brushes Grown in Porous Substrates

3.1. Introduction

While the previous chapter discussed the synthesis of ultrathin polymer films at the surface of porous substrates to prepare high-flux membranes, this chapter explores the growth of brushes in the interior of porous substrates to prepare membranes with unusually high adsorption capacities. Such systems may prove useful for rapid purification of proteins, which is important because potential therapeutic applications of proteins along with rapid developments in biotechnology and genetic engineering have greatly increased protein production and the need for fast, convenient purification technologies.[1, 2] Affinity chromatography is currently the most convenient way to purify proteins due to its ability to separate biomolecules based on their biological interactions,[2, 3] but the rate of separations with packed-bead affinity columns is limited by slow diffusion of biomacromolecules within bead pores.[3-5]

Affinity membrane chromatography, which was initially introduced by Henis and coworkers in 1987,[6] has the potential to overcome this disadvantage of packed-bead columns because the protein solutions being treated must flow through the membrane pores.[7-9] Additionally, membrane chromatography avoids challenges in packing of columns, which makes it an attractive technique for large-scale separation processes. A number of adsorptive membranes are now available commercially,[10] and a wide range of

porous materials such as cellulose,[11] chitin,[12, 13] chitosan,[14] and nylon[15] have been used as substrates that can be modified for protein immobilization.

This research aims at utilizing the controlled growth of polymer brushes in porous substrates to develop affinity membranes with remarkably high protein-binding capacities. The use of ATRP to grow PHEMA from initiators bound to a porous alumina surface affords relatively fine control over polymer molecular weight, which allows large increases in capacity without clogging of membrane pores. PHEMA brushes are particularly attractive because they can be functionalized to exploit a number of affinity interactions.[16-18] Specifically, functionalization of PHEMA with nitrilotriacetate-Cu^{2+} complexes results in protein binding via metal-ion affinity interactions, and the microporous alumina support provides a ~500-fold increase in surface area relative to two-dimensional supports. Overall, the combination of the alumina supports and functionalized polymer brushes described here yields a remarkable binding capacity of 0.9 mg of bovine serum albumin (BSA) per cm^2 of external membrane surface (150 mg/cm^3 of membrane). Typical membrane absorbers have protein capacities of 4 - 20 mg/cm^3.[19-21]

A few recent studies demonstrated the possibility of using ATRP and other polymerization techniques to prepare protein-adsorbing polymer brushes.[2, 19, 22-24] Matyjaszewski and coworkers reported electrostatic adsorption of 10 to 15 monolayers of BSA to poly(dimethylamino ethylmethacrylate) brushes grown on flat surfaces.[22] Luzinov and coworkers used ATRP to prepare poly(2-vinylpyridine) brushes in porous PVDF. Although these brushes were reported to enhance lysozyme adsorption, no

capacity was provided.[25]   The PHEMA-modified membranes described here clearly demonstrate the advantages of polymer brushes for membrane-based affinity separations.

3.2.   Experimental Section

3.2.1.   Materials

Anodisc™ porous alumina membranes with 0.2 μm-diameter surface pores were obtained from Fisher Scientific.   SEM images suggest that pore diameters in the bulk of these membranes are about 0.25 μm.   Dimethylformamide (DMF, anhydrous, 99.8%), 11-mercaptoundecanol (97%), 2-bromoisobutyryl bromide (98%), CuCl (99.999%), $CuBr_2$ (99%), 2,2'-bipyridyl (bpy, 99%), 1-[3-(dimethylamino)propyl]-3-ethylcarbodiimide hydrochloride (EDC), N-hydroxysuccinimide (NHS), 4-dimethylaminopyridine (DMAP), ethylenediamine tetraacetic acid (EDTA), bovine serum albumin (BSA), and myoglobin were used as received from Sigma Aldrich. $CuSO_4 \cdot 5H_2O$ (Columbus Chemical), $N_\alpha N_\alpha$-bis(carboxymethyl)-L-lysine hydrate (Fluka, aminobutyl-NTA), succinic anhydride (SA, Matheson Coleman & Bell), and Coomassie protein assay reagent (Pierce) were also used as received.   2-Hydroxyethyl methacrylate (HEMA, Aldrich, 97%, inhibited with 300 ppm hydroquinone monomethyl ether) was purified by passing it through a column of activated basic alumina (Spectrum), and the trichlorosilane initiator (11-(2-bromo-2-methyl)propionyloxy)undecyltrichlorosilane) was synthesized according to a literature procedure.[26]   Buffers were prepared using analytical grade chemicals and deionized (Milli-Q, 18.2 MΩ cm) water.

3.2.2. Polymerization of HEMA in Porous Alumina Membranes and on Au Substrates

The alumina membrane was first cleaned in a UV/ozone cleaner (Boekel model 135500) for 12 minutes and sandwiched inside a membrane cell (Millipore, Swinnex 25). A Masterflex 7518-60 peristaltic pump was used to circulate 1 mM trichlorosilane initiator in DMF solution through the membrane for 3 h at a rate of 10 mL/min, and subsequent rinsing with ethanol (20 mL), water (20 mL) and acetone (20 mL) at a flow rate of 10 mL/min yielded an initiator-modified membrane. Polymerization of HEMA occurred by circulating a solution containing 15 mL of purified HEMA, 15 mL methanol, 82.5 mg (0.825 mmol) of CuCl, 54 mg (0.24 mmol) of $CuBr_2$, and 320 mg (2.04 mmol) of bpy through the initiator-modified membrane using a peristaltic pump (7 mL/min) for 1 h. This HEMA solution was initially degassed using 3 freeze-pump-thaw cycles and prepared as described in Chapter 2.[16] After polymerization, the membrane was cleaned by flowing ethanol (20 mL), water (20 mL) and acetone (20 mL) through the membrane at 7 mL/min.

To prepare films for reflectance FTIR characterization, Au-coated silicon wafers were modified with a mercaptoundecanol monolayer that was subsequently derivatized with 2-bromoisobutyryl bromide as described previously.[27, 28] Polymerization of HEMA from these substrates occurred as described above, except the substrate was simply immersed in a degassed polymerization solution that was kept in a glove bag.

3.2.3. PHEMA Derivatization and Protein Immobilization

To derivatize PHEMA-coated alumina membranes, a 55 °C DMF solution containing SA (10 mg/mL) and DMAP (15 mg/mL) was passed through the membrane

for 3 h at 7 mL/min followed by rinsing with DMF (20 mL), water (20 mL) and ethanol (20 mL) at 7 mL/min (Scheme 3.1). Next, a room-temperature solution containing EDC/NHS (0.1 M of each in pure water) was circulated for 30 min (6.8 mL/min) through the membrane, which was then briefly washed with water and ethanol (20 mL each). The EDC/NHS-activated membrane was allowed to react with a flowing (6.5 mL/min) 0.1 M aminobutyl-NTA solution (adjusted to pH 10.2) for 1 h, rinsed with 20 mL water, and finally exposed to a 0.1 M $CuSO_4$ solution (6.5 mL/min) for 30 min and rinsed with 20 mL of water. The membrane was then taken out of the Swinnex 25 cell, rinsed sequentially with 5 mL of water, ethanol and acetone using a pipette, and dried with a flow of nitrogen. The water remaining in the pump tubing was next pumped out, and the membrane was put back into the cell. A solution containing BSA or myoglobin (in pH 7.2 phosphate buffer) was then forced through the membrane, and the permeate was collected for analysis at specific time intervals. Permeate volume was estimated using a graduated cylinder. Subsequently, the membrane was rinsed with pH 7.2 phosphate buffer, and protein was eluted using a 50 mM EDTA solution (pH adjusted to 7.2). To prepare films for reflectance FTIR characterization, a PHEMA film on a gold substrate was treated in a similar procedure by immersing the substrate in appropriate solutions and rinsing with solutions from a pipette.
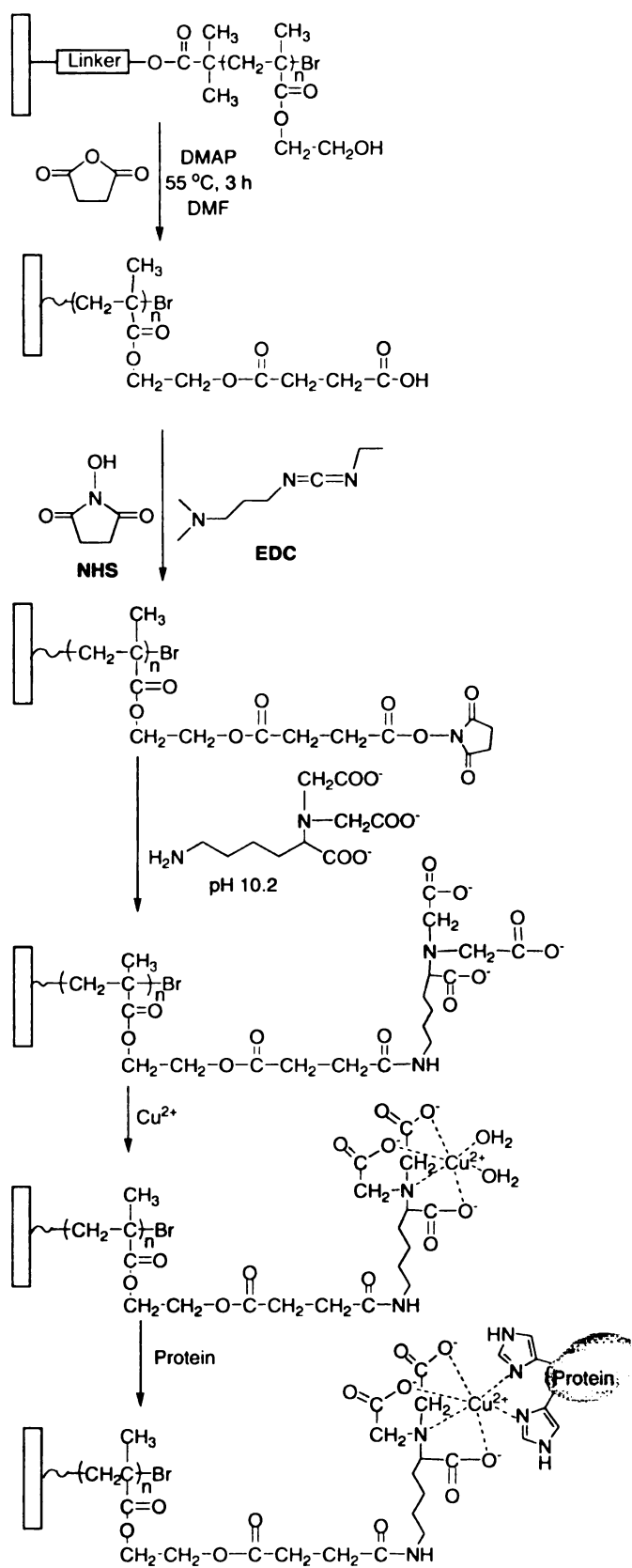
Scheme 3.1. Derivatization of PHEMA for protein immobilization.

3.2.4. Determination of Protein Concentrations

To determine the concentration of protein in permeate and eluent solutions, 50 μL of the sample was added to 2.95 mL of a solution of Coomassie reagent, and the mixture was shaken a few times and allowed to react for 5 min at room temperature. The UV/vis absorbance spectra of these solutions were then obtained with a Perkin-Elmer UV/Vis (model Lambda 40) spectrophotometer. Calibration curves for the absorbance of BSA and myoglobin/Coomassie solutions at 595 nm were obtained using a series of protein solutions (concentration range of 100 μg to 2 mg of protein per mL) that were mixed with Coomassie reagent. All spectra were measured against a Coomassie reagent background.

3.2.5. Film Characterization Methods

Film growth inside alumina membranes was verified using field-emission scanning electron microscopy (FESEM, Hitachi S-4700II, acceleration voltage of 15 kV) and energy dispersive X-ray spectroscopy (EDS, Phoenix EDAX instrument). For SEM and EDS observations, the alumina membrane was attached to a Si wafer by double-sided tape, and the alumina was dissolved by immersing it into 1 M NaOH at 25 °C for two hours followed by careful washing several times with distilled water and ethanol. Subsequently, 7 nm of gold was sputtered onto the remaining polymer prior to FESEM and EDS examination. Reflectance FTIR spectra of films on gold-coated wafers were obtained with a Nicolet Magna-IR 560 instrument using a Pike grazing angle (80°) accessory. The spectrum of reflection from a UV/ozone-cleaned gold-coated wafer was used as a background.

3.3. Results and Discussion

3.3.1. FTIR Characterization of PHEMA Derivatization and Protein Binding

Reflectance FTIR spectra of PHEMA films and their derivatives on Au-coated Si confirm the steps of the derivatization and protein-adsorption procedure shown in Scheme 3.1. To prepare brushes capable of protein binding, we first reacted PHEMA
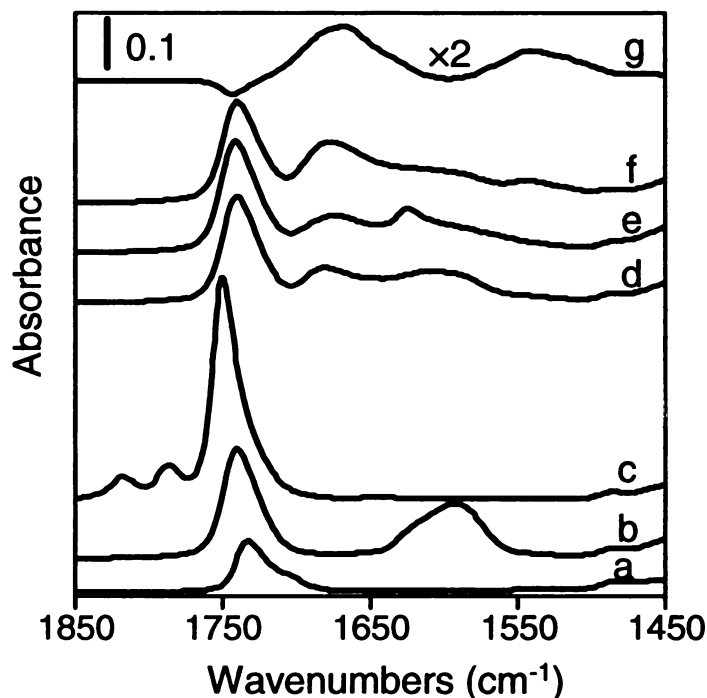
Figure 3.1. Reflectance FTIR spectra of a PHEMA film before (a) and after the following sequential steps: (b) reaction with SA, immersion in a pH 9.9 buffer, and rinsing with ethanol; (c) activation with EDC/NHS; (d) reaction with aminobutyl NTA followed by immersion in pH 9.9 buffer; (e) exposure to 0.1 M Cu^{2+} to form NTA-Cu^{2+} complexes; (f) exposure to 1 mg/mL BSA followed by immersion in pH 9.9 buffer. Spectrum (g) is the difference spectrum resulting from subtraction of (d) from (f) and multiplication by a factor of 2.

with SA to create free –COOH groups in the film. Prior to obtaining the reflectance IR spectrum of SA-derivatized films, we immersed the film-coated gold slide in pH 9.9 buffer for 15 min and rinsed with ethanol. At pH 9.9, the newly introduced carboxylic acid groups should be deprotonated,[29] and consistent with derivatization and deprotonation, the FTIR spectrum of these films contains a new peak around 1594 cm^{-1} (Figure 3.1b), which is likely due to the –COO$^-$ symmetric stretch. The absorbance at
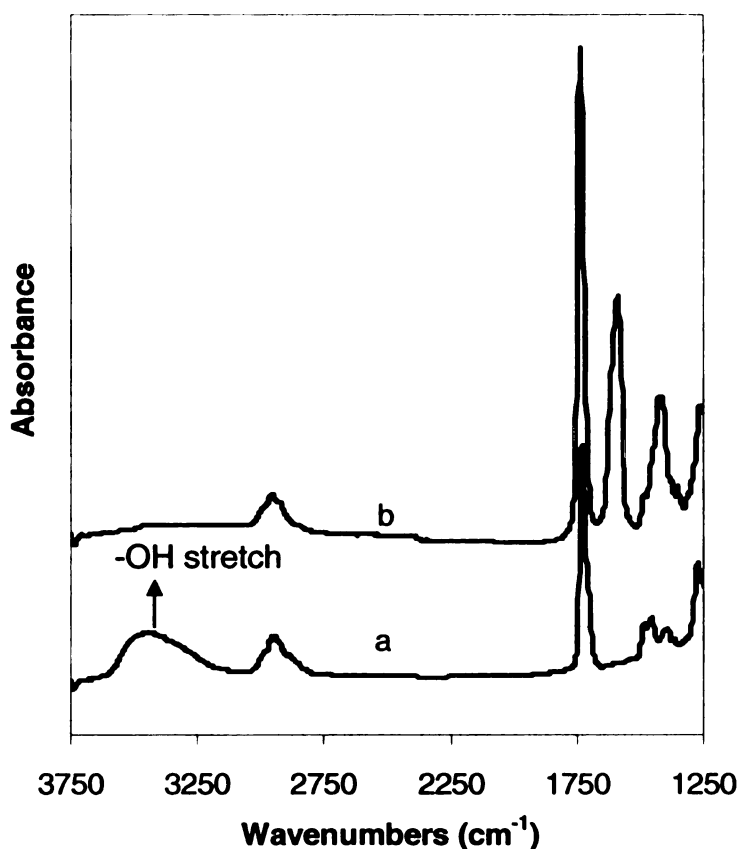
Figure 3.2. Reflectance FTIR spectra of a PHEMA film (3750 to 1250 cm^{-1}) on Au (a) before and (b) after derivatization with succinic anhydride, immersion in pH 9.9 buffer, and rinsing in ethanol.

~1740 cm^{-1}, which is assigned to ester carbonyl groups, approximately doubled after SA derivatization, suggesting a high degree of conversion of the –OH groups of PHEMA to ester groups. The disappearance of the –OH stretch of PHEMA (3650 - 3100 cm^{-1}, Figure 3.2) also indicates nearly 100% derivatization.

After activation of the –COOH groups of modified PHEMA using EDC/NHS, peaks due to the succinimide ester appeared at 1817 and 1786 cm^{-1} (Figure 3.1c).[30-32] The asymmetric stretch of succinimide (~1753 cm^{-1}) overlaps with the C=O stretch (1740 cm^{-1}) of the previously formed esters to yield a broad peak with an absorbance that is about double that for the ester carbonyl after SA derivatization. The new peak at 1817 cm^{-1} is due to the carbonyl stretch of the active ester formed by reaction with NHS, while the absorbance at 1786 cm^{-1} results from the symmetric succinimide stretch.

The EDC/NHS activated PHEMA was then reacted with aminobutyl-NTA ($N_\alpha N_\alpha$–bis(carboxymethyl)-L-lysine hydrate) and immersed in pH 9.9 buffer for 15 min and rinsed with ethanol. Reaction of the active ester with both aminobutyl NTA and water resulted in the loss of the active ester absorbances, and the shift of the 1753 cm^{-1} peak back to 1740 cm^{-1} (Figure 3.1d). The new peak at 1680 cm^{-1} provides evidence for NTA immobilization and is probably due to the COO$^-$ groups from NTA as well as the amide bond formed between SA and NTA. The broad absorbance centered at 1600 cm^{-1} could result from carboxylate groups in either NTA or the hydrolyzed active esters. Exposure of NTA-derivatized PHEMA to 0.1 M CuSO$_4$ followed by rinsing with water yielded immobilized NTA-Cu^{2+} that is capable of binding proteins through their histidine groups. Unfortunately, there was no significant change in the IR spectrum (Figure 3.1e) of the film after Cu^{2+} coordination except that the peak at 1600 cm^{-1} appeared to shift to

1630 cm^{-1} and become sharper. However, this shift could be due to the fact that spectrum (d) was measured after treatment with pH 9.9 buffer, while the sample for spectrum (e) was not treated with this buffer because $Cu(OH)_2$ might precipitate in the film at high pH. XPS data confirmed the presence of Cu^{2+} in the film and showed a Cu : N ratio of 0.4 : 1, which is consistent with our previous results and indicative of nearly one Cu^{2+} per NTA moiety.[33]

After an overnight exposure of the PHEMA-NTA-Cu^{2+} film to a 1 mg/mL BSA solution in pH 7.2 buffer followed by immersion in pH 9.9 buffer for 15 min and rinsing in EtOH, we saw growth in the absorbance at 1680 cm^{-1} (amide I band) and the appearance of a small peak at 1545 cm^{-1} (amide II band) (Figure 3.1f). Subtracting the spectrum of PHEMA-NTA (Figure 3.1d) from that of PHEMA-NTA-Cu^{2+}-BSA (Figure 3.1f) yielded a bound-BSA spectrum, which is dominated by amide absorbances (Figure 3.1g). We chose to subtract the PHEMA-NTA rather than the PHEMA-NTA-Cu^{2+} spectrum because the former was taken after immersion in a pH 9.9 buffer as was the spectrum of PHEMA-NTA-Cu^{2+}-BSA. Comparison of the amide intensities in Figure 3.1g with those of spin-coated films of pure BSA suggests that about 40 nm of BSA adsorbed to this film.[33] Assuming a monolayer height of 4.0 nm,[34] this thickness corresponds to 10 monolayers of bound BSA. The PHEMA film was initially 50 nm thick.

3.3.2. SEM and EDS Characterization of PHEMA inside Alumina Membranes
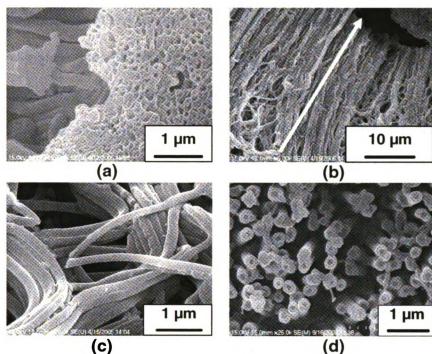
Figure 3.3.   FESEM images of PHEMA nanotubes synthesized by ATRP in porous alumina substrates.   (a) Top view of the nanotubes. (b) Cross-sectional image showing the length of the nanotubes.   (c) Highly flexible PHEMA nanotubes. (d) Top view of the nanotubes obtained by removing the surface layer by polishing with sand paper.   The arrow in (b) shows the approximate length of the tubes.

In chapter 2, we used ATRP to graft PHEMA from the surface of porous alumina substrates and form composite membranes with ultrathin PHEMA skins.[16]   In contrast, this work aimed at grafting PHEMA within the pores of the membrane to achieve a high surface area for protein capture.   By pumping the initiator and monomer solutions through the membrane, we were able to achieve polymerization throughout the support

and increase the surface area from which polymerization occurred by 500 fold. One challenge in such polymerizations is to grow polymer brushes without clogging the membrane. To overcome this difficulty, we used methanol instead of water as the solvent for brush growth to decrease the rate of polymerization.[35]

The SEM images in Figure 3.3 clearly demonstrate the formation of hollow PHEMA tubes in the membrane pores.[36, 37] To obtain these images, we dissolved the alumina template in 1 M NaOH and collected the polymer tubes before taking SEM images. (PHEMA likely does not dissolve in 1 M NaOH because it is lightly cross-linked.[38]) The right side of Figure 3.3a shows an image of the top of the brushes, which is similar to images of bare porous alumina. Figure 3.3b indicates that the length of the resulting nanotubes is about 45 μm, which is slightly less than the thickness of the alumina support (60 μm), perhaps because the tubes curled up. Figure 3.3c shows the flexibility of the tubes. The image in Figure 3.3d was obtained after removing the skin layer of the membrane by polishing with sandpaper to reveal that the interior of the pores is open. (Although Figure 3.3a shows that the pores are open at the surface of the membrane, it does not necessarily imply that the interior of the pores is open.) Figure 3.3d shows open, interior pores, but the thickness of the polymers is much higher than what we calculated from flow experiments (see below). Because the sanding process may cause the pores to appear thicker than they are, we do not think that Figure 3.3d can be employed to determine the inner diameter of the tubes.

The energy dispersive X-ray spectrum of the nanotubes (Figure 3.4) reveals C and

O and not Al, demonstrating that these images are indeed those of PHEMA.
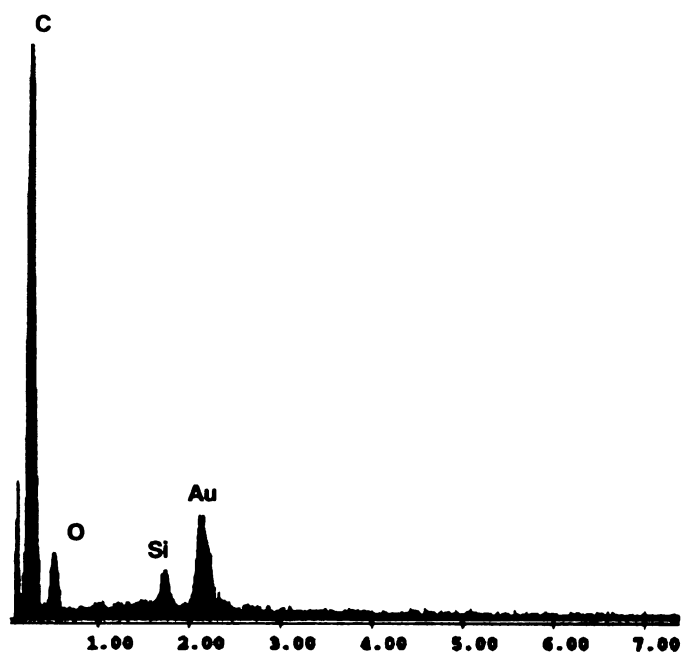
Figure 3.4. Energy dispersive X-ray spectrum of PHEMA nanotubes grown

by ATRP in porous alumina membranes. The nanotubes were obtained by

attachment of the membrane onto Si wafers and dissolution of the alumina in

1.0 M NaOH. These samples were sputtered with 7 nm of Au prior to

imaging. Peaks due to Si and Au are due to the support and sputtering,

respectively.

3.3.3. BSA Binding to PHEMA-NTA-Cu^{2+} Brushes

To test the binding capacity of PHEMA-NTA-Cu^{2+} films, we initially pumped a 0.56 mg/mL BSA solution through the membrane, collected the permeate over specific
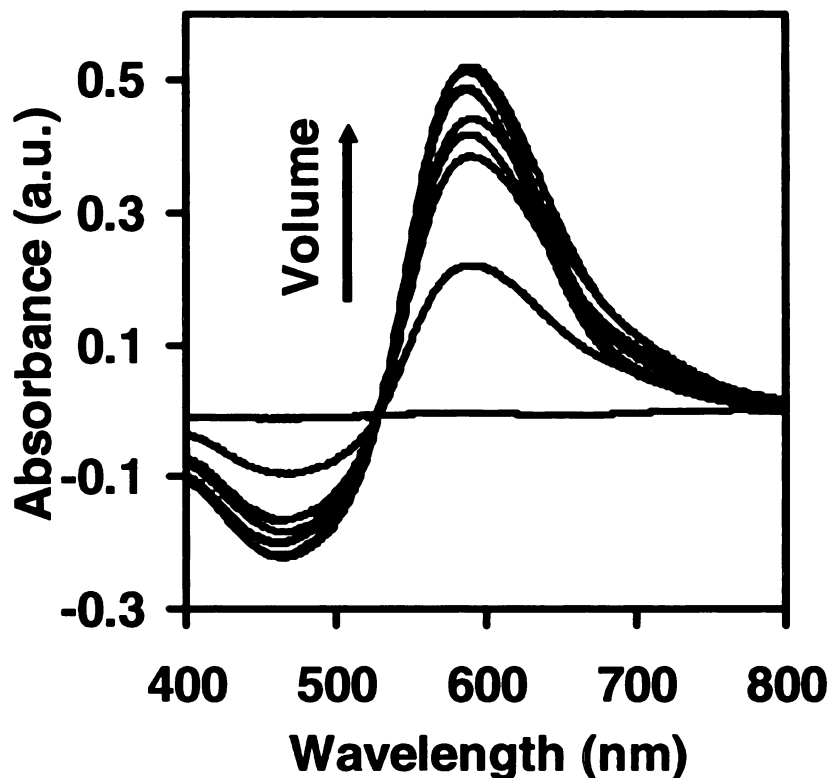
Figure 3.5. UV-vis spectra of the permeate collected at certain time intervals when 0.56 mg/mL BSA solution was pumped through porous alumina membranes coated with PHEMA-NTA-Cu^{2+}. The permeate flow rate was initially 2.4 mL/min and 0.9 mL/min at the end of the experiment. Prior to measurement of the UV-vis spectra, 50 μL of permeate was mixed with 2.95 mL of Coomassie reagent. Pure Coomassie reagent was used as the background.

time intervals, and analyzed these solutions using the absorbance at 595 nm in a Bradford

assay. Figure 3.5 presents typical UV-vis spectra from the Bradford assays.

The breakthrough curve (Figure 3.6) obtained from these measurements shows

that essentially all of the BSA was adsorbed until breakthrough occurred, and that

saturation of the membrane took less than 15 min.[34, 39, 40] Integration of the difference

between the feed concentration and the concentrations given in Figure 3.6 yielded a
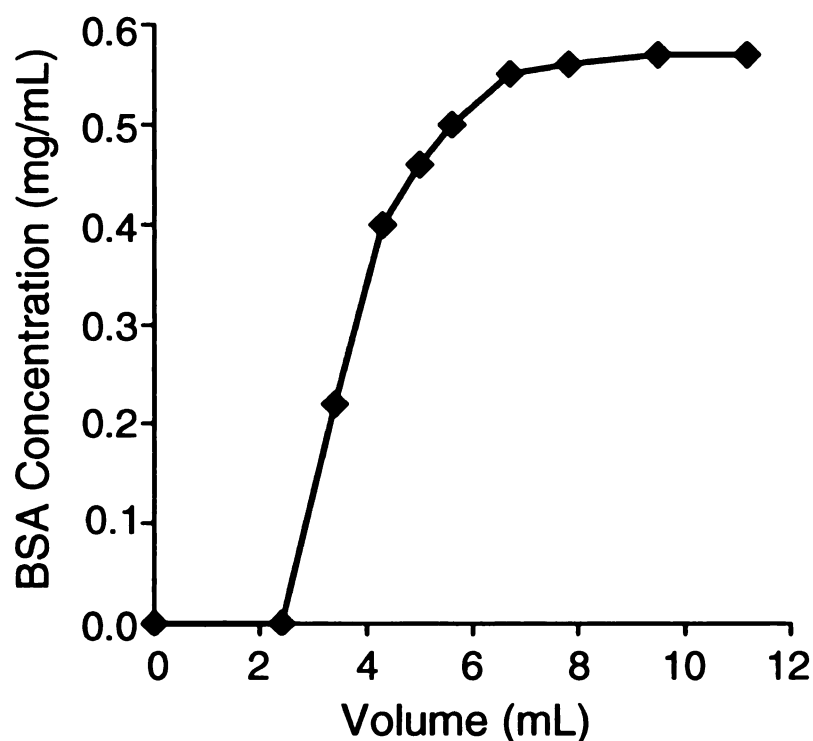
Figure 3.6. Breakthrough curve for BSA adsorption in porous alumina

membranes coated with PHEMA-NTA-Cu^{2+}. The BSA concentration in the

feed solution was 0.56 mg/mL and the initial flow rate was 2.4 mL/min,

decreasing to 0.9 mL/min at the end of the experiment.

remarkable 0.8 mg of bound BSA per cm^2 of external membrane surface area. Repetition

of this experiment on 4 different membranes yielded an average BSA binding of 0.82 ±

0.07 mg/cm^2. This very high capacity is due in part to the high internal surface area of the alumina, but even taking into account the surface area of the pores (assuming 50% porosity, pore diameters of 0.25 μm, and a membrane thickness of 60 μm), the capacity is 1.6 μg of BSA per cm^2 of pore area or about 4 monolayers of BSA (assuming a BSA density of 1 g/cm^3 and a monolayer thickness of 4.0 nm) adsorbed throughout the pores of these membranes.

Figure 3.7 shows how the amount of equilibrium binding of BSA to PHEMA-
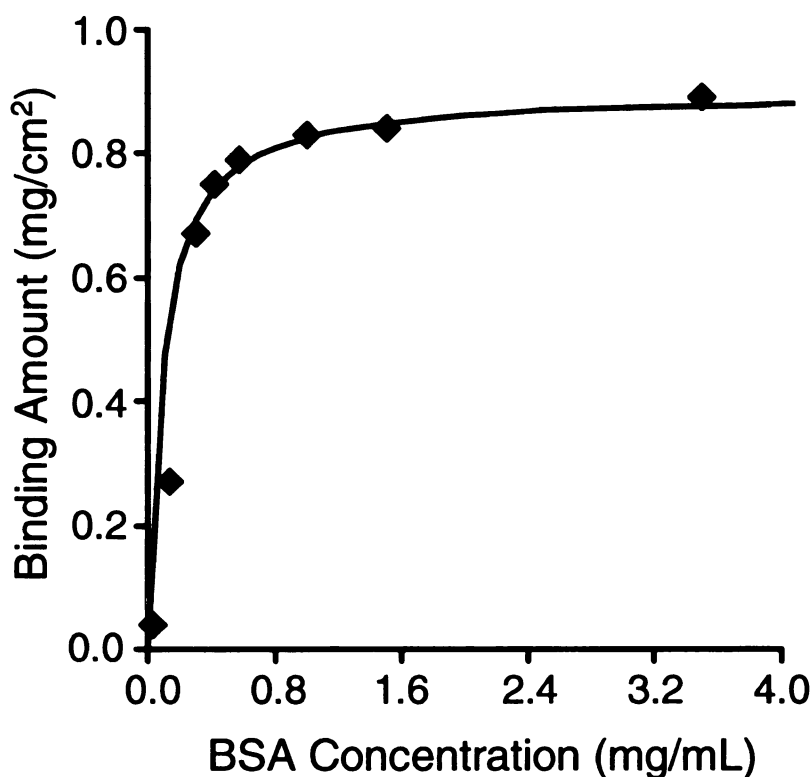
Figure 3.7. Equilibrium binding capacity of PHEMA-NTA-Cu^{2+}-coated alumina membranes as a function of BSA concentration. The solid line represents the fit of the data to the Langmuir isotherm.

NTA-Cu^{2+} films in alumina membranes varies with the concentration of BSA. In this experiment, binding was performed at a specific BSA concentration, and the membrane

98

was regenerated with 0.05 M EDTA (pH 7.2) followed by 0.1 M Cu^{2+} prior to examining

adsorption at another BSA concentration. As can be seen, BSA binding increases with its

concentration in the feed solution until approaching saturation at concentrations around 1

mg/mL. The data are reasonably described by the Langmuir isotherm,[9, 41-43] $q = q_m C/(K_d$

$+ C)$, where q is the amount of protein bound, q_m represents the saturation capacity, C is

the concentration of protein in solution, and K_d is the dissociation equilibrium constant.

The value of q_m determined from the Langmuir plot is 0.9 mg per cm^2 of external

membrane surface area, and the dissociation constant is 0.09 mg/mL, which also

corresponds to 1.3 μM. This K_d value is reasonably consistent with the previously

reported value of 2.3 μM for Chitosan-Cu^{2+}-BSA,[44] and indicates a strong binding

affinity between BSA and immobilized NTA-Cu^{2+} complexes.

The high protein-binding capacity of these membranes is also consistent with

decreases in flow rate after protein binding. As noted in Figure 3.6, flow rate decreased

from 2.4 to 0.9 mL/min during binding of 0.8 mg of BSA per cm^2 of external membrane

surface area (130 mg/cm^3). We achieved a similar decrease in flow rate when we loaded

protein in the membrane using a dead-end filtration cell (Millipore, Model 8010) with a

controlled pressure of 6.9 × 10^4 pascals (10 psig). Assuming Poiseuille flow in the

membranes (flow rate is proportional to pore radius raised to the 4th power), the drop in

flow rate suggests that the radius of the membrane pores decreased by a factor of 1.28

after protein binding. Using an open pore radius of 0.112 μm after PHEMA-NTA-Cu^{2+}

deposition (see below) and assuming a 50% porosity prior to film deposition, the

decrease in radius by a factor of 1.28 upon protein binding would yield a decrease in pore

volume of 0.16 cm^3/cm^3 of total membrane. With a protein density of 1 g/cm^3, this

decrease in pore volume agrees well with both the BSA binding capacity of 130 mg/cm^3 for the membrane used to obtain Figure 3.6 and the saturated binding capacity of 150 mg/cm^3 (Figure 3.7). Thus, the high protein-binding capacity is consistent with the flow rates through the membrane.

Flow rates before polymerization and after deposition of PHEMA-NTA-Cu^{2+} were 10 mL/min and 6.5 mL/min, respectively, suggesting that the pore radius decreased from 0.125 μm before polymerization (radius estimated from FESEM images) to 0.112 μm after deposition of the PHEMA-NTA-Cu^{2+} film. This implies a film thickness of 10 nm, which appears to be less than that in the SEM images of PHEMA tubes in Figure 3.3, but as mentioned previously, the polymers might be much thicker at their sanded surface than in the bulk of the membrane. We should note that flow rate dropped from 6.5 mL/min to 2.5 mL/min almost instantaneously when we began filtering the BSA solution. We think that a thin layer of contaminants may quickly adsorb at the membrane surface. Elution with EDTA and/or regeneration with 0.1 M Cu^{2+} did not return the flow rate to 6.5 mL/min.

Table 3.1. Comparison of the protein-binding capacity of alumina-PHEMA-NTA-Cu^{2+} membranes with other membrane absorbers.

Membrane	Thickness (μm)	Surface Area (cm^2)	Pore Size (μm)	Porosity	Ligate	Binding capacity (mg/cm^2)	Binding capacity (mg/cm^3)
Glass fiber[20]	8000	17.3	3	87%	BSA	6.9	8.6
Poly (acrylic acid) (Polypropylene base polymer)[19]	150	3.14	0.4	-----	Lysozyme	0.3	20
Cellulose[21]	64	125	0.2	-----	BSA	0.027	4.2
PHEMA (This work) (Alumina support)	60	3.14	0.2	50%	BSA	0.9	150

Table 3.1 compares the BSA-binding capacity of PHEMA-NTA-Cu^{2+}-coated alumina membranes with several other membrane systems. Ruckenstein and Guo modified glass fiber filters with trypsin or papain to bind proteins.[20, 45] They then packed 20 modified glass membrane filters (about 8 mm thick) into a cartridge and achieved an extremely high binding capacity of 6.9 mg of BSA per cm^2 of external membrane surface area. However, if one takes the membrane thickness into account and converts binding capacity into mg/cm^3, the modified alumina membranes described here show a 17-fold higher capacity (compare rows 1 and 4 in Table 3.1). Very recently, Ulbricht and Yang used UV-initiated graft polymerization to grow poly (acrylic acid) from porous polypropylene microfiltration membranes.[19] The resulting membranes showed a promising performance in adsorption of lysozyme using ion-exchange interactions (Table 3.1, row 2). Still the capacity of those membranes was 7-fold lower than that described here. Kubota and coworkers modified porous cellulose membranes with iminodiacetate-Cu^{2+} complexes,[21] but those membranes (Table 3.1, row 3) gave only 1/36 of the binding

capacity described here . The growth of brushes from alumina using ATRP provides an

unusually productive method for introducing a high concentration of binding groups into

membranes.

3.3.4. Elution of BSA and Reuse of Alumina-PHEMA-NTA-Cu^{2+} Membranes

In addition to rapid, high-capacity adsorption, elution and regeneration are also

vital in the use of membrane absorbers.[46-48] Figure 3.8 shows results from multiple
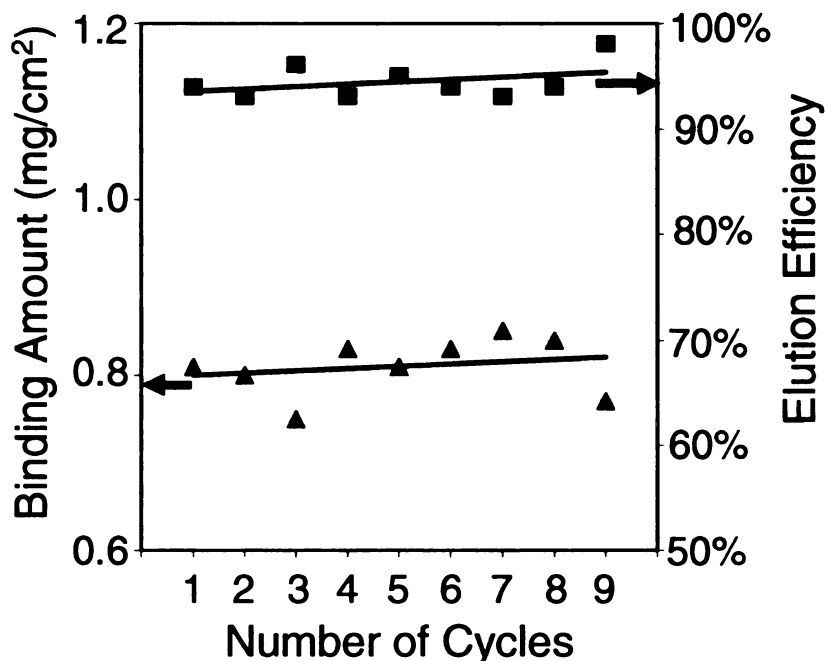
Figure 3.8. Binding amounts (triangles) and elution efficiencies (squares) for

several cycles of BSA adsorption and elution followed by Cu^{2+} reloading of an

alumina membrane modified with PHEMA-NTA. (Flow rate - 0.9 mL/min;

BSA concentration - 0.6 mg/mL; Elution buffer – 50 mM EDTA, pH 7.2)

experiments comprising cycles of absorption of BSA, elution with 50 mM EDTA, and

regeneration with 0.1 M Cu^{2+} on a single alumina-PHEMA-NTA-Cu^{2+} membrane.

Within experimental error (<15%), there was no loss in binding amount over 9 cycles,

and >93% recovery of protein occurred in each cycle. The consistency in capacity over 9

loadings implies that the elution buffer removed essentially all of the adsorbed protein from the membranes, even though the average calculated elution efficiency was only 94%. There likely was a systematic error in the analyses that resulted in an underestimation of elution efficiencies. Given the small volumes involved in the breakthrough experiments along with inaccuracies in the volume measurements and the need to integrate data such as those in Figure 3.5 to obtain adsorption amounts, this is certainly possible.

To more accurately assess elution efficiency, we passed 10 mL of 0.56 mg/mL BSA in pH 7.2 buffer through the membrane and analyzed this entire solution to determine how much BSA was adsorbed in the membrane. We also passed 5-10 mL of rinsing buffer through the membrane to rinse the system and determined the amount of protein in this effluent. We subtracted the total amount of protein that came through the membrane from the amount of protein added to the initial 10 mL BSA solution to determine the amount of bound BSA. (In these experiments we used weight rather than volume to more accurately determine the amount of solution passing through the membrane.) We eluted the protein with 10-15 mL of 0.1 M EDTA and analyzed the protein concentration in the entire solution. For three cycles of adsorption, elution, and Cu^{2+} binding, the average amount bound to the membrane was 0.78±0.02 mg/cm^2, which is in reasonable agreement with the previous measurements. The elution efficiency was 101 ± 1 %. Hence, essentially all of the protein is eluted.

Control experiments with membranes that were derivatized with PHEMA-NTA films but not exposed to Cu^{2+} showed elution of <0.02 mg/cm^2 BSA from a membrane loaded by a 0.56 mg/mL BSA solution and rinsed with buffer. These control experiments

help to validate the experimental procedure and also indicate that the PHEMA-NTA films are not prone to high levels of non-specific BSA adsorption under these conditions.

3.3.5. Adsorption of Myoglobin

We also examined the adsorption of myoglobin to alumina-PHEMA-NTA-Cu^{2+} membranes to see if molecular weight affects protein adsorption. BSA has a molecular weight of 67 kDa, an isoelectric point of 4.9, 17 histidine residues, and dimensions of 4.0 nm × 4.0 nm × 11.5 nm.[34] In contrast, myoglobin has a molecular weight of 17 kDa, an isoelectric point of 7.0, 11 histidine residues and a size of 4.4 nm × 4.4 nm × 2.5 nm.[49] Figure 3.9 shows the breakthrough curves for the two proteins on the same membrane.
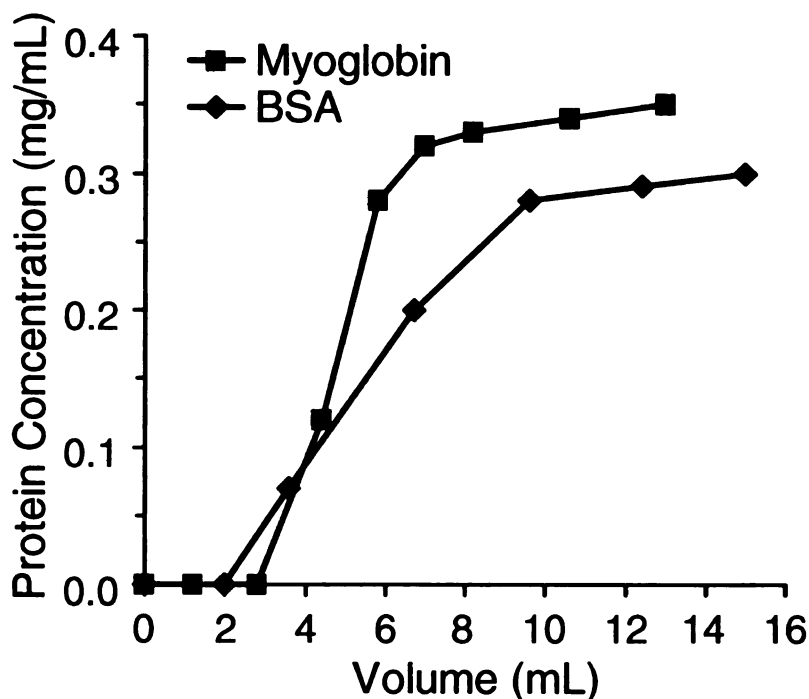
Figure 3.9. Breakthrough curves for adsorption of 0.3 mg/mL BSA and 0.35 mg/mL myoglobin on the same alumina-PHEMA-NTA-Cu^{2+} membrane. After adsorption of BSA, the membrane was regenerated with 0.05 M EDTA and 0.1 M Cu^{2+}.

The membrane showed high binding capacities for both BSA (0.67 mg/cm^2, feed concentration: 0.30 mg/mL) and myoglobin (0.50 mg/cm^2, feed concentration: 0.35 mg/mL), but the breakthrough curve is sharper for myoglobin. This could be due to more rapid diffusion of the smaller myoglobin in the brushes, but this needs further investigation. Future studies examining how the rate of binding varies with brush thickness and density should be helpful in this regard. (Brush thickness can be controlled by varying the polymerization time, while density can be controlled by changing the denisyt of initiators.[38, 50]) The fraction of histidine residues in myoglobin is also higher, and this could result in more rapid binding.[41]

3.4. Conclusions

Immobilized metal-affinity membranes were prepared by ATRP of HEMA inside the pores of alumina substrates followed by a series of derivatization steps to immobilize NTA-Cu^{2+} complexes. FESEM measurements confirmed the growth of PHEMA brushes inside the pores of alumina membranes, and reflectance FTIR spectroscopy verified the efficacy of the derivatization procedures. Equilibrium binding essentially followed the Langmuir isotherm, and the saturation binding capacity of PHEMA-NTA-Cu^{2+} for BSA was 0.9 mg per cm^2 of membrane. Moreover, saturation of the membrane with protein occurred in less than 15 min. After 9 cycles of adsorption, elution, and regeneration, the membranes showed no detectable loss of capacity, and elution efficiencies were essentially 100%. The derivatized PHEMA brushes also showed rapid, high capacity binding of myoglobin. Hence, the use of polymer brushes in the pores of membranes is an effective means for creating high-capacity protein adsorbers.

3.5. References

1. Arica, M. Y.; Testereci, H. N.; Denizli, A., *J. Chromatogr. A* **1998**, *799*, 83-91.

2. Kawai, T.; Saito, K.; Lee, W., *J. Chromatogr. B* **2003**, *790*, 131-142.

3. Zou, H.; Luo, Q.; Zhou, D., *J. Biochem. Biophys. Methods* **2001**, *49*, 199-240.

4. Clairbois, A. S.; Letourneur, D.; Muller, D.; Jozefonvicz, J., *J. Chromatogr. B* **1998**, *706*, 55-62.

5. Sun, G.-Y.; Shi, Q.-H.; Sun, Y., *J. Chromatogr. A* **2004**, *1061*, 159-165.

6. Henis, J. M. S.; Tripodi, M. K.; Stimpson, D. I. European Patent 0,221,046B1, October 30, 1987.

7. Charcosset, C., *J. Chem. Technol. Biotechnol.* **1998**, *71*, 95-110.

8. Urmenyi, A. M.; Poot, A. A.; Wessling, M.; Mulder, M. H. V., *J. Membr. Sci.* **2005**, *259*, 91-102.

9. Wu, C.-Y.; Suen, S.-Y.; Chen, S.-C.; Tzeng, J.-H., *J. Chromatogr. A* **2003**, *996*, 53-70.

10. Roper, D. K.; Lightfoot, E. N., *J. Chromatogr. A* **1995**, *702*, 3-26.

11. Sarfert, F. T.; Etzel, M. R., *J. Chromatogr. A* **1997**, *764*, 3-20.

12. Ruckenstein, E.; Zeng, X., *Biotechnol. Bioeng.* **1997**, *56*, 610-617.

13. Zeng, X.; Ruckenstein, E., *J. Membr. Sci.* **1999**, *156*, 97-107.

14. Zeng, X.; Ruckenstein, E., *J. Membr. Sci.* **1996**, *117*, 271-278.

15. Castilho, L. R.; Deckwer, W. D.; Anspach, F. B., *J. Membr. Sci.* **2000**, *172*, 269-277.

16. Sun, L.; Baker, G. L.; Bruening, M. L., *Macromolecules* **2005**, *38*, 2307-2314.

17. Miller, M. D.; Baker, G. L.; Bruening, M. L., *J. Chromatogr. A* **2004**, *1044*, 323-330.

18. Bayramoglu, G.; Yilmaz, M.; Arica, M. Y., *Colloids Surf., A* **2004**, *243*, 11-21.

19. Ulbricht, M.; Yang, H., *Chem. Mater.* **2005**, *17*, 2622-2631.

20. Guo, W.; Ruckenstein, E., *J. Membr. Sci.* **2003**, *215*, 141-155.

21. Kubota, N.; Nakagawa, Y.; Eguchi, Y., *J. Appl. Polym. Sci.* **1996**, *62*, 1153-1160.

22. Kusumo, A.; Bombalski, L.; Qiao, L.; Kowalewski, T.; Matyjaszewski, K.; Schneider, J. W.; Tilton, R. D., AIChe Annual Meeting, Cincinnati, OH, **2005**, *01C14*, 123d.

23. Ito, H.; Nakamura, M.; Saito, K.; Sugita, K.; Sugo, T., *J. Chromatogr. A* **2001**, *925*, 41-47.

24. Okamura, D.; Sait, K.; Sugita, K.; Tamada, M.; Sugo, T., *J. Chromatogr. A* **2002**, *953*, 101-109.

25. Singh, N.; Husson, S. M.; Zdyrko, B.; Luzinov, I., *J. Membr. Sci.* **2005**, *262*, 81-90.

26. Matyjaszewski, K.; Miller, P. J.; Shukla, N.; Immaraporn, B.; Gelman, A.; Luokala, B. B.; Siclovan, T. M.; Kickelbick, G.; Vallant, T.; Hoffmann, H.; Pakula, T., *Macromolecules* **1999**, *32*, 8716-8724.

27. Kim, J.-B.; Bruening, M. L.; Baker, G. L., *J. Am. Chem. Soc.* **2000**, *122*, 7616-7617.

28. Kim, J.-B.; Huang, W.; Bruening, M. L.; Baker, G. L., *Macromolecules* **2002**, *35*, 5410-5416.

29. Hong, Y. K.; Hong, W. H., *Sep. Purif. Technol.* **2005**, *42*, 151-157.

30. Dordi, B.; Schoenherr, H.; Vancso, G. J., *Langmuir* **2003**, *19*, 5780-5786.

31. Lahiri, J.; Isaacs, L.; Tien, J.; Whitesides, G. M., *Anal. Chem.* **1999**, *71*, 777-790.

32. Xiao, S.-J.; Brunner, S.; Wieland, M., *J. Phys. Chem. B* **2004**, *108*, 16508-16517.

33. Dai, J.; Bao, Z.; Sun, L.; Hong, S. U.; Baker, G. L.; Bruening, M. L., *Langmuir* **2006**, *22*, 4274-4281.

34. Tsuneda, S.; Saito, K.; Furusaki, S.; Sugo, T., *J. Chromatogr. A* **1995**, *689*, 211-218.

35. Robinson, K. L.; Khan, M. A.; de Banez, M. V.; Wang, X. S.; Armes, S. P., *Macromolecules* **2001**, *34*, 3155-3158.

36. Hou, S.; Wang, J.; Martin, C. R., *J. Am. Chem. Soc.* **2005**, *127*, 8586-8587.

37. Martin, C. R., *Science* **1994,** *266,* 1961-1966.

38. Huang, W.; Kim, J.-B.; Bruening, M. L.; Baker, G. L., *Macromolecules* **2002,** *35,* 1175-1179.

39. Shi, W.; Zhang, F.; Zhang, G., *J. Chromatogr. A* **2005,** *1081,* 156-162.

40. Hao, W.; Wang, J., *Chromatographia* **2005,** *62,* 55-62.

41. Iwats, H.; Saito, K.; Furusaki, S., *Biotechnol. Progr.* **1991,** *7,* 412-418.

42. Arica, M. Y.; Denizli, A.; Salih, B.; Piskin, E.; Hasirci, V., *J. Membr. Sci.* **1997,** *129,* 65-76.

43. Bayramoglu, G., *J. Appl. Polym. Sci.* **2003,** *88,* 1843-1853.

44. Shi, Q.-H.; Tian, Y.; Dong, X.-Y.; Bai, S.; Sun, Y., *Biochem. Eng. J* **2003,** *16,* 317-322.

45. Guo, W.; Ruckenstein, E., *J. Chromatogr. B* **2003,** *795,* 61-72.

46. Avramescu, M.-E.; Girones, M.; Borneman, Z.; Wessling, M., *J. Membr. Sci.* **2003,** *218,* 219-233.

47. Garipcan, B.; Andac, M.; Uzun, L.; Denizli, A., *React. Funct. Polym.* **2004,** *59,* 119-128.

48. Kubota, N.; Kounosu, M.; Saito, K.; Sugita, K.; Watanabe, K.; Sugo, T., *J. Membr. Sci.* **1997,** *134,* 67-73.

49. Kent, M. S.; Yim, H.; Sasaki, D. Y.; Satija, S.; Seo, Y.-S.; Majewski, J., *Langmuir* **2005,** *21,* 6815-6824.

50. Bao, Z.; Bruening, M. L.; Baker, G. L., *Macromolecules* **2006,** *39,* 5251-5258.

Chapter 4

Purification of Histidine$_x$-Tagged Proteins Using Membranes

Modified with Polymer Brushes

4.1. Introduction

Advances in genetic engineering have generated an ongoing need for efficient purification of recombinant proteins.[1] One of the most powerful methods for isolating such proteins, affinity chromatography, is based on specific interactions between immobilized ligands and an affinity tag (e.g., glutathione-S-transferrase (GST)[2], Streptavidin,[3] or polyhistidine[4]) that is appended to the protein of interest. Polyhistidine, the most frequently employed tag, allows purification by immobilized metal-affinity chromatography (IMAC),[5-8] where selectivity is usually based on the interaction of the polyhistidine with an immobilized Ni^{2+} complex. Proteins containing a polyhistidine tag (his tag) are selectively bound to the chromatographic matrix, while other cellular proteins are washed away.[9]

The advantages of IMAC, which include ligand stability, high protein loading, mild elution conditions, simple regeneration and low cost,[10] are very important when developing purification procedures. Nevertheless, this technique has some serious limitations, including long separation times, difficulties in packing large columns, relatively high pressure drops, and slow intra-bead diffusion of solutes.[11-13] These limitations will be particularly important for large scale separations.

In an effort to solve some of these problems that are general to affinity chromatography, membrane chromatography was first introduced in 1987.[14] In this technique flow of solution through membrane pores containing immobilized ligands enhances the rate of mass transport to the ligands, and scale up is in principle relatively simple.[9] Despite their potential, however, the major disadvantage of membrane absorbers is that their low specific surface area (when compared to porous beads) yields a relatively low binding capacity. To overcome this problem, we and others are developing membranes modified with polymer brushes that have multiple protein-binding sites.[15-18] The controlled growth of polymers in membrane pores using ATRP is particularly attractive because the thickness of the resulting polymer brushes can be readily controlled to optimize capacity without completely filling pores. Our previous study (Chapter 3 of this thesis) showed that growth of PHEMA from initiators bound to a porous alumina membrane followed by functionalization of the PHEMA with nitrilotriacetate-Cu^{2+} (NTA-Cu^{2+}) complexes resulted in membranes that bind large amounts of BSA and myoglobin, presumably via formation of a complex between the histidine groups of the proteins and the immobilized NTA-Cu^{2+}. Overall, the combination of a porous alumina support and functionalized polymer brushes yielded a remarkable binding capacity of 0.9 mg of BSA per cm^2 of external membrane surface (150 mg/cm^3 of membrane).

However, the NTA-Cu^{2+} complex, as suggested from the high BSA-binding capacity of membranes containing PHEMA-NTA-Cu^{2+} brushes, is prone to binding of many proteins and is not sufficiently selective to effectively purify his tagged proteins. This chapter describes the use of PHEMA-NTA-Ni^{2+}, rather than PHEMA-NTA-Cu^{2+}, brushes to modify membranes and selectively purify his tagged proteins. It is well

known that NTA-Ni^{2+} is highly selective for binding of his tagged proteins because the
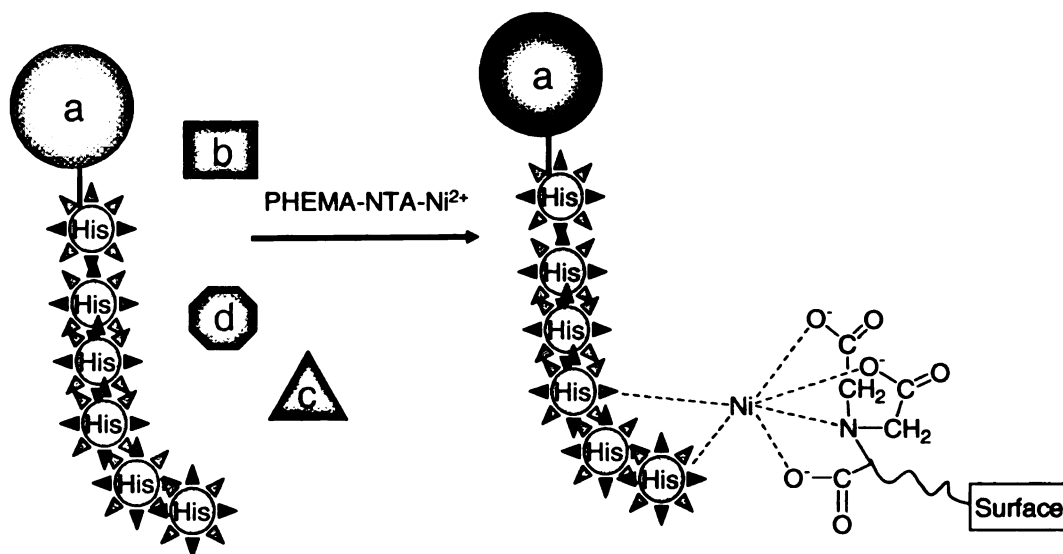
Figure 4.1. Selective binding of PHEMA-NTA-Ni^{2+} to a his tagged protein. (a: his tagged protein; b-d: non his tagged proteins).

interaction of NTA-Ni^{2+} with histidine is much weaker than the interaction of NTA-Cu^{2+} with histidine (Figure 4.1).[4, 19] Thus, polyhistidine is required for efficient binding to the NTA-Ni^{2+} complex. This work demonstrates that membranes modified with PHEMA-NTA-Ni^{2+} selectively bind his tagged ubiquitin (HisU) from solutions containing equal amount of HisU, myoglobin, and BSA or a 20-fold excess of BSA relative to HisU. Gel electrophoresis revealed that the purity of HisU recovered from such solutions is >99%, and that the binding capacity of these membranes is as high as 120 mg HisU/cm^3 of membrane (for a 0.3 mg/mL HisU solution).

4.2. Experimental Section

4.2.1. Materials

Anodisc^{TM} porous alumina membranes with 0.2 μm-diameter surface pores were obtained from Fisher Scientific. Dimethylformamide (DMF, anhydrous, 99.8%), 11-mercaptoundecanol (97%), 2-bromoisobutyryl bromide (98%), CuCl (99.999%), CuBr$_2$ (99%), 2,2'-bipyridyl (bpy, 99%), 1-[3-(dimethylamino)propyl]-3-ethylcarbodiimide hydrochloride (EDC), N-hydroxysuccinimide (NHS), 4-dimethylaminopyridine (DMAP), ethylenediamine tetraacetic acid (EDTA), imidazole (99%), TWEEN-20 surfactant, bovine serum albumin (BSA), ubiquitin (N-terminal histidine$_6$ tagged) and myoglobin were used as received from Sigma Aldrich. NiSO$_4$·5H$_2$O (Columbus Chemical), NaH$_2$PO$_4$ (CCI), Na$_2$HPO$_4$ (Aldrich), $N_\alpha N_\alpha$-bis(carboxymethyl)-L-lysine hydrate (Fluka, aminobutyl-NTA), succinic anhydride (SA, Matheson Coleman & Bell), and Coomassie protein assay reagent (Pierce) were also used as received. 2-Hydroxyethyl methacrylate (HEMA, Aldrich, 97%, inhibited with 300 ppm hydroquinone monomethyl ether) was purified by passing it through a column of activated basic alumina (Aldrich), and trichlorosilane initiator (11-(2-bromo-2-methyl)propionyloxy)undecyltrichlorosilane) was synthesized according to a literature procedure.[20] Buffers were prepared using analytical grade chemicals and deionized (Milli-Q, 18.2 MΩ cm) water.

4.2.2. Polymerization of HEMA in Porous Alumina Membranes and on Au Substrates

The procedure for polymerizing HEMA inside alumina membranes was reported in the last chapter. Briefly, the alumina membrane was sandwiched inside a membrane cell (Millipore, Swinnex 25), and the trichlorosilane initiator solution was first passed
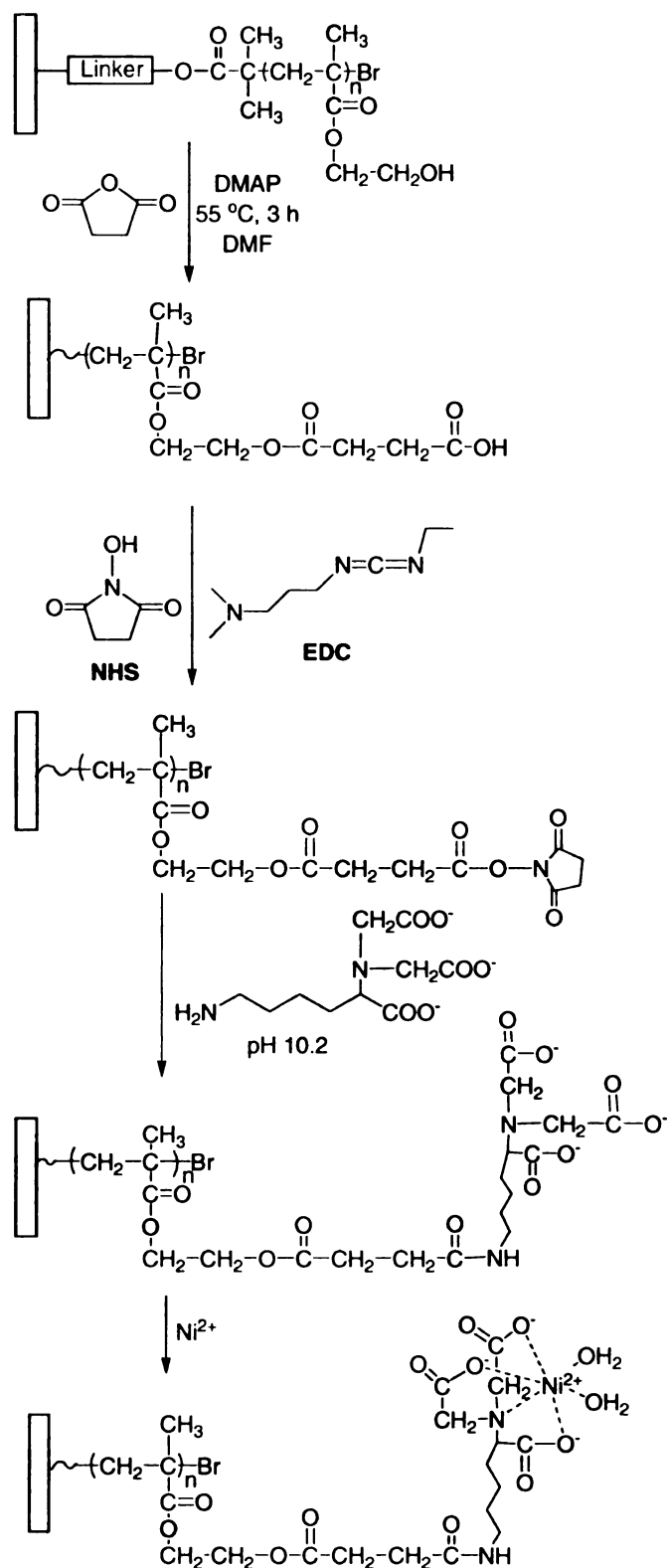
Scheme 4.1. Derivatization of PHEMA with NTA-Ni^{2+} before protein immobilization.

113

through the membrane followed by subsequent rinsing. Polymerization of HEMA occurred by circulating a degassed solution containing 15 mL of purified HEMA, 15 mL methanol, 82.5 mg (0.825 mmol) of CuCl, 54 mg (0.24 mmol) of $CuBr_2$, and 320 mg (2.04 mmol) of bpy through the initiator-modified membrane for 1 hour. After polymerization, the membrane was cleaned with flowing ethanol (20 mL), water (20 mL) and acetone (20 mL).

To prepare films for reflectance FTIR characterization, Au-coated silicon wafers were coated with a mercaptoundecanol monolayer that was subsequently derivatized with 2-bromoisobutyryl bromide as described previously.[21, 22] Polymerization of HEMA from these substrates occurred as described above, except that the substrate was simply immersed in a polymerization solution that was kept in a glove bag.

4.2.3. PHEMA Derivatization and Protein Immobilization

The derivatization procedure was also described in the last chapter and is shown in Scheme 4.1. However, in this case the NTA-derivatized membrane was exposed to a 0.1 M $NiSO_4$, rather than 0.1 M $CuSO_4$, solution and rinsed with solvents. A solution containing pure protein or a mixture of proteins (in 20 mM phosphate buffer, pH 7.2) was then pumped through the membrane using a peristaltic pump, and the permeate was collected for analysis at specific time intervals. Subsequently, the membrane was rinsed with 20 mL pH 7.2 washing buffer (20 mM phosphate buffer containing 0.1% Tween-20 surfactant and 0.15 M NaCl) and 20 mL phosphate buffer, and protein was eluted using 5-10 mL elution buffer (20 mM sodium phosphate, 0.5 M NaCl, 0.5 M imidazole, pH 7.4). Ni^{2+} was later eluted using a 50 mM EDTA solution (pH adjusted to 7.2), and the PHEMA-NTA film was recharged with Ni^{2+} prior to reuse. To prepare derivatized films

for reflectance FTIR characterization, a PHEMA film on a gold substrate was treated in a similar procedure by immersing the substrate in appropriate solutions and rinsing with solutions from a pipette.

4.2.4. Determination of the Amount of Coordinated Ni^{2+} in the Membrane

A calibration curve was obtained by measuring the UV-vis spectra of Ni^{2+}-EDTA standard solutions (5, 10, 20, 40 mM $NiSO_4$ in 50 mM EDTA at pH 7.2), and a sample solution was prepared by using 5.0 mL of 50 mM EDTA (pH 7.2) to remove Ni^{2+} from a PHEMA-NTA-Ni^{2+}-coated membrane. The UV-vis spectrum of the stripping solution was acquired, and the amount of Ni^{2+} in the solution was calculated using the calibration curve.

4.2.5. Determination of Protein Concentrations

To determine the concentration of protein in permeate and eluent solutions, 50 μL of the sample was added to 2.95 mL of a solution of Coomassie reagent, and the mixture was shaken a few times and allowed to react for 5 min at room temperature. The UV/vis absorbance spectra of these solutions were then obtained with a Perkin-Elmer UV/Vis (model Lambda 40) spectrophotometer. Calibration curves for the absorbance of BSA, HisU and myoglobin solutions at 595 nm were obtained using a series of protein solutions (concentration range of 100 μg to 1 mg of protein per mL) that were mixed with Coomassie reagent. All spectra were measured against a Coomassie reagent background.

4.2.6. Determination of Protein Purity by SDS-PAGE

The protein soutions were analyzed by SDS-PAGE with a 15% cross-linked separating gel and a 4% cross-linked stacking gel (acrylamide). Protein bands were visualized using a standard silver staining procedure.[13]

4.2.7. Film Characterization Methods

Reflectance FTIR spectra of films on gold-coated wafers were obtained with a Nicolet Magna-IR 560 instrument using a Pike grazing angle (80°) accessory. The spectrum of reflection from a UV/ozone-cleaned gold-coated wafer was used as a background. Film growth inside alumina membranes was verified using Transmission FTIR (Mattson Galaxy Series 3000) with an air background.

4.3. Results and Discussion

4.3.1. Characterization of PHEMA Derivatization

In the last chapter, we examined PHEMA formation inside the pores of alumina membrane using SEM and EDS, and verified derivatization of PHEMA only for films on Au-coated Si. Here I present transmission FTIR spectroscopy that demonstrates both the formation and derivatization of PHEMA within alumina membranes. Figure 4.2 shows the transmission FTIR spectra of PHEMA films and their derivatives inside the alumina membrane. To ensure that derivatization happens throughout the pores, we passed the reactant solutions through the membrane using a peristaltic pump. After each derivatization step, the membrane was taken out of the membrane cell, immersed in appropriate buffers, rinsed with ethanol and acetone and dried under a flow of nitrogen. We then placed the membrane in a holder for taking IR spectra, and a spectrum of air was used as a background. The transmission IR data are consistent with the spectra of films on gold surface and prove successful derivatization inside the alumina.
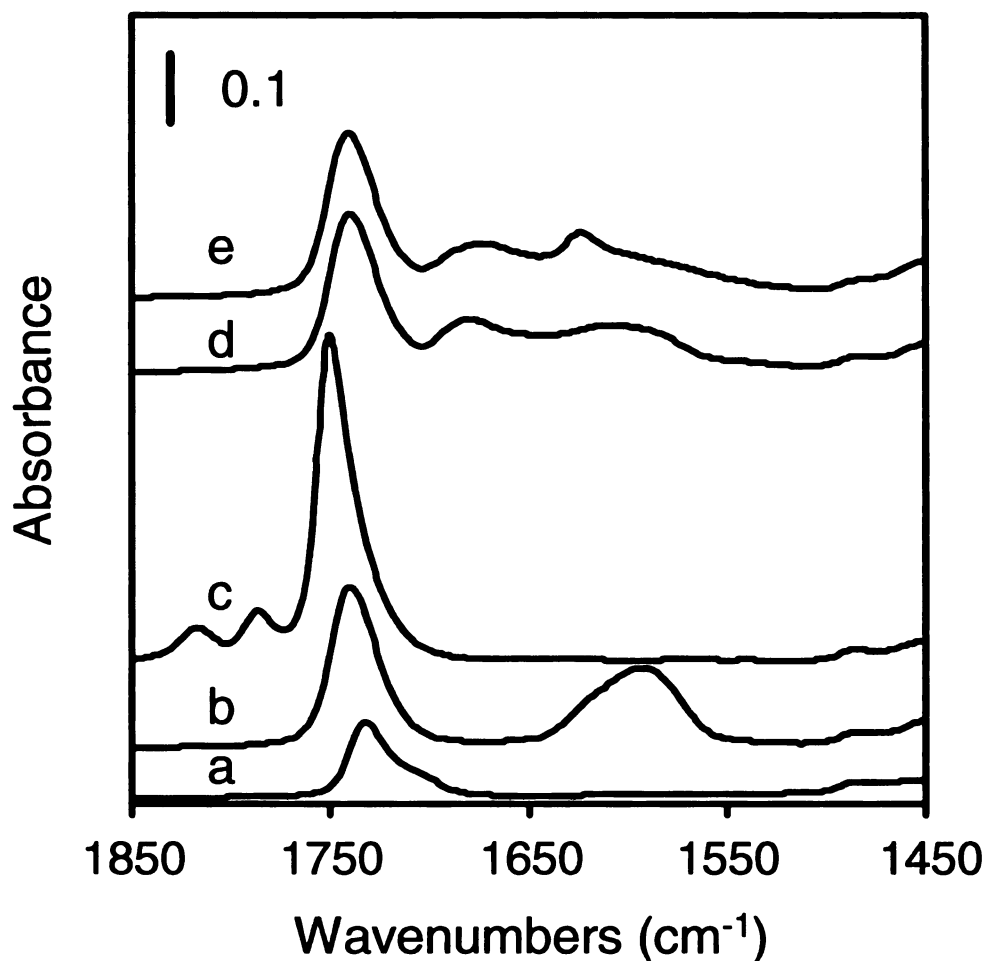
Figure 4.2. Transmission IR of (a) PHEMA films inside an alumina membrane before (a) and after the following sequential steps: (b) reaction with SA, immersion in a pH 9.9 buffer. (c) activation with EDC/NHS; (d) reaction with aminobutyl NTA followed by immersion in a pH 9.9 buffer; (e) exposure to 0.1 M Ni^{2+} to form NTA-Ni^{2+} complexes.

To be specific, we first passed a solution of SA in DMF through a PHEMA-derivatized membrane to create free –COOH groups in the film. We then immersed the membrane in pH 9.9 buffer for 15 min and rinsed with ethanol and acetone before taking a transmission IR spectrum. The absorbance at ~1740 cm⁻¹, which is assigned to ester

117

carbonyl groups, approximately doubled after SA derivatization (Figure 4.2b), suggesting a high degree of conversion of the –OH groups of PHEMA to ester groups. A new peak also appeared at ~1594 cm^{-1}, which is consistent with the deprotonation of the newly introduced carboxylic acid groups.

Passing a 0.1 M mixture of EDC and NHS in water (pH~4.9) through the membrane converted —COOH groups to succinimidyl esters. The membrane was then rinsed with water, ethanol and acetone. Peaks due to the succinimide ester appeared at 1817 and 1786 cm^{-1} (Figure 4.2c). The asymmetric stretch of succinimide (~1753 cm^{-1}) overlaps with the C=O stretch (1740 cm^{-1}) of the previously formed esters to yield a broad peak with an absorbance that is about double that for the ester carbonyl after SA derivatization. The new peak at 1817 cm^{-1} is due to the carbonyl stretch of the active ester formed by reaction with NHS, while the absorbance at 1786 cm^{-1} results from the symmetric succinimide stretch.

The EDC/NHS-activated PHEMA was then reacted with aminobutyl-NTA ($N_{\alpha}N_{\alpha}$-bis(carboxymethyl)-L-lysine hydrate) and immersed in pH 9.9 buffer for 15 min and rinsed with ethanol and acetone. Reaction of the active ester with both aminobutyl NTA and water resulted in the loss of the active ester absorbances, and the shift of the 1753 cm^{-1} peak back to 1740 cm^{-1} (Figure 4.2d). The new peak at 1680 cm^{-1} provides evidence for NTA immobilization and is probably due to the COO$^-$ groups from NTA as well as the amide bond formed between SA and NTA. The broad absorbance centered at 1600 cm^{-1} could result from carboxylate groups in either NTA or the hydrolyzed active esters.

Exposure of NTA-derivatized PHEMA to 0.1 M NiSO$_4$ followed by rinsing with water yielded immobilized NTA-Ni^{2+} that is capable of binding proteins through their histidine groups. Unfortunately, there was no large change in the IR spectrum (Figure 4.2e) of the film after Ni^{2+} coordination except that the peak at 1600 cm^{-1} appeared to shift to 1630 cm^{-1} and become sharper. The shift could be due to the fact that spectrum (d) was measured after treatment with pH 9.9 buffer, while the sample for spectrum (e) was not treated with this buffer because Ni(OH)$_2$ might precipitate in the film at high pH. The similarity is probably due to the high spectral similarity of the Na$^+$ and Ni^{2+} salts of NTA. XPS data for a PHEMA-NTA-Ni^{2+} film on a gold substrate (Figure 4.3) confirmed the presence of Ni^{2+} in these films and showed a Ni : N ratio of 0.5 : 1, which is consistent with our previous results and indicative of one Ni^{2+} per NTA moiety.[15, 17]
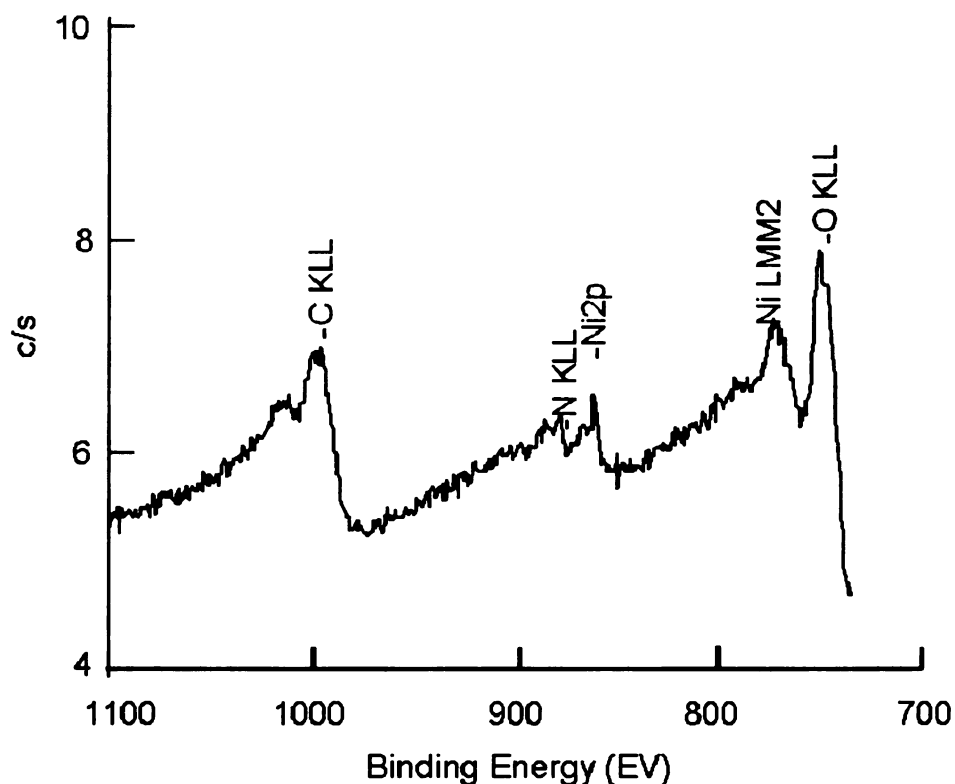
Figure 4.3.   XPS spectrum of a PHEMA-NTA-Ni^{2+} film on a gold substrate.

To determine how much Ni^{2+} was bound to the PHEMA-NTA films inside

alumina membranes, we passed 5 mL of 50 mM EDTA through a PHEMA-NTA-Ni^{2+}-
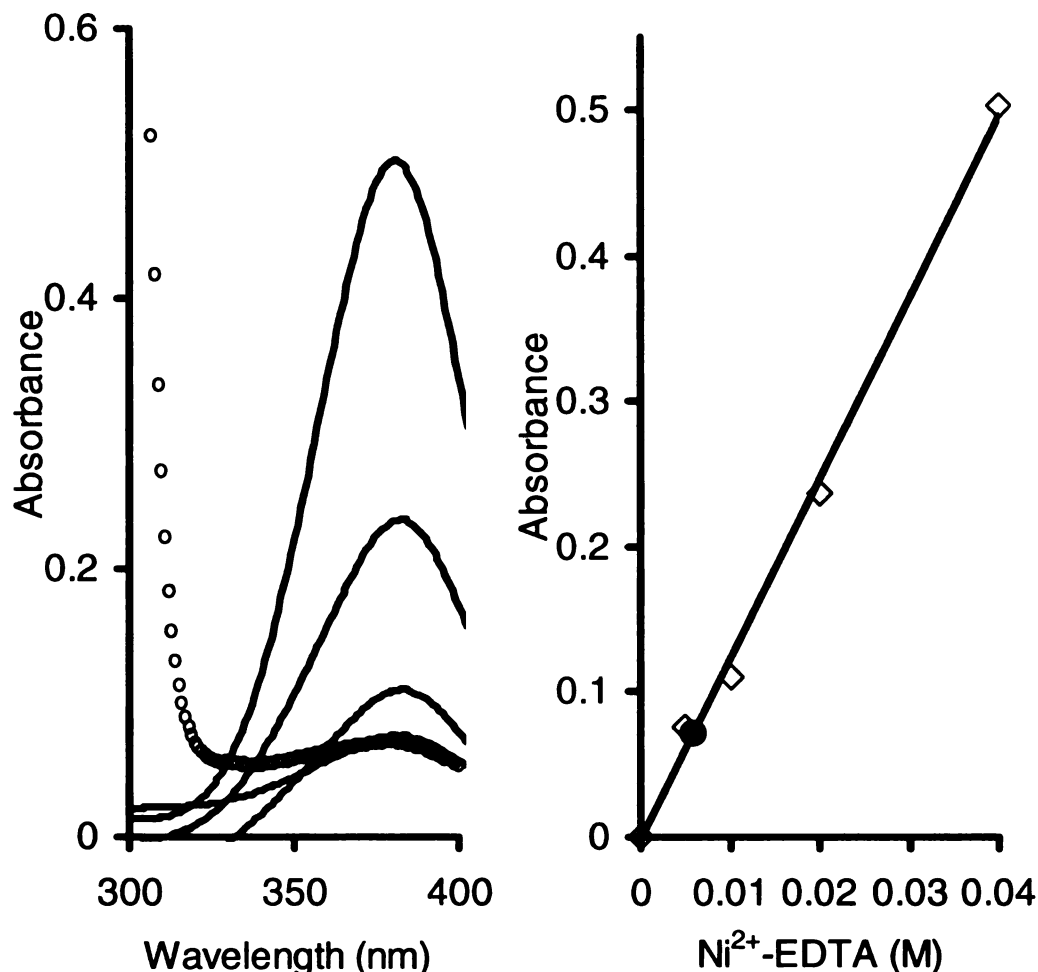
Figure 4.4. Determination of the amount of immobilized Ni^{2+} in a PHEMA-NTA-Ni^{2+} film in the membrane. The figure on the left shows the calibration spectra for Ni^{2+}-EDTA standards (solid lines) as well as the spectrum of the sample (circle), which was prepared by passing 5.0 mL of 50 mM EDTA (pH 7.2) through a PHEMA-NTA-Ni^{2+}-derivatized alumina membrane. The plot on the right shows the calibration curve for absorbance at 384 nm and indicates the absorbance of the sample.

coated membrane and subsequently analyzed the EDTA solution for Ni^{2+} using UV-vis spectroscopy (Figure 4.4). According to this procedure, the amount of Ni^{2+} bound in the membrane is 29.5 μmol. Considering the effective surface area of the membrane is ~1500 cm^2 (pore diameter of 0.25 μm, 50% porosity, and a membrane thickness of 60 μm), this corresponds to a Ni^{2+} coverage of 18.4 $nmol/cm^2$. Bruening and coworkers reported Cu^{2+} coverage to be 70 $nmol/cm^2$ for a 55 nm PAA film derivatized with NTA-Cu^{2+} on a gold substrate.[15] Our Ni^{2+} coverage is ~¼ of the previously reported Cu^{2+} coverage, presumably because of a thinner PHEMA film (10 nm according to flow experiments).[17]

4.3.2. HisU Binding to PHEMA-NTA-Ni^{2+} Brushes on Gold Substrates

A gold substrate modified with PHEMA-NTA-Ni^{2+} was immersed in a solution containing 0.01 mg/mL HisU in pH 7.2 phosphate buffer for 2 hours followed by immersion in pH 7.2 phosphate buffer (no HisU) for 15 min and rinsing in EtOH. The spectrum of the film showed growth in the absorbance at 1680 cm^{-1} (amide I band) and the appearance of a small peak at 1545 cm^{-1} (amide II band), similar to the BSA binding spectrum shown in last chapter (Figure 3.1). Subtracting the spectrum of PHEMA-NTA-Ni^{2+} from that of PHEMA-NTA-Ni^{2+}-HisU yielded a bound-HisU spectrum, which is dominated by amide absorbances (Figure 4.5a). (The negative peak at 1740 cm^{-1} likely result from deprotonation of some –COOH groups.)

Comparison of the amide intensities in Figure 4.5a with those of spin-coated films of pure HisU with known thicknesses suggests that about 31 nm of HisU adsorbed to this film. This corresponds to a binding capacity of 3.1 $\mu g/cm^2$ or about 8 monolayers of HisU (assuming a HisU density of 1 g/cm^3 and a monolayer thickness of 4.0 nm).[17]
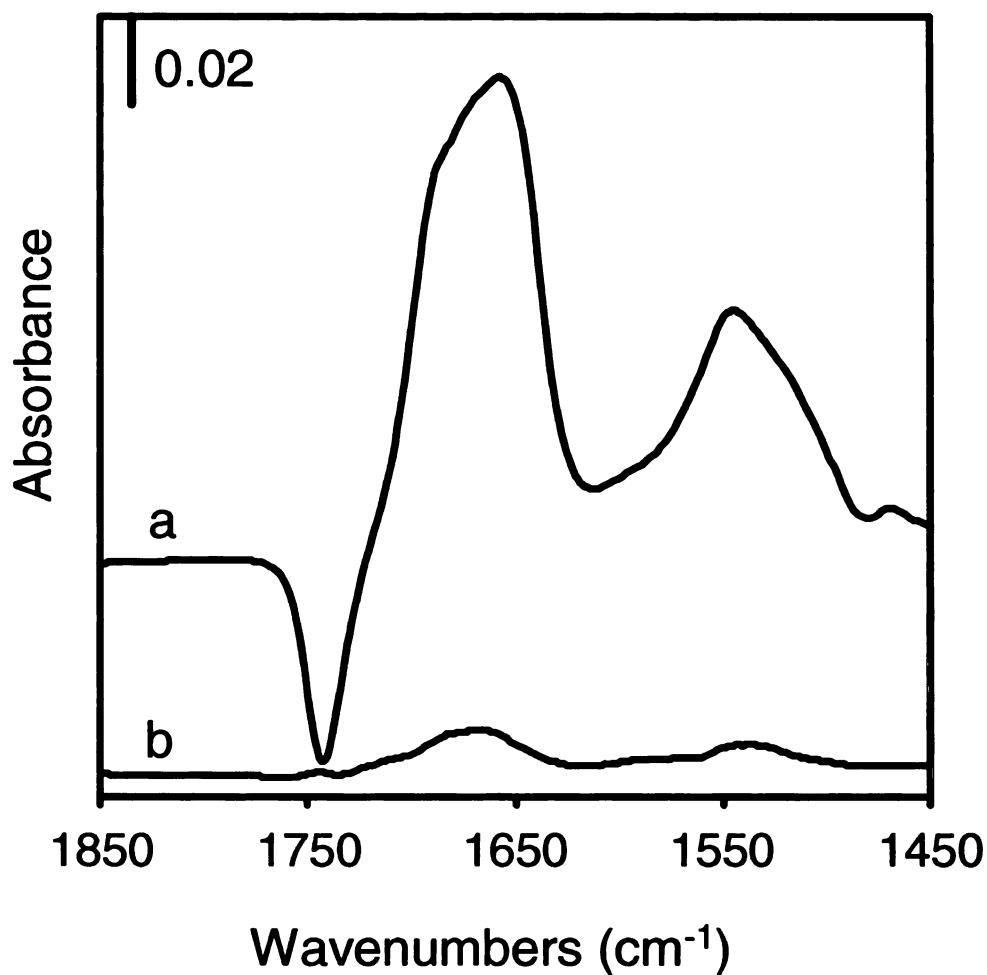
Figure 4.5. Subtracted reflectance FTIR spectra of protein immobilized on PHEMA-NTA-Ni^{2+} films after exposure of the films to (a) 0.01 mg/mL HisU or (b) 1 mg/mL BSA. The spectra were obtained by subtracting the spectrum of PHEMA-NTA-Ni^{2+} from that of PHEMA-NTA-Ni^{2+}-protein (both films were rinsed with buffer and ethanol prior to the measurement).

To show that PHEMA-NTA-Ni^{2+} films bind his tagged species selectively over other proteins, we also immersed these coatings in 1 mg/mL, stirred BSA solutions for ~15 h. The amide intensities in the bound BSA spectrum (Figure 4.5b) show that only 3.2 nm of

BSA was absorbed to the film, or <10% of the amount of HisU that bound to these coatings. Moreover, the concentration of HisU in solution was 0.01 mg/mL, while that of BSA was 100-fold higher. At concentrations of 0.01 mg/mL, no BSA binding to PHEMA-NTA-Ni^{2+} was detected.

4.3.3. HisU Binding to PHEMA-NTA-Ni^{2+} Brushes in Membranes

To test the HisU binding capacity of PHEMA-NTA-Ni^{2+} films in membranes, we pumped 10 mL of a 0.3 mg/mL HisU solution in pH 7.2 phosphate buffer through the membrane, collected the permeate over specific time intervals and analyzed the permeate samples using a Bradford assay. The breakthrough curve for HisU binding to PHEMA-NTA-Ni^{2+} in membranes and similar curves for BSA and myoglobin binding to PHEMA –NTA-Cu^{2+}-modified membranes are shown in Figure 4.6. PHEMA-NTA-Cu^{2+} modified membranes showed high binding capacities for both BSA (0.67 mg/cm^2) and myoglobin (0.50 mg/cm^2), but the PHEMA-NTA-Ni^{2+}-modified membrane showed an even higher binding capacity for HisU (0.72 mg/cm^2). Moreover, the breakthrough curve was much sharper for HisU. The sharpness of the breakthrough curves increases with decreasing molecular mass of the absorbing species, and suggests more rapid diffusion of smaller proteins into the polymer brushes. Full breakthrough curves for BSA and myoglobin binding to membranes with PHEMA-NTA-Ni^{2+} brushes could not be obtained because of the minimal binding in this case.
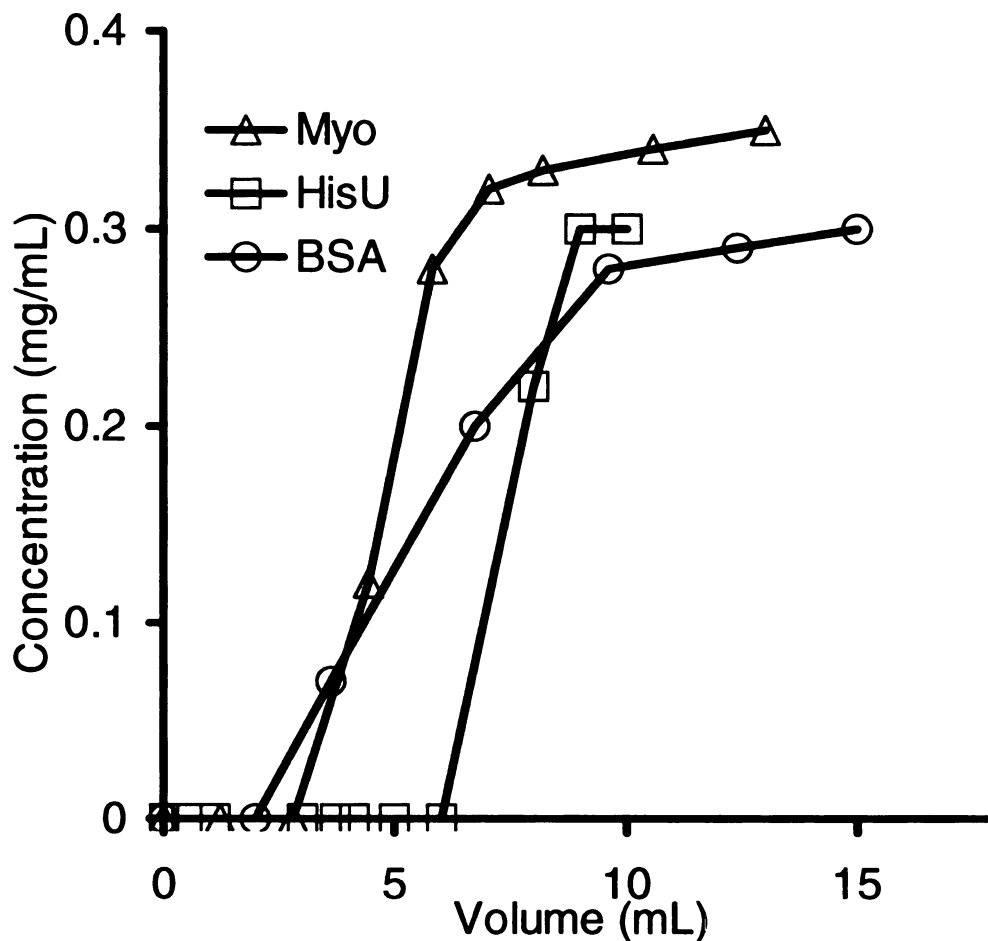
Figure 4.6. Breakthrough curves for adsorption of 0.3 mg/mL HisU, 0.3 mg/mL BSA, and 0.35 mg/mL myoglobin in membranes modified with PHEMA-NTA-Ni^{2+} (HisU) or PHEMA-NTA-Cu^{2+} (BSA and myoglobin). The permeate flow rate was initially 2.4 mL/min and 0.9 mL/min at the end of the experiment.

After measuring the breakthrough curve of HisU, the PHEMA-NTA-Ni^{2+}-HisU membrane was washed with 20 mL washing buffer followed by 20 mL phosphate buffer, and HisU was then eluted with 5-10 mL elution buffer (imidazole). Analysis of the eluent using a Bradford assay showed that 99% of the bound HisU was recovered.

To prove that PHEMA-NTA-Ni^{2+} films selectively bind HisU, we also investigated the binding of BSA and myoglobin to PHEMA-NTA-Ni^{2+} films in membranes. A PHEMA-NTA-Ni^{2+}-derivatized membrane was first loaded with 10 mL of 0.2 mg/mL BSA or 10 mL of 0.2 mg/mL myoglobin in buffer. After washing the membrane with washing buffer, we passed 6 mL of elution buffer through the membrane and analyzed both the feed solutions before passing through the membrane and eluents. Figure 4.7 a is the UV-vis spectrum of the 0.2 mg/mL BSA feed solution, while Figure 4.7 b is the spectrum of the eluent from the membrane loaded with BSA. The absorbance of the eluent at 595 nm is <0.001, showing that an undetectable amount of BSA was bound to and eluted from the membrane. Similar spectra for myoglobin (spectra 4.7 c and d show that the membrane binds a small amount (0.05 mg) myoglobin. However, the amount of myoglobin bound is only 3% of the amount of HisU bound under similar conditions.
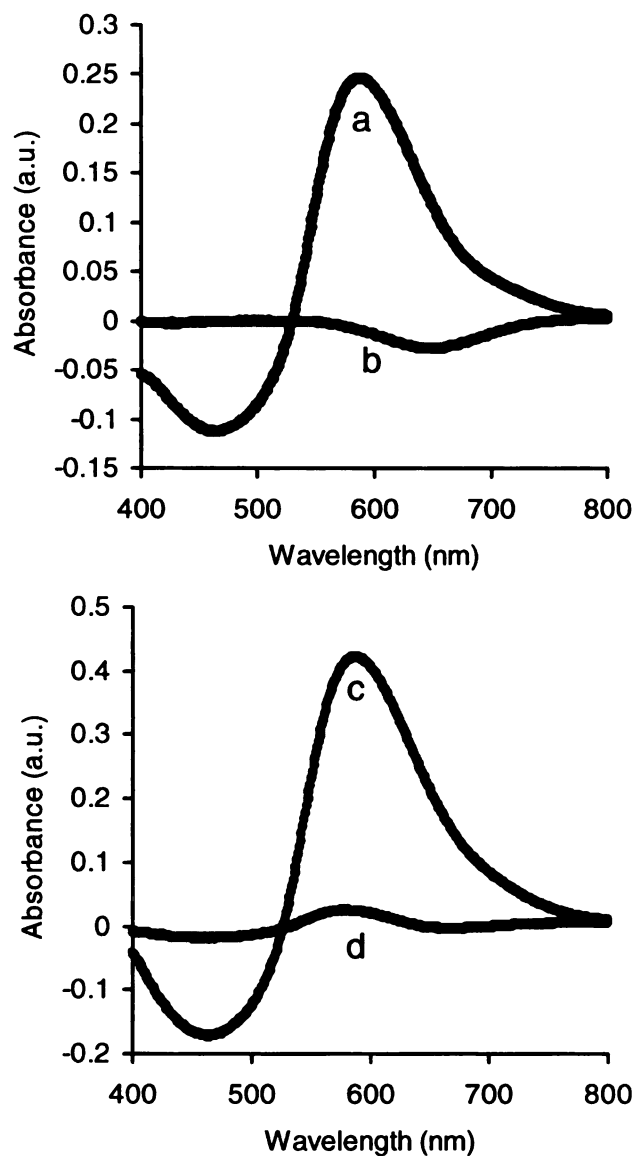
Figure 4.7. UV-vis spectra of (a) a 0.2 mg/mL BSA solution; (b) eluent (imidazole

solution) from an alumina-PHEMA-NTA-Ni^{2+}membrane treated with 10 mL of 0.2

mg/mL BSA solution and washing buffer; (c) a 0.2 mg/mL myoglobin solution; (d)

Eluent (imidazole solution) from an alumina-PHEMA-NTA-Ni^{2+}membrane treated

with 10 mL of 0.2 mg/mL myoglobin solution and washing buffer. All solutions

were mixed with Coomassie reagent prior to measurement of the spectra, and blank

Coomassie reagent was used as a background.

4.3.4. Separation of Protein Mixtures

Two sets of experiment were carried out to test the ability of alumina-PHEMA-NTA-Ni^{2+} membranes to purify his tagged proteins. In the first experiment, 6 mL of phosphate buffer containing BSA, myoglobin and HisU (0.05 mg/mL each) was passed through the PHEMA-NTA-Ni^{2+}-derivatized membrane, and the membrane was then rinsed with 20 mL washing buffer followed by 20 mL phosphate buffer. Finally, we used 5-10 mL elution buffer to recover the bound protein and then analyzed the eluent by electrophoresis. We then washed the membrane with 10 mL of 50 mM EDTA and rinsed it with water. After recharging the membrane with 0.1 M Ni^{2+} and rinsing with 20 mL water and 20 mL phosphate buffer, in a second experiment, 10 mL of phosphate buffer containing 1 mg/mL BSA and 0.05 mg/mL HisU was passed through the membrane, and the membrane was rinsed, treated with elution buffer, and analyzed using the procedure described above.

Figure 4.8 shows SDS-PAGE analyses of the protein samples. Lanes 2 and lane 6 are the feed and eluent of the first experiment. Bands for all three proteins are clearly visible for the feed solution, but only a HisU band appears in the eluent, showing that the membrane selectively binds HisU. The gel suggests that the purity of the HisU is >99%. Lanes 7 and 8 demonstrate the results for the second experiment with a solution containing 1 mg/mL BSA and 0.05 mg/mL HisU. In this case, only HisU appears in the electropherogram of the eluent, even though BSA was in 20-fold excess in the feed. Purity of the HisU relative to BSA is at least 99%. Analysis of the protein concentration in the eluent using a Bradford assay showed that essentially all of the bound HisU

(>99%) was eluted. These experiments clearly demonstrate the ability of PHEMA-NTA-Ni^{2+}-modified membranes to purify his tagged proteins.
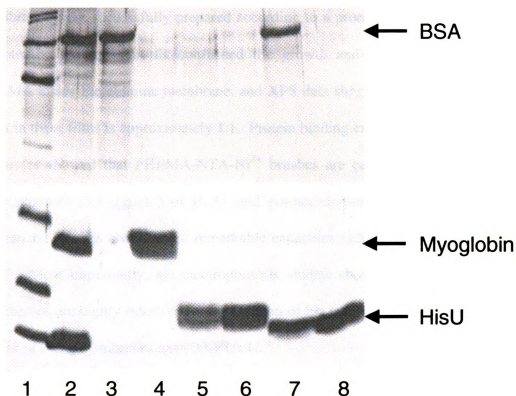
Figure 4.8. SDS-PAGE analysis (silver staining) of protein solutions and eluents from alumina-PHEMA-NTA-Ni^{2+} membranes loaded with proteins. Samples are: lane 1, standard broad range ladder; lane 2, mixture of BSA, myoglobin and HisU (0.05 mg/mL each); lane 3, pure BSA; lane 4, pure myoglobin; lane5, pure HisU; lane 6, eluent from a membrane loaded with a mixture of BSA, myoglobin and HisU (0.05 mg/mL each); lane 7, mixture of BSA and HisU; lane 8, eluent from a membrane loaded with 10 mL of a solution containing 1 mg/mL BSA and 0.05 mg/mL HisU.

4.4. Conclusions

PHEMA-NTA-Ni^{2+} brushes immobilized on both gold substrates and alumina membranes were successfully prepared according to a procedure similar to that given in Chapter 3. Transmission IR confirmed the growth and successful derivatization of PHEMA inside the alumina membrane, and XPS data suggested that the ratio of Ni^{2+} to NTA in these films is approximately 1:1. Protein binding experiments with films on gold substrates showed that PHEMA-NTA-Ni^{2+} brushes are capable of selectively binding large amounts (3.1 μg/cm^2) of HisU, and porous alumina membranes modified with derivatized brushes also showed remarkable capacities (120 mg/cm^3) for the binding of HisU. Most importantly, gel electrophoresis studies showed that these high-capacity membranes are highly selective for purification of his tagged proteins. Even in a 20-fold excess of BSA, membranes gave 99% HisU.

4.5. References

1. Zhen, G.; Falconnet, D.; Kuennemann, E.; Voros, J.; Spencer, N. D.; Textor, M.; Zurcher, S., *Adv. Funct. Mater.* **2006**, *16*, 243-251.

2. Draveling, C.; Ren, L.; Haney, P.; Zeisse, D.; Qoronfleh, M. W., *Protein Expression Purif.* **2001**, *22*, 359-366.

3. Skerra, A.; Schmidt, T. G., *Biomol. Eng.* **1999**, *16*, 79-86.

4. Stiborova, H.; Kostal, J.; Mulchandani, A.; Chen, W., *Biotechnol. Bioeng.* **2003**, *82*, 605-611.

5. Gaberc-Porekar, V.; Menart, V., *J. Biochem. Biophys. Methods* **2001**, *49*, 335-360.

6. Everson, R. J.; Parker, H. E., *Bioinorg. Chem. Appl.* **1974**, *4*, 15-20.

7. Porath, J.; Olin, B., *Biochemistry* **1983**, *22*, 1621-1630.

8. Porath, J.; Carlsson, J.; Olsson, I.; Belfrage, G., *Nature* **1975**, *258*, 598-599.

9. Suen, S.-Y.; Liu, Y.-C.; Chang, C.-S., *J. Chromatogr. B* **2003**, *797*, 305-319.

10. Ozkara, S.; Yavuz, H.; Denizli, A., *J. Appl. Polym. Sci.* **2003**, *89*, 1567-1572.

11. Zou, H.; Luo, Q.; Zhou, D., *J. Biochem. Biophys. Methods* **2001**, *49*, 199-240.

12. Che, S.; Liu, Z.; Ohsuna, T.; Sakamoto, K.; Terasaki, O.; Tatsumi, T., *Nature* **2004**, *429*, 281-284.

13. Clairbois, A. S.; Letourneur, D.; Muller, D.; Jozefonvicz, J., *J. Chromatogr. B* **1998**, *706*, 55-62.

14. Henis, J. M. S.; Tripodi, M. K.; Stimpson, D. I. European Patent 0,221,046B1, October 30, 1987.

15. Dai, J.; Bao, Z.; Sun, L.; Hong, S. U.; Baker, G. L.; Bruening, M. L., *Langmuir* **2006**, *22*, 4274-4281.

16. Kawai, T.; Saito, K.; Lee, W., *J. Chromatogr. B* **2003**, *790*, 131-142.

17. Sun, L.; Dai, J.; Baker, G. L.; Bruening, M. L., *Chem. Mater.* **2006**, *18*, 4033-4039.

18. Ulbricht, M.; Yang, H., *Chem. Mater.* **2005**, *17*, 2622-2631.

19.   Johnson, R. D.; Arnold, F. H., *Biotechnol. Bioeng.* **1995,** *48*, 437-443.

20.   Matyjaszewski, K.; Miller, P. J.; Shukla, N.; Immaraporn, B.; Gelman, A.; Luokala, B. B.; Siclovan, T. M.; Kickelbick, G.; Vallant, T.; Hoffmann, H.; Pakula, T., *Macromolecules* **1999,** *32*, 8716-8724.

21.   Kim, J.-B.; Bruening, M. L.; Baker, G. L., *J. Am. Chem. Soc.* **2000,** *122*, 7616-7617.

22.   Kim, J.-B.; Huang, W.; Bruening, M. L.; Baker, G. L., *Macromolecules* **2002,** *35*, 5410-5416.

Chapter 5

Summary and Future Work

The research in this dissertation investigated the application of polymer brushes in two areas: high flux pervaporation and high capacity protein binding. In chapter 2, I discussed the synthesis of ultrathin polymer films at the surface of porous substrates to prepare high-flux pervaporation membranes. Chapter 3 explored the growth of brushes in the interior of porous substrates to prepare membranes with unusually high protein adsorption capacities. Chapter 4 expanded on the protein adsorption work and demonstrated that polymer brushes derivatized with Ni^{2+} complexes are very attractive for purification of his tag proteins.

In applications of polymer brush-containing membranes as adsorbers, although brush-modified alumina membranes are capable of high-capacity protein binding, they
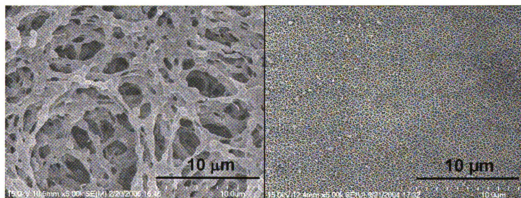
Figure 5.1. FESEM image of a PVDF membrane (left) with a nominal cutoff of 0.45 µm and an alumina membrane (right) with pore size of 0.25 µm.

suffer from low flux, fragility, and high cost. The largest pores available in commercial alumina membranes are 0.25 μm in diameter (Figure 5.1), and this greatly limits the flux available with these systems. To overcome this challenge, our future research aims at extending the very promising results with BSA and HisU binding to derivatized PHEMA brushes in porous alumina to the preparation of polymer brushes in porous polymer supports (Figure 5.1). The PVDF membrane shown in Figure 5.1 has a nominal filtration cutoff of 0.45 μm, but as can be seen pore sizes are much larger than this. Most polymer supports are both more robust and less expensive than the alumina substrates, and more importantly, careful control over pore geometry in the polymeric substrates will allow the increased permeabilities needed for high-flux, high-capacity membrane separations. Nevertheless, formation of high-capacity absorbers in polymer supporters will require new chemistries for initiator attachement, and could be quite difficult because of the incompatibilitiy of many polymeric materials with organic solvents. Relatively thick, highly adsorbing brushes will also be needed to maintain high capacities in large pores.

PHEMA-NTA-Ni^{2+}-modified membranes showed excellent performance in selectively recovering HisU from protein mixtures. However, much more research needs to be done with complex systems such as whole cell extracts and sera. Additionally, after demonstrating separations from complex mixtures, we will need to remove imidazole from the isolated protein and cleave the his tag to obtain the desired product. However, literature procedures including size exclusion chromatography and dialysis are already available for these final purification steps.[1, 2]

In the case of pervaporation membranes, we have demonstrated that ultrathin, brush skins allow high flux and reasonable selectivity. However, further research into

polymerization of monomers which are more suitable for pervaporation should give membranes with an order of magnitude improvement in both flux and selectivity. The appendix describes some unfinished research in this direction. Brush membranes prepared from high performance monomers will provide far superior performance to that of commercial membrane systems.

References

1.   Colangeli, R.; Heijbel, A.; Williams, A. M.; Manca, C.; Chan, J.; Lyashchenko, K.; Laura Gennaro, M., *J. Chromatogr. B* **1998**, *714*, 223-235.

2.   Casey, J. L.; Keep, P. A.; Chester, K. A.; Robson, L.; Hawkins, R. E.; Begent, R. H. J., *J. Immunol. Methods* **1995**, *179*, 105-116.

Appendix

Preliminary Work in Separating Organic Solvent Mixtures Using Other Ultrathin Polymer Membranes

Introduction

Ethyl acetate–hexane mixtures are used as eluents in liquid chromatography in academic laboratories, as well as in the pharmaceutical and chemical industry. Conventional distillation-based separations of ethyl acetate and hexane for recycling are not possible, however, due to the formation of an azeotropic mixture (Figure A1). In this study, I examined the possibility of using a polymer membrane to recover hexane from
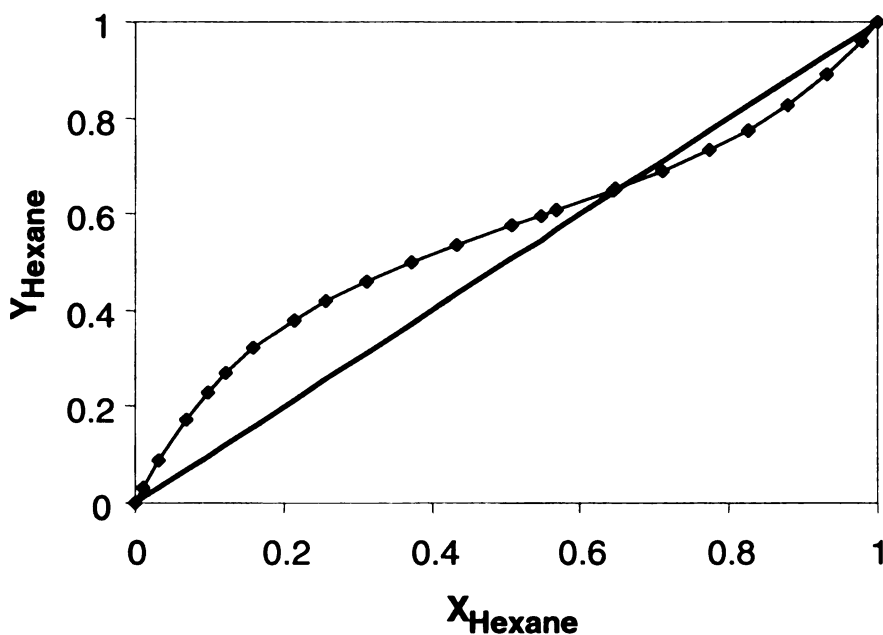
Figure A1. Vapor liquid equilibrium of ethyl acetate-hexane mixtures at 101.32 kPa. (The X and Y axes are the fractions of hexane in the liquid and vapor phases, respectively.)

ethyl acetate-hexane mixture. This appendix also describes efforts aimed at the polymerization of dimethyldi(methacryloyloxy-1-ethoxy)silane (DMDMAES) from a surfac to prepare ultrathin membranes with pervaporation properties similar to those of PDMS.

Experiments and Results

Materials

Poly(allylamine hydrochloride) (PAH) (Mw = 70,000), sodium poly(styrenesulfonate) (PSS) (Mw = 70,000), 3-mercaptopropionic acid (MPA), dimethylformamide (DMF, anhydrous, 99.8%), tetrahydrofuran (THF, anhydrous, inhibitor free, 99.8%), acetone (anhydrous, 99%), 2-bromopropionylbromide (2-BPB), and CuBr (99.999%) were used as received from Aldrich. $MnCl_2$ (Acros) and NaBr (Spectrum) were also used as received. HEMA (Aldrich, 97%, inhibited with 300 ppm hydroquinone monomethyl ether) was purified by passing it through a column of activated basic alumina (Spectrum). Dichlorodimethylsilane (99%), triethylamine (Et_3N, 99.5%), and N, N, N', N', N''-Pentamethyldiethylenetriamine (PMDETA,99%) were also purchased from Aldrich and used as received. Pervaporation experiments were performed using analytical grade ethyl acetate and hexane (Aldrich). Anodisc™ porous alumina membranes (Fisher) with 0.02 μm-diameter surface pores were used as supports for membrane formation, while gold-coated wafers (200 nm of sputtered Au on 20 nm Cr on a Si (100) wafer) were employed as substrates for ellipsometry and reflectance Fourier Transform Infrared (FTIR) spectroscopy.

Monomer Synthesis

Dimethyldi(methacryloyloxy-1-ethoxy)silane (DMDMAES, Figure A2), was prepared following a literature by the etherification reaction of HEMA with dichlorodimethylsilane in anhydrous THF in the presence of Et_3N (base).[1] Specifically, THF (100 mL), Et_3N (24.7 mL, 17.9 g, 0.177 mol), and HEMA (18.3 mL, 19.6 g, 0.151 mol) were added to a 250 mL round-bottom flask and kept under a dry nitrogen atmosphere. The contents were stirred and cooled to 0-5 °C in an ice bath.. Next, dichlorodimethylsilane (7.3 mL, 7.8 g, 0.060 mol) was added slowly for 5 minutes to the mixture while stirring, giving an exotherm (3.2-10.8 °C), and the reaction mixture was stored in a refrigerator overnight. Filtering of the reaction mixture removed the precipitated triethylamine hydrochloride, and THF (50 mL) was then added to wash the filtrate. THF and unreacted Et_3N were subsequently removed under reduced pressure using a rotary evaporator at room temperature. The resulting oily residue was purified by column chromatography (silica gel/CH_2Cl_2: hexane 75:25) to give an oily liquid, which was then distilled under vacuum. The purity (>95%) of this cross-linkable monomer was confirmed by 1H NMR spectroscopy, and the relevant spectrum is displayed in Figure A2.
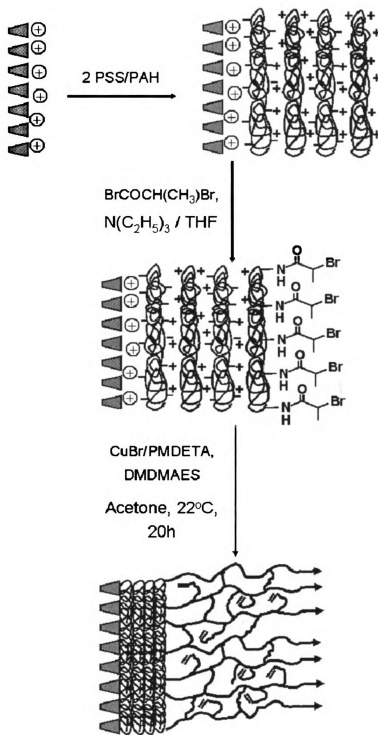
Polymerization of DMDMAES

Before polymerization, we first deposited a multilayer polyelectrolyte film on the substrate and subsequently attached initiators to these modified surfaces. The initiator anchoring was done according to the literature procedure outlined in scheme A1.[2] Polymerization of DMDMAES occurred by immersion of the initiator-coated substrate in a degassed acetone solution containing DMDMAES and a CuBr/PMDETA catalyst system (Scheme A1). To be specific, 43.2 mg CuBr, 10 mL
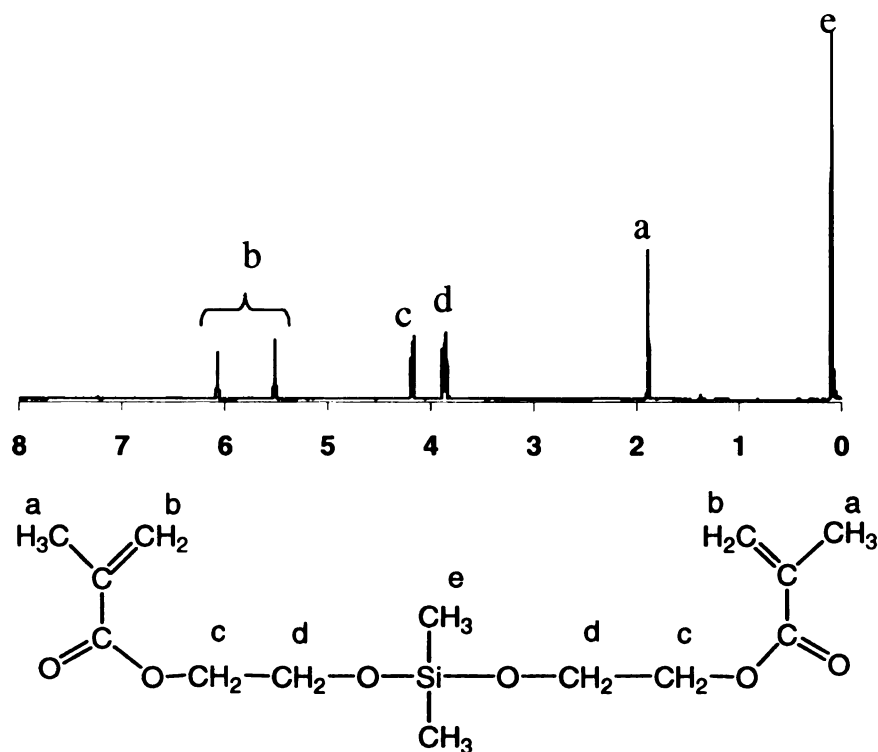
Figure A2. ¹H NMR spectrum of DMDMAES in CDCl₃.

DMDMAES and 10 mL acetone were first mixed in a Schlenk flask and degassed via three freeze-pump-thaw cycles. Then, 62.7 µL of PMDETA was quickly added to the mixture, which was then subjected to another freeze-pump-thaw cycle and stirred until a clear blue solution formed. Initiator-coated substrates and the sealed flask containing the polymerization solution were then transferred to a glove bag that was purged with nitrogen for about 1 h. The polymerization solution was finally transferred to the container holding the substrates, and polymerization was carried out for 20 h.

Scheme A1. Schematic diagram showing polymerization of DMDMAES from a polyelectrolyte surface modified with an initiator. PSS stands for poly(styrenesulfonate), and PAH represents protonated poly(allylamine).

FTIR Characterization of Membranes

The FTIR spectrum (Spectrum a, Fig. A3) of initiator attached to 5 PSS/PAH bilayers has a strong peak intensity in the amide region (1650–1560 cm^{-1}), indicating initiator attachment. After growth of a PDMDMAES film, a strong carbonyl peak appeared at 1730 cm^{-1} in the spectrum (Spectrum b, Fig. A3) as well as a C=C stretching band (1637 cm^{-1}) from unpolymerized vinyl groups. Ellipsometry results show that the polymerized film has a thickness of about 25 nm, including the polyelectrolyte layer which was 15 nm thick.
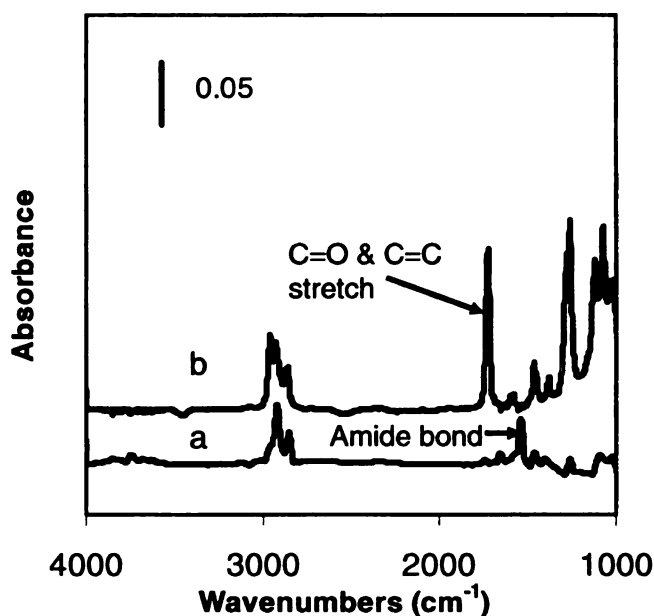

Figure A3. Reflectance FTIR spectra of (a) the initiator attached onto 5 bilayers of PSS/PAH film, (b) PDMDMAES film after 20 h growth from (a).

Pervaporation Experiments

Pervaporation was performed at room temperature with mixtures of ethyl acetate and hexane. Figure A4 shows the effect of feed concentration on the performance of the membrane. As the weight fraction of hexane in the feed solution increases from 20% to 80%, the weight fraction of hexane in the permeate rapidly increase until it reaches a limiting value. Our membrane greatly outperformed the vapor–liquid equilibrium separation achievable by vacuum distillation, and permeate compositions were not affected by the formation of the hexane/ethyl acetate azeotrope, as shown in Figure A4 (a). The hydrophobic nature of the membrane allows preferential adsorption of hexane, which likely swells the membrane due to its hydrophobicity. The total flux of hexane/ethyl acetate mixture increases with the hexane concentration in the feed, while selectivity, initially increases and then decreases as the hexane concentration in the feed increases. This is presumably because at the initial stage, the membrane is swollen by hexane and preferentially absorbs hexane molecules. At extremely high swelling, however, both hexane and ethyl acetate can diffuse through the membrane at similar rates, and selectivity declines.

Future Work

Growth of a series of PDMS-like polymers from porous alumina supports using ATRP should be investigated. The pervaporation performance of these polymers also needs to be examined.
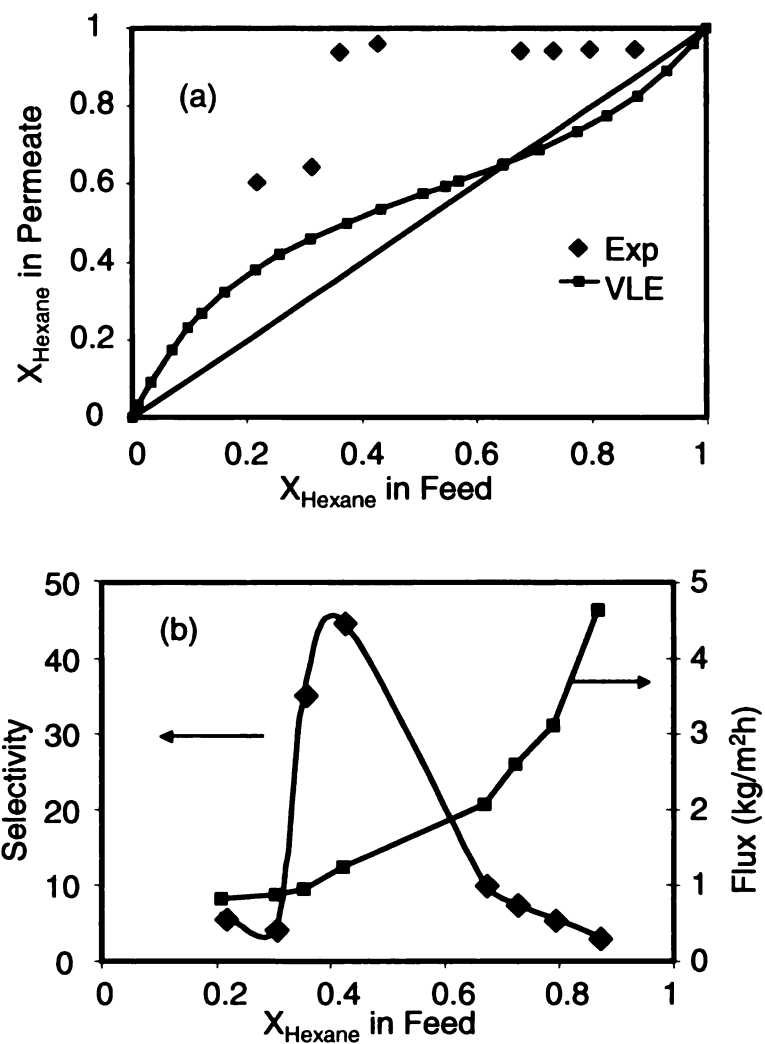
Figure A4. (a) Hexane/ethyl acetate vapor–liquid equilibrium (VLE) relative to separation achieved by PDMDMAES membrane(Exp); (b) Effect of hexane concentration in the feed on separation factor and flux.

References

1.   Themistou, E.; Patrickios, C. S., *Macromolecules* **2004,** *37*, 6734-6743.

2.   Balachandra, A. M.; Baker, G. L.; Bruening, M. L., *J. Membr. Sci.* **2003,** *227*, 1-14.